ANZCOP21

Australian and New Zealand Conference on Optics and Photonics 2021

18-19 November 2021

Conference Program and Book of Abstracts

Version 1.1 –9/11/2021

CONTENTS

Acknowledgement of First Nations 5
Australia 5
Aotearoa - New Zealand 5
Welcome to ANZCOP21 6
From the Organising Committee 6
From the President of ANZOS 6
About ANZCOP 6
ANZCOP21 Conference organisation team 7
Organising committee 7
Hub Leads 7
ANZCOP/AIP Congress/WSOF 2022 8
About ANZOS 8
ANZOS 2021 Annual General Meeting 8
Equity Diversity and Inclusion 9
Conference Code of conduct 9
Support for Parents and carers 9
Statistics on registrants and presenters 10
Conference sponsors 11
Guidelines for the MeetAnyway Platform 12
Before the meeting 12
During the meeting 12
Plenary session and invited speakers 13
Plenary session 13
Partner society addresses 13
Plenary speaker - Professor Halina Rubinsztein-Dunlop 13
ANZOS Prizes 13
Panel session – Your future in photonics 14
Invited speakers 15
ANZOS Prize winners – 2020 and 2021 16
2020 AWARD RECIPIENTS 16
2021 AWARD RECIPIENTS 16
Program schedule 17
Thursday 18 November 2021 17

Friday 19 November 2021 18

List of oral papers 20

List of poster papers 21

PA - Quantum optics 21

PB - Novel lasers and nonclassical light sources 22

PC - Metadevices and nanophotonics 23

PD - Optomechanics and Brillouin scattering 23

PE - Integrated photonics, optical devices and space-based applications 24

PF - Optical sensing, characterisation and biophotonics 25

ACKNOWLEDGEMENT OF FIRST NATIONS

ANZCOP21 is taking place on the traditional lands of many First Nations peoples across Australia and Aotearoa/New Zealand.
The organisers of ANZCOP21 acknowledge and pay respect to the traditional owners of all the lands on which the conference will take place.

AUSTRALIA

We acknowledge the ancestors past, present and emerging and all Aboriginal and Torres Strait Islander people participating in the conference.
We particularly acknowledge the following peoples on whose land our gatherings at city hubs will take place:

- Ngunnawal and Ngambri people - Australian National University, Canberra
- Gadigal and Guring-gai people of the Eora nation- University of Technology, Sydney; University of Sydney
- Wurundjeri people of the Kulin nation - RMIT University, Melbourne:
- Wallumedegal people of the Darug nation - Macquarie University, Sydney
- Kaurna people - University of Adelaide, University of South Australia
- Whadjuk Noongar people - University of Western Australia
- Turrbal/Jagera people - University of Queensland
- Yugarabul, Yuggera, Jagera and Turrbal peoples - Griffith University
- Turrbal and Yugara people - Queensland University of Technology

AOTEAROA - NEW ZEALAND

- Ngā Kaitiaki o tēnei whenua e noho nei mātou, Ngāti Whātua Ōrākei – Waipapa Taumata Rau | The University of Auckland
- Nei rā ka tai o mihi ki a koutou i raro i te maru o ka rūnaka o Kāti Huirapa ki Puketeraki me Ōtākou. Nau mai, haere mai ki Te Whare Wānaka o Ōtākou | The University of Otago

WELCOME TO ANZCOP21

FROM THE ORGANISING COMMITTEE

On behalf of the organising committee and the ANZOS Council, welcome to ANZCOP21, the first ever hybrid ANZCOP online and hub-based conference.

Following the cancellation of our 2020 meeting, ANZCOP21 has been designed to facilitate a mix of in-person and online communication that is best suited for our unpredictable present. Recognising the severe impact COVID-19 has had on networking opportunities for young researchers, ANZCOP21 has an explicit focus on highlighting the work of early career and postgraduate researchers, enabling opportunities for networking, collaboration, and ideas exchange in a hybrid setting.

We have been greatly encouraged by the enthusiasm for this meeting. At the time of writing in late October, the conference has attracted over 170 registrants and well over 80 papers.

We truly hope you find ANZCOP21 an enriching intellectual experience and an opportunity to begin reconnecting with colleagues.

ANZCOP21 Organising Committee

FROM THE PRESIDENT OF ANZOS

It is with great pleasure that I, on behalf of the Australian and New Zealand Optical Society, welcome you to ANZCOP-21. That we are able to have any meeting at all is due to the sheer determination of the fantastic organising committee, whose full membership you will find listed on the next page.

This group, widely dispersed over two countries, imagined what could be in a time of shutdowns, lockdowns, and restrictions. This meeting is not your average ANZCOP meeting. It is a triumph over adversity and recognises that fundamentally we, as humans, need to interact, to group and cluster, speak and share, for our own wellbeing as much as for the progression of our science.

Personally, I have a femtosecond spectroscopy facility shutdown since 5th August, a developing fast scanning LiDAR facility that moves in a van outdoors, slowed down but not stopped, and student projects on diffuse media scattering now back running 24/7 since restrictions have eased. The impact of COVID restrictions on post-doctoral careers, student progression through Undergraduate, Honours and Ph.D. stages has been profound and this imaginative ANZCOP will provide to the group most affected, the opportunity to share their science and bolster confidence.

Equally, the opportunity to gather allows us to engage with our international society partners, SPIE and Optica, who will provide prizes and international talks for the event. Their participation reinforces the global impact that our science has, even as we use the photonic engineering in the optical communications network to engage.

Recognition of outstanding members in restricted times means that we will have not one, but two, Beattie Steel Medals to present amongst the full program of ANZOS awards.

I look forward to seeing you virtually this time, in person in December 2022, and my congratulations again to the organising team.

John Holdsworth, ANZOS President.

ABOUT ANZCOP

The Australian and New Zealand Conference on Optics and Photonics, presented annually by the Australian and New Zealand Optical Society (ANZOS) is the primary domestic conference for optics research in our two countries. The ANZCOP series integrates several former events including ACOFT, ACOLS and the AOS conference. The conference is open to submissions from all areas of contemporary photonics and optics including

- lasers and novel light sources
- nonlinear optics
- fibre optics, communication systems and microwave photonics
- optical materials
- nanophotonics
- optoacoustics
- integrated photonics and optical nano- and micro-fabrication
- metamaterials, metasurfaces and other engineered optical materials
- optical spectroscopy
- biophotonics and biomedical photonics
- laser processing
- astronomical instrumentation
- quantum optics
- modelling and theoretical photonics

ANZCOP21 CONFERENCE ORGANISATION TEAM

ORGANISING COMMITTEE

- Dr Shahna Haneef, University of Auckland
- Dr Rocio Camacho, Australian National University
- Dr Haoran Ren, Macquarie University
- Dr Rohan Glover, University of Adelaide
- Amy Van der Hel, University of Queensland
- Farhan Azeem, University of Otago
- Prof. Igor Aharonovich, University of Technology, Sydney
- A/Prof. Frederique Vanholsbeeck, University of Auckland
- Prof. Michael Steel, Macquarie University

HUB LEADS

Our sincere thanks to the following people who are leading local coordination in each of our hubs.

Hub	Hub champions	Contact details
Auckland	Ashly Jose Sam Esan	ajos486@aucklanduni.ac.nz aesa598@aucklanduni.ac.nz
Otago	Finnian Smith	smifi252@student.otago.ac.nz
Sydney	Alessandro Tuniz (U. Sydney) Mikolaj Schmidt (MQ) Alexander Solntsev (UTS)	alessandro.tuniz@sydney.edu.au mikolaj.schmidt@mq.edu.au a.s.solntsev@gmail.com
Canberra	Anastasia Zalogina Shridhar Manjunath Lorcan Conlon	anastasiia.zalogina@anu.edu.au
Brisbane	Amy van der Hel Leo Sementilli Jordan Scarabel	a.vanderhel@uq.edu.au
Melbourne	Andreas Boes	andreas.boes@rmit.edu.au
Adelaide	Stephen Warren-Smith Anna Radionova	Stephen.Warren-Smith@unisa.edu.au anna.radionova@adelaide.edu.au
Online	Rhona Hamilton Tieshan Yang	rhona.hamilton@student.adelaide.edu.au

ANZCOP/AIP CONGRESS/WSOF 2022

The next ANZCOP conference will be a co-located event in December 2022 with the Australian Institute of Physics Congress (AIPC) and the Workshop on Specialty Optical Fibres and Their Applications (WSOF). The combined conferences and workshop will be held as in-person event in Adelaide at the Adelaide Convention Centre from 11-17 Dec 2022.

Please look out for detailed announcements about the congress early in 2022. The elements of the meeting are as follows:

- The 24th Australian Institute of Physics (AIP) Congress brings the Australian Physics community together in the first major post-pandemic physics meeting in Australia.
- The 6th Australian and New Zealand Conference on Optics and Photonics (ANZCOP) is the annual conference of the Australian and New Zealand Optical Society and provides a forum for researchers from academia and industry working any area of photonics and optics to meet and discuss latest results.
- The 7th International Workshop on Specialty Optical Fibers and Their Applications (WSOF) is a technical workshop and exhibit, which brings together students and researchers from academia and industry, with an interest in fibre optics in a small and familiar setting that affords one-on-one opportunities for technical discussions and fellowship.

aip AUSTRALIAN INSTITUTE OF PHYSICS

ANZCOP

Workshop on SPECIALTY OPTICAL FIBERS AND THEIR APPLICATIONS

ABOUT ANZOS

The Australian and New Zealand Optical Society (ANZOS) is a non-profit organisation for the advancement of optics in Australia. Formed in 1983 as the Australian Optical Society (AOS), the Society embraces anyone contributing to or interested in optics in the widest sense. In January 2020 the Council of the Australian Optical Society (AOS) changed the "trading name" of the Society to the Australian and New Zealand Optical Society (ANZOS) and adopted a new logo.

ANZOS contributions to the community include organising the ANZCOP meetings, offering annual prizes for outstanding work in optics and photonics, maintaining the optics.org.au website including a free job-hosting service, and representing the optics community at the national level through membership of Science and Technology Australia (STA).

ANZOS membership is affordable and offers a discount rate in partnership with major international societies. Student membership is free for the first year. For more information, see the membership page on the society web site.

ANZOS 2021 ANNUAL GENERAL MEETING

The 2021 ANZOS AGM will be held online on Wednesday 1st December, 12pm-1.30 pm Sydney time. Watch your members' emails for the meeting invitation and call for nominations for office holders.

EQUITY DIVERSITY AND INCLUSION

CONFERENCE CODE OF CONDUCT

ANZCOP21 is governed by the ANZOS Code of Conduct.

This Code of Conduct (or code with substantially similar provisions) applies to any event which ANZOS runs, technically sponsors or promotes and must be adopted by the event organisers.

The Australian Optical and New Zealand Society (ANZOS) is dedicated to providing a harassment-free experience for everyone attending events it organises or promotes. Anyone who violates this code of conduct may be sanctioned or expelled from these spaces at the discretion of the Organising Committee of the event.

We require that all attendees:

- Behave professionally
- Are considerate and respectful to others; Do not insult or put down other attendees
- Critique ideas rather than individuals
- Do not monopolise discussion; Sustained disruption of talks or other events may be considered harassment
- Do not engage in photography or recording of an individual without consent.
- Do not harass any attendees, staff or volunteers associated with the conference.

If you witness any breaches of this code, in particular discrimination or harassment, you are encouraged to immediately inform the alleged violator that their comments or behaviour are unwelcome. Individuals may be unaware that their conduct is offensive and are often willing to moderate their behaviour if so informed.

However, please note that you are not required to directly address or confront a person you believe is discriminating against or harassing you or another person.

Each event will nominate at least one person to whom you may wish to report the incident.

Complaints will be investigated confidentially, fairly and discreetly and within the bounds of any relevant legislation. Following the completion of an inquiry, any action to be taken will be determined and may include a request for private or public apologies, discharge from the conference or restrictions on future invitations and attendance.

This code applies equally to in-person, online and mixed mode events.

Definition: Harassment includes but is not limited to: verbal comments that reinforce social structures of domination (related to gender, gender identity and expression, sexual orientation, disability, physical appearance, body size, race, age, religion, etc); sexual images in public spaces; deliberate intimidation, stalking, or following; harassing photography or recording; sustained disruption of talks or other events; inappropriate physical contact; unwelcome sexual attention; and advocating for or encouraging any of the above behaviour.

SUPPORT FOR PARENTS AND CARERS

Through support from ANZOS and our sponsors, ANZCOP21 has some capacity to fund babysitter or substitute carer costs for registrants whose normal parental or carer duties would significantly affect their engagement with the conference, including hub-based social activities. As free registration means our funds are limited, preference will be given to registrants whose home institutions do not offer such support schemes. Interested registrants should contact anzcop21info@gmail.com.

STATISTICS ON REGISTRANTS AND PRESENTERS

As of 20 October 2021, intended participation with ANZCOP21 was as follows:

Gender identity	Participants	Invited talks	Submissions	Contributed Talks	Contributed Posters	Rejected
Female	42 (26 %)	2 (50 %)	18 (24 %)	5 (42 %)	13 (21 %)	0
Male	116 (72 %)	2 (50 %)	56 (75 %)	7 (58 %)	49 (78 %)	0
Non-binary/Do not identify/Prefer not to say	4 (2.5 %)	0	1 (1 %)		1 (1 %)	0
Total	164	4	75	12	63	0

CONFERENCE SPONSORS

ANZOS and the organisers of ANZCOP21 are grateful for the support of the following organisations

- ANZOS - the Australian and New Zealand Optical Society
- Coherent Scientific
- Lastek: Photonics Technology Solutions
- TMOS - The ARC Centre of Excellence for Transformative Meta-Optical Systems
- The ARC Centre of Excellence for Exciton Science
- The Dodd-Walls Centre for Photonic and Quantum Technologies
- OzGrav - The ARC Centre of Excellence for Gravitational Wave Discovery
- Department of Physics, The University Auckland
- Centre for Quantum Science, University of Otago
- SPIE-OSA Otago student chapter

GUIDELINES FOR THE MEETANYWAY PLATFORM

ANZCOP21 is running on the MeetAnyway platform at https://meetanyway.com/events/anzcop-2021. Please use the following instructions to connect to the conference. A visual walk-through is also available.

BEFORE THE MEETING

Visit the main seminar platform under https://meetanyway.com/events/anzcop-2021, click on the "Attend meeting" button and register (or login if you already have an account).

- Firstly, make sure that your computer has a good camera and microphone or headset. Make sure that you test both before the meeting!
- Please register with your full name and institution (in the Headline field) and upload a photograph. That will make networking and poster sessions more effective for you.
- When ready, click the orange "Enter event space" button on the right.
- Make sure that you only use **one** computer per room to join the event to avoid echoes and interferences!
- Google Chrome is currently the most stable and reliable browser for video conferencing. Firefox and Safari should work but may offer reduced performance.
- It is recommended to disable any Ad Blocker extensions from your web browsers for an uninterrupted experience.
- Further information on MeetAnyway and its functionalities is available at this YouTube video: www.youtube.com/watch?v=3JwgF9pHVuU

DURING THE MEETING

- Once you are in the event space you will see different floors such as the Information space, Welcome Hall, Main Stage, Poster Session etc, and you will be able to move freely between them.
- Each floor has different elements such as stages and tables. Hover on a button to see a tooltip on its use. **Join** will connect to a video chat or a stage. The **Open** button in the information space will redirect you to the conference website via a popup with embedded websites, PDFs, or similar.
- When you join a stage in order to listen to a talk, you will automatically be connected via a video call. Your audio and video will be turned off, but you may turn both on and off on your own.
- If presenting a talk, please turn on your microphone and camera, open your presentation on your computer and use the *Share your Screen* option so that the audience may see your slides. Please remember the time limits for contributed presentations: 14 minutes for the talk plus 4 minutes discussion.
- To ask a question, please use the chat or turn on your microphone and camera and ask directly.
- Please make sure that you leave the Auditorium properly during the breaks. You will then return to the main floors in MeetAnyway.
- Throughout the whole conference, all posters can be viewed by visiting the two **Poster Session** floors. To discuss a poster, you can join a video call with the poster presenter during the poster sessions. During a video call each participant can share their screen. To leave a video call, click on the arrow in the red box at the bottom-left corner or simply directly join another video call.
- During breaks, you are strongly encouraged to use the networking elements provided by MeetAnyway. In the **Welcome Hall,** you will find a Networking area with multiple tables and a mingling area. If you join the Mingling area, you will be randomly matched with other conference attendees for a 3 minute video chat. When you join a table in the Networking floor you enter a video call with all the people on that table. There are two kinds of tables, open and private ones. Open ones can be joined by everyone anytime. For the private ones we ask that you only join them after being invited to do so. The magnifier at the upper-right corner in MeetAnyway allows you to search for any participant and subsequently visit their current room or send them a message by hovering on their icon.
- If you need technical support, in the first instance approach your hub champion. You can start a chat with MeetAnyway staff by clicking on the steering wheel or sending an e-mail to support@meetanyway.com .

PLENARY SESSION AND INVITED SPEAKERS

PLENARY SESSION

The opening session of ANZCOP21 features several distinguished speakers.

PARTNER SOCIETY ADDRESSES

We are delighted to welcome the incoming presidents of both SPIE and Optica to continue the tradition of presentations at ANZCOP by members of their leadership teams.

SPIE will be represented by incoming 2022 SPIE President, **Professor Anita Mahadevan-Jansen** of Vanderbilt University, a global leader in biomedical engineering.

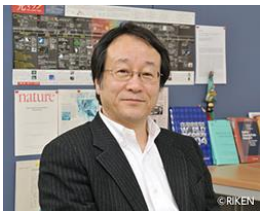

Optica will be represented by incoming President **Professor Satoshi Kawata** of Osaka University and RIKEN, known for numerous contributions in nanophotonics, biophotonics and other branches of optics.

PLENARY SPEAKER - PROFESSOR HALINA RUBINSZTEIN-DUNLOP

The plenary address of ANZCOP21 will be delivered by **Professor Halina Rubinsztein-Dunlop AO FFP** of the School of Mathematics and Physics at the University of Queensland. Prof. Rubinsztein-Dunlop is renowned for her many contributions to spectroscopy, nonlinear optics, laser trapping and micromanipulation, quantum chaos and quantum optics. A 2021 SPIE Luminary, she has an accomplished record of service in physics and optics, including as ANZOS Councillor, member of the Board of Directors of SPIE, as Chair of the SPIE Equity, Diversity, and Inclusion Committee.

Sculpted light – one good turn deserves another

The way light can apply forces to a nano- or micro-sized object is easily understood as an exchange of momentum between the light beam and the object. This applies both to linear momentum and to angular momentum exchange. Methods based on these phenomena promise high flexibility and an

opportunity for trapping and driving these objects or even using them inside a biological cell for evaluation and better understanding of cellular responses. Optical drive of micron scale devices promises the ability to carry out measurements and operations on microscopic systems in a flexible way. The energy that is needed can be transmitted without harm through many materials including a membrane of a cell. Optical tweezers have been already used in atom optics as well as to measure mechanical properties of cells and their components, and also for studies of molecular motors. The stimulation of cells by forces and torques applied to them has allowed studies of cell response and signal transduction.

Sculpted light produced using programmable spatial light modulators have significantly enhanced the configurable optical trapping. These sculpted light beams can be used for optical trapping of Bose Einstein Condensate and their manipulation. They can also provide beams carrying angular momentum that enables introduction of rotation. Quantitative measurements of this rotation are possible through a measurement of the change of polarisation state of light after passing through the object. The transfer of the angular momentum can then be used for several applications in biology and medicine. Sculpted light can also be used to substantially enhance the trapping efficiency and therefore increase the applied forces.

ANZOS PRIZES

The plenary session will conclude with the formal presentation of ANZOS awards for both 2020 and 2021 by the respective ANZOS presidents for those years, Prof. John Harvey (University of Auckland) and A/Prof. John Holdsworth (University of Newcastle).

PANEL SESSION – YOUR FUTURE IN PHOTONICS

The plenary session and first poster session will be followed by a panel session chaired by optical scientist and entrepreneur Prof. Cather Simpson of the University of Auckland. Alongside her academic work, Professor Simpson was the founding director of the Photon Factory and a founder of two spin-off companies, Engender Technologies and Orbis Diagnostics.

We are delighted to welcome the following distinguished speakers to the panel:

- **Dr Xiaoli Tang,**
  Optical engineering team leader, Baraja Pty. Ltd
- **Dr Steve Frisken**
  Optical researcher, inventor and entrepreneur Cylite
- **Dr Matheus J. T. Vargas**
  Chief Technology Officer, Orbis Diagnostics
- **Dr Maria Maragkou**
  Senior Business Development Manager, Riverlane


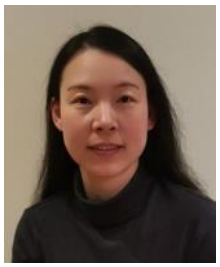


INVITED SPEAKERS

The day two sessions will feature invited presentations from the following four exciting speakers.

Dr Daria Smirnova,
Australian National University

Topological photonics with all-dielectric nanostructures

Daria Smirnova received her Ph.D. in Physics in 2016 from the Australian National University (ANU), followed by work experience in the USA, Russia and Australia. Currently, she holds a prestigious Discovery Early Career Research Fellow position supported by the Australian Research Council at the ANU. In 2020 she was honoured as one of Australia's leading young researchers in The Australian's Special Report. Her research interests include nonlinear physics, nanophotonics and topological photonics.

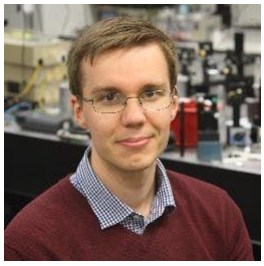

Dr Miro Erkintalo,
University of Auckland

Spontaneous breaking of polarisation symmetry in nonlinear resonators

Miro is an associate professor at the Department of Physics at the University of Auckland, New Zealand, and a principal investigator of the Dodd-Walls Centre for Photonic and Quantum Technologies. He obtained his PhD in 2012 from the Tampere University of Technology in Tampere, Finland, and has worked at the University of Auckland ever since. Miro's research encompasses a wide range of subjects across nonlinear and ultrafast photonics, including microresonator optical frequency combs, mode-locked lasers, physics of conservative and dissipative solitons, and supercontinuum generation. He is the recipient of the 2019 New Zealand Prime Minister's MacDiarmid Emerging Scientist Prize.

Dr Andreas Boes,
RMIT University

Unlocking all-optical processing with lithium thin-film niobate

Andy obtained his PhD from RMIT in 2016, exploring strongly focused laser light to engineer ferroelectric domains in lithium niobate crystals. Since then, Andy has shifted his focus from engineering the material properties of lithium niobate to using its attractive properties in photonic integrated circuits. To deepen his understanding, Andy visited the research group of Prof. John Bowers (UCSB) in 2017/18, deepening his knowledge in highly efficient nonlinear optical waveguides. Andy is currently the team leader of the precision sensing team in the Integrated Photonics and Applications Centre (InPAC) at RMIT, concentrating on the industrial translation of lithium niobate circuits.

Dr Jiawen Li,
University of Adelaide

Freeform 3D printed micro-lenses for optical coherence tomography probes

Dr Jiawen Li is a Lecturer and NHMRC Fellow at School of Electrical and Electronic Engineering, the University of Adelaide. She received her Bachelor's degree in Optical Engineering from Zhejiang University (China) in 2010, and her PhD degree in Biomedical Engineering from University of California Irvine (USA) in 2015. Jiawen is developing ultrathin, flexible, multimodal fibre-optic devices that will enable cross-sectional visualisation deep inside the body, with cellular resolution and molecular contrast. She is inventor on three patents, and has won numerous prestigious awards/honours (including Superstar of STEM, Australian Optical Society Geoff Opat Prize, SA Women in Innovation Award).

ANZOS PRIZE WINNERS – 2020 AND 2021

The Australian and New Zealand Optical Society offers a series of prestigious awards for society members.

The awards are:

- *W. H. (Beattie) Steel Medal* – the Society's highest award
- *Geoff Opat Early Career Researcher Prize*
- *John Love Award* for innovation and technical advances in optics
- *ANZOS Postgraduate Student Prize*
- *Warsash Science Communication Prize*

In 2022, the Society will introduce a new award targeting mid-career researchers.

For details on criteria and nomination procedures for all awards, see the awards web page at https://optics.org.au/prizes. Nominations for ANZOS awards typically open in early April.

2020 AWARD RECIPIENTS

Congratulations to the following recipients of ANZOS awards in 2020:

- *W. H. (Beattie) Steel Medal*
  Professor Benjamin Eggleton, University of Sydney
- *Geoff Opat Early Career Researcher Prize*
  Dr Andreas Boes, RMIT University
- *John Love Award*
  Professor Warwick Bowen, University of Queensland
- *ANZOS Postgraduate Student Prize*
  Kirill Koshelev, Australian National University

2021 AWARD RECIPIENTS

Recipients of 2021 ANZOS awards will be announced during the first session of the conference following the formal announcement of prizes by the ANZOS presidents for 2020 and 2021.

PROGRAM SCHEDULE

THURSDAY 18 NOVEMBER 2021

Session Th1 – Plenary session and ANZOS prize presentation

Chair: A/Prof. Frederique Vanholsbeeck, *University of Auckland*

Activity	Sydney	New Zealand	Brisbane	Adelaide	Perth
Welcome address **Prof. Igor Aharonovich** *University of Technology, Sydney*	13:00	15:00	12:00	12:30	10:00
SPIE Partner Society Talk **Dr. Anita Mahadevan-Jansen** *SPIE President, 2022*	13:10	15:10	12:10	12:40	10:10
Optica Partner Society Talk **Dr Satoshi Kawata** *Optica President, 2022*	13:35	15:35	12:35	13:05	10:35
Plenary talk **Prof. Halina Rubinsztein-Dunlop** *University of Queensland*	14:00	16:00	13:00	13:30	11:00
ANZOS prize presentations 2020/2021 **Prof. John Harvey** *ANZOS President, 2020* **A/Prof. John Holdsworth** *ANZOS President, 2021*	14:50	16:50	13:50	14:20	11:50
Session close	15:05	17:05	14:05	14:35	12:05

Coffee break (25 mins)	Sydney	New Zealand	Brisbane	Adelaide	Perth
	15:05-15:30	17:05-17:30	14:05-14:30	14:35-15:00	12:05-12:30

Session Th2 – Poster session 1 and discussion panel

Chair: A/Prof. Frederique Vanholsbeeck, *University of Auckland*

Activity	Sydney	New Zealand	Brisbane	Adelaide	Perth
Poster Session 1	15:30	17:30	14:30	15:00	12:30
Discussion panel - *Your future in optics and photonics* **Chair: Prof. Cather Simpson** *University of Auckland*	16:30	18:30	15:30	16:00	13:30
Hub-based networking	17:45	19:45	16:45	17:15	14:45

FRIDAY 19 NOVEMBER 2021

Session FrA - Nonlinear optics and plasmonics

Chair: Dr Shahna Haneef, *University of Auckland*

Activity	Sydney	New Zealand	Brisbane	Adelaide	Perth
(*Invited*) Dr Miro Erkintalo (U. of Auckland) *Spontaneous breaking of polarisation symmetry in nonlinear resonators*	9:00	11:00	8:00	8:30	6:00
Mr Liam Quinn (U. of Auckland) *Random number generation using spontaneous symmetry breaking in a Kerr resonator*	9:30	11:30	8:30	9:00	6:30
Mr Geraud Hennin Arencibia (U. of Auckland) *Catching quantum jumps through heterodyne monitoring of a thermal drive*	9:50	11:50	8:50	9:20	6:50
Dr Alessandro Tuniz (U. of Sydney) *Revisiting plasmonic sensors: a non-Hermitian perspective*	10:10	12:10	9:10	9:40	7:10
Session close	10:30	12:30	9:30	10:00	7:30

Coffee break (30 mins)	**Sydney** 10:30-11:00	**New Zealand** 12:30-13:00	**Brisbane** 9:30-10:00	**Adelaide** 10:00-10:30	**Perth** 7:30-8:00

Session FrB - Metadevices and quantum optics

Chair: Dr Rocio Camacho, *Australian National University*

Activity	Sydney	New Zealand	Brisbane	Adelaide	Perth
(*Invited*) Dr Daria Smirnova (Australian National U.) *Topological photonics with all-dielectric nanostructures*	11:00	13:00	10:00	10:30	8:00
Dr Yana Izdebskaya (Australian National U.) *Magnetic Tuning of Liquid Crystal Metasurfaces*	11:30	13:30	10:30	11:00	8:30
Ms Ritika Ritika (U. of Technology, Sydney) *Coupling spin defects in a layered material to nanoscale plasmonic cavities*	11:50	13:50	10:50	11:20	8:50
Mr Shaban Sulejman (U. of Melbourne) *Classical ghost phase imaging using optical metasurfaces*	12:10	14:10	11:10	11:40	9:10
Session close	12:30	14:30	11:30	12:00	9:30

Lunch and poster session 2 (60 mins)	**Sydney** 12:30-13:30	**New Zealand** 14:30-15:30	**Brisbane** 11:30-12:30	**Adelaide** 12:00-13:00	**Perth** 9:30-10:30

Session FrC - Integrated devices and materials

Chair: Dr Haoran Ren, *Macquarie University*

Activity	Sydney	New Zealand	Brisbane	Adelaide	Perth
(Invited) Dr Andreas Boes (RMIT U.) *Unlocking all-optical processing with lithium thin-film niobate*	13:30	15:30	12:30	13:00	10:30
Mr Saurabh Bhardwaj (Macquarie U.) *Morphology of femtosecond laser inscribed point-by-point Bragg gratings*	14:00	16:00	13:00	13:30	11:00
Dr Ziyuan Li (Australian National U.) *GaAsSb nanowire array based filter-free wavelength-selective photodetectors*	14:20	16:20	13:20	13:50	11:20
Ms Sophie Muusse (U. of Adelaide) *Independent absorption and extrinsic scatter measurements in low loss glasses*	14:40	16:40	13:40	14:10	11:40
Session close	15:00	17:00	14:00	14:30	12:00

Coffee break (30 mins)	Sydney	New Zealand	Brisbane	Adelaide	Perth
	15:00-15:30	17:00-17:30	14:00-14:30	14:30-15:00	12:00-12:30

Session FrD - Novel imaging and characterisation

Chair: Dr Rohan Glover, *University of Adelaide*

Activity	Sydney	New Zealand	Brisbane	Adelaide	Perth
(Invited) Dr Jiawen Li (U. of Adelaide) *Freeform 3D printed micro-lenses for optical coherence tomography probes*	15:30	17:30	14:30	15:00	12:30
Dr Lu Peng (U. of Adelaide) *Particle size characterisation using a multimoded fibre*	16:00	18:00	15:00	15:30	13:00
Dr Mickael Mounaix (U. of Queensland) *Spectrally resolved point-spread-function engineering using scattering media*	16:20	18:20	15:20	15:50	13:20
Dr Michael Taylor (U. of Queensland) *Heterodyne Brillouin microscopy for biomechanical imaging*	16:40	18:40	15:40	16:10	13:40
Closing session: Student prizes Introduction of ANZCOP 2022 Closing remarks	17:00	19:00	16:00	16:30	14:00
Conference close	17:15	19:15	16:15	16:45	14:15

LIST OF ORAL PAPERS

Papers are indexed in the following pages by the paper number shown in these tables.

Paper number	Lead author	Institution	Title
FrA-1	Dr Miro Erkintalo	University of Auckland	Spontaneous breaking of polarisation symmetry in nonlinear resonators (Invited)
FrA-2	Mr Liam Quinn	University of Auckland	Random number generation using spontaneous symmetry breaking in a Kerr resonator
FrA-3	Mr Geraud Hennin Arencibia	University of Auckland	Catching quantum jumps through heterodyne monitoring of a thermal drive
FrA-4	Dr Alessandro Tuniz	University of Sydney	Revisiting plasmonic sensors: a non-Hermitian perspective
FrB-1	Dr Daria Smirnova	Australian National University	Topological photonics with all-dielectric nanostructures (Invited)
FrB-2	Dr Yana Izdebskaya	Australian National University	Magnetic Tuning of Liquid Crystal Metasurfaces
FrB-3	Ms Ritika Ritika	University of Technology, Sydney	Coupling spin defects in a layered material to nanoscale plasmonic cavities
FrB-4	Mr Shaban Sulejman	University of Melbourne	Classical ghost phase imaging using optical metasurfaces
FrC-1	Dr Andreas Boes	RMIT University	Unlocking all-optical processing with lithium thin-film niobate (Invited)
FrC-2	Mr Saurabh Bhardwaj	Macquarie University	Morphology of femtosecond laser inscribed point-by-point Bragg gratings
FrC-3	Dr Ziyuan Li	Australian National University	GaAsSb nanowire array-based filter-free wavelength-selective photodetectors
FrC-4	Ms Sophie Muusse	University of Adelaide	Independent absorption and extrinsic scatter measurements in low loss glasses
FrD-1	Dr Jiawen Li	University of Adelaide	Freeform 3D printed micro-lenses for optical coherence tomography probes (Invited)
FrD-2	Dr Lu Peng	University of Adelaide	Particle size characterisation using a multimoded fibre
FrD-3	Dr Mickael Mounaix	University of Queensland	Spectrally resolved point-spread-function engineering using scattering media
FrD-4	Dr Michael Taylor	University of Queensland	Heterodyne Brillouin microscopy for biomechanical imaging

LIST OF POSTER PAPERS

Papers are indexed in the following pages by the paper number shown in these tables.

PA - QUANTUM OPTICS

Paper number	Lead author	Institution	Title
PA-1	Prof. Geoff Pryde	Griffith University	Detection-loophole-free quantum steering with vector vortex states
PA-2	Dr Jihua Zhang	Australian National University	Single-shot characterization of two-photon distinguishability with dielectric metasurfaces
PA-3	Dr Sergei Slussarenko	Griffith University	Experimental quantum channel correction via heralded amplification
PA-4	Mr Soroush Khademi	University of Queensland	Conditional quantum states of macroscopic objects at room temperature
PA-5	Mr Jordan Scarabel	Griffith University	Zeeman sub-level Raman sideband cooling with 171Yb+
PA-6	Mr Kenji Shimizu	Griffith University	Ultrafast coherent excitation of an Ytterbium ion with single laser pulses
PA-7	Mr. Jacob Ngaha	University of Auckland	A better method for calculating filtered photon correlations
PA-8	Dr Mehran Kianinia	University of Technology, Sydney	Creation and properties of spin-bearing defects in hBN
PA-9	Ms Sabrina Slimani	University of Adelaide	Developing a space-based quantum-secure time transfer system
PA-10	Mr Ben White	University of Adelaide	Towards a compact ytterbium magneto optical trap for use in precision timekeeping applications
PA-11	Dr Zachary Koumi	University of Adelaide	Determining the advantage of Quantum Lidar
PA-12	Dr Sri Kasi Matta	RMIT University	Low bandgap Janus semiconductors from carbon and nitrogen family of elements - property analysis through Density Functional Theory
PA-13	Dr Mikolaj Schmidt	Macquarie University	Quantum engineering the effective optomechanical coupling
PA-14	Mr Jaret Vasquez-Lozano	RMIT University	Mapping the geometry of quantum correlation microscopy: Voronoi cells in the Hanbury Brown and Twiss experiment

PB - NOVEL LASERS AND NONCLASSICAL LIGHT SOURCES

Paper number	Lead author	Institution	Title
PB-1	Dr. Jinyong Ma	Australian National University	Photon-pair generation enhanced by extended resonances in metasurfaces
PB-2	Mr. Chi Li	University of Technology, Sydney	Scalable and Deterministic Fabrication of hBN Quantum Emitter Arrays
PB-3	Mr Alexander Elliott	University of Auckland	Quantum states of light generated from a single atom through cavity-assisted Raman transitions
PB-4	Ms Lesley Spencer	University of Technology Sydney	Coupling spin defects in hexagonal boron nitride to monolithic bullseye cavities
PB-5	Mr Simon White	University of Technology Sydney	Phonon dephasing and spectral diffusion of quantum emitters in hexagonal Boron Nitride
PB-6	Dr Zaiquan Xu	University of Technology Sydney	Enhanced spin readout in hBN via coupling to nanoscale plasmonic cavities
PB-7	Mr. Zachary Holmes	University of Adelaide	Delay-limited phaselocking for stable narrow-linewidth laser diodes
PB-8	Ms Georgia Bolingbroke	University of Adelaide	Single-frequency 1950nm, 1980nm, and 2035nm thulium-doped fiber lasers
PB-9	Mr Alexandros Kolovinos	University of Adelaide	Optimisation of dispersion-compensation fiber length in a SESAM-Soliton hybrid mode-locked laser
PB-10	Mr Milad Nonahal	University of Technology, Sydney	Bottom-up synthesis of single-crystal diamond pyramids containing germanium vacancy centers
PB-11	Mr Farhan Azeem	University of Otago	Investigating a titanium doped sapphire whispering-gallery mode resonator as a laser and amplifier

PC - METADEVICES AND NANOPHOTONICS

Paper number	Lead author	Institution	Title
PC-1	Dr Alireza Maleki	Macquarie University	Nanorubies for multiplexed imaging of cells
PC-2	Dr Quanlong Yang	Australian National University	Terahertz topological meta-devices
PC-3	L. Weseman	University of Melbourne	Meta-optics for edge detection and enhanced phase contrast imaging
PC-4	Mr Sangeeth Soman Thandasseril	University of Technology, Sydney	Polarisation-independent gratings for high-reflectivity LCoS in near-infrared
PC-5	Ms. Luyao Wang	Australian National University	Tunable metasurfaces with electro-optic materials
PC-6	Mr. Heyou Zhang	University of Melbourne	Direct assembly of single nanocrystal arrays
PC-7	Mr Ibrahim Al-Ani	University of New South Wales, Canberra	Strong coupling in all-perovskite metasurface via bound state in the continuum
PC-8	Mr. Fanlu Zhang	Australian National University	Selective area growth of InGaAs/InP multiple quantum well nanowire for optoelectronic device applications
PC-9	Mr Declan Armstrong	University of Queensland	Aberration correction for printed microstructures

PD - OPTOMECHANICS AND BRILLOUIN SCATTERING

Paper number	Lead author	Institution	Title
PD-1	Mr Walter Wasserman	University of Queensland	An integrated platform for superfluid optomechanics
PD-2	Dr Christopher Baker	University of Queensland	Superfluid Brillouin optomechanics
PD-3	Miss Amy van der Hel	University of Queensland	Optical-to-mechanical state transfer through feedback in optomechanics
PD-4	Mr Matthew Garrett	University of Sydney	Microwave photonic notch filter for suppression of multi-band interferers
PD-5	Mr Luke McKay	The University of Sydney	Ultra-deep image rejection mixer using stimulated Brillouin scattering in a chip-based platform
PD-6	Mr Raymond Harrison	University of Queensland	Trapping sound with light

PE - INTEGRATED PHOTONICS, OPTICAL DEVICES AND SPACE-BASED APPLICATIONS

Paper number	Lead author	Institution	Title
PE-1	Miss Paramjeet Kaur	RMIT University	Progress toward the integration of high-speed photodetectors in lithium niobate on insulator photonic circuits
PE-2	Mr Oliver Bickerton	University of Sydney	CMOS-compatible high-efficiency silicon photodetector with suspended nano-photonic structures
PE-3	Mr Long Qiang	University of Sydney	Generalised sixth order dispersion solitons
PE-4	Ms Rebecca Russell	RMIT University	Simulation and design of circulators in lithium niobate on insulator
PE-5	Mr Jonathan Hedger	University of Adelaide	Measuring the fundamental thermal phase fluctuations in a passive fibre resonator
PE-6	Mr Pierce Qureshi	University of Auckland	Soliton linear-wave scattering in a Kerr microresonator
PE-7	Dr Timothy Davis	University of Melbourne	Ultra-fast vector imaging of surface plasmon polaritons
PE-8	Dr Alessandro Tuniz	The University of Sydney	Terahertz bend losses in cm-scale polyurethane flexible hollow-core fibers
PE-9	Mr Daniel Dahl	University of Queensland	High-dimensional Stokes-space Spatial Beam Analyser
PE-10	Nusrat Alim	University of New South Wales	Personal thermal management with large scale kevlar textile
PE-11	Mr Sam Dekkers	Monash University	Optical fibre photodetector for COMET Phase-I
PE-12	Mr Luyi Xu	Macquarie University	Fabrication of thermally stable fiber Bragg gratings with high reflectivity for the mid-infrared
PE-13	Dr Kerry Mudge	Defence Science Technology Group	Laboratory Scintillation Emulator for the Optical Low Earth Orbit Satellite Downlink Channel
PE-14	Dr Vladimyros (Vladimir) Devrelis	Gadzooks PtyLtd	Cloud free sky comparison for optical ground station sites in Australia
PE-15	Mr Marcus Birch	Australian National University	The Mount Stromlo optical communication ground station
PE-16	Dr Nicholas Lambert	University of Otago	Ultrastable dual frequency combs generation using whispering gallery resonators
PE-17	Mrs Sobia Rehman	Macquarie University	Parametric study of waveguide inscription into mid-infrared compatible glasses
PE-18	Mr Josh Christensen	University of Otago	High-Q yttrium lithium fluoride whispering-gallery mode resonator
PE-19	Dr Wen Qi Zhang	University of South Australia	Using convolutional neural networks for nonlinear frequency division multiplexing

PF - OPTICAL SENSING, CHARACTERISATION AND BIOPHOTONICS

Paper number	Lead author	Institution	Title
PF-1	Mr Mark Watson	University of Queensland	Successful intracellular microrheology of living macrophages
PF-2	Mr Shridhar Manjunath	Australian National University	Biosensing with high Q-factor dielectric metasurfaces
PF-3	Mr Ziqian Zhang	University of Sydney	Centimetre-spatial-resolution photonic radar using low-speed electronics
PF-4	Dr. Shahna Muhammad Haneef	University of Auckland	Distributed temperature and strain measurements at an active plate-bounding fault using fiber optic sensors
PF-5	Mr Darcy Smith	University of Adelaide	Machine learning for sensing with a multimode exposed core fiber specklegram sensor
PF-6	Mr Mohammad Istiaque Reja	University of Adelaide	Simultaneous measurement of high temperature and pressure using pure silica microstructured optical fiber
PF-7	Dr Mikolaj Schmidt	Macquarie University	Probing the electromagnetic response of dielectric antennas by vortex electron beams
PF-8	Mr Ling Zhang	University of Technology, Sydney	Trapped aerosol sizes in dual beam optical fiber-based traps
PF-9	Dr Jamie Laird	University of Melbourne	System for high-speed transient absorption microscopy
PF-10	Ms Caitlin Smith	University of Auckland	Quantitative photoacoustic velocimetry technique using multi-angle observations

Spontaneous Breaking of Polarization Symmetry in Nonlinear Optical Resonators

M. Erkintalo[1,2], G. Xu[1,2], A. U. Nielsen[1,2], L. Quinn[1,2], B. Garbin[1,2,3], L. Hill[4,5], G.-L. Oppo[4], J. Fatome[1,2,6], S. G. Murdoch[1,2], & S. Coen[1,2]

[1]*Department of Physics, University of Auckland, Auckland 1010, New Zealand*
[2]*The Dodd-Walls Centre for Photonic and Quantum Technologies, New Zealand*
[3]*Centre de Nanosciences et de Nanotechnologies (C2N), CNRS, Université Paris-Saclay, F-91120 Palaiseau, France*
[4]*SUPA and Department of Physics, University of Strathclyde, Glasgow G4 0NG, Scotland, EU*
[5]*National Physical Laboratory, Hampton Road, Teddington, TW11 0LW, UK*
[6]*ICB, UMR 6303 CNRS, Université Bourgogne-Franche-Comté, 9 Av. Alain Savary, BP 47870, F-21078 Dijon, France*
email: m.erkintalo@auckland.ac.nz

***Abstract**: We report on a sequence of experiments that explore the process of spontaneous polarization symmetry breaking in coherently-driven, Kerr nonlinear optical resonators, and we show that the symmetry breaking dynamics can be leveraged for robust physical random number generation.*

Coherently-driven nonlinear optical resonators display incredibly rich physics that has been leveraged for applications from sensing to optical frequency comb generation [1-4]. Here we describe a sequence of experiments that demonstrate and explore, for the first time to the best of our knowledge, the breaking of polarization symmetry in optical resonators with Kerr nonlinearity [5-7]. Our experiments are performed in macroscopic optical fibre ring resonators that display two orthogonal mode families corresponding to the principal polarization components of the fibres that form the resonators. We judiciously engineer symmetry (equal driving and detuning) for the two polarization modes, yet find that the nonlinear cavity dynamics can enact spontaneous breaking of this symmetry.

In our experiments, we observe for the first time the polarization symmetry breaking for homogeneous steady-state solutions of the intracavity field [5], as predicted theoretically more than two decades ago [8]. Moreover, we theoretically and experimentally demonstrate that the symmetry breaking dynamics are not limited to homogeneous states but extend to so-called dissipative Kerr solitons [6] that have recently attracted significant attention as the time-domain counterparts of microresonator optical frequency combs [1,2]. To the best of our knowledge, these experiments [6] represent the first observation of spontaneous symmetry breaking of dissipative solitons in any two-component physical system.

Our experiments also reveal a new dynamical regime, whereby the system self-symmetrizes itself so as to develop complete immunity against residual asymmetries [7]. Operation in this regime enables spontaneous symmetry breaking to take place with unprecedented robustness, a feature we leverage to realise a physical random number generator operating at MHz rates. We rigorously verify the true randomness of the resulting bit sequences using state-of-the-art statistical tests.

In summary, we report on experiments performed in macroscopic optical fibre ring resonators that demonstrate and explore the spontaneous breaking of polarization symmetry of light circulating in the resonators. Our results elucidate the fundamental dynamics of (multimode) nonlinear optical resonators and could find applications from physical random number generators to photonic Ising machines.

References:

1. A. Pasquazi et al., *Phys. Rep.* **729**, 1-81 (2018).
2. T. J. Kippenberg et al., *Science* **361**, eaan8083 (2018).
3. Q.-T. Cao et al., *Phys. Rev. Lett.* **2**, 023244 (2017).
4. L. Del Bino et al., *Sci. Rep.* **7**, 43142 (2017).
5. B. Garbin et al. *Phys. Rev. Research* **2**, 023244 (2020).
6. G. Xu et al., *Nature Commun.* **12**, 4023 (2021)
7. J. Fatome et al., arXiv:2106.07642 (2021)
8. M. Haelterman et al., J. Opt. Soc. Am. B **11**, 446-456 (1994).

Random number generation using spontaneous symmetry breaking in a Kerr resonator

Liam Quinn[1,2], Gang Xu[1,2], Zongda Li[1,2], Julien Fatome[1,2], Stuart G. Murdoch[1,2], Miro Erkintalo[1,2], Stéphane Coen[1,2]

[1]*Department of Physics, University of Auckland, Auckland 1010, New Zealand*
[2]*The Dodd-Walls Centre for Photonic and Quantum Technologies, New Zealand*
email: liam.quinn@auckland.ac.nz

***Abstract**: We present a novel, all-optical random number generator relying on polarization SSB in a passive, driven nonlinear cavity. The random numbers are produced at MHz generation rates and require no post-processing. The system is stable, with a statistically high degree of randomness.*

A variety of applications, including numerical modelling, cryptography, gambling, and finance, rely on random number generators (RNGs) [3]. For these systems, the ideal RNG has a high rate of number generation and is truly random. While there are many accessible computer algorithms for generating random numbers, these sources output pseudo-random numbers known to be deterministic. There has been recent improvement and research into RNGs based on quantum mechanical systems [3]. However, these techniques are often limited by requiring either substantial post-processing or the characterization of associated devices.

We have developed a new method for random number generation based on spontaneous symmetry breaking (SSB). We use a fiber ring cavity with two polarization modes with a π phase defect between them. In this configuration, only one mode is driven, yet we can describe the system in terms of two hybrid modes that are mixtures of the cavity modes and have exact interchange symmetry over two cavity roundtrips. This so-called self-symmetrization mechanism (also known as P2 [1]) leads to the realization of SSB in ideal conditions. For low intracavity intensities, the hybrid polarization modes have equal intensities, and only one symmetric state will occur. Above a certain threshold, however, spontaneous symmetry breaking (SSB) results in the emergence of two asymmetric states that are mixtures of the two modes as described previously by Garbin et. al. [2].

When tuning the system across the SSB bifurcation point, the two asymmetric states emerge with equal probability, enabling the realization of an RNG [see Fig. 1a]. By rapidly scanning the laser frequency across the bifurcation point in a fibre ring resonator, we obtain a MHz RNG scheme by measuring a single polarization mode [see Fig. 1b]. The degree of randomness of the bit sequence is rigorously assessed using the NIST Statistical Test Suite for Random Number Generators [4], where all tests are passed on 100 samples of one million bits. The generation of genuinely random numbers also serves to demonstrate that the self-symmetrization induced by the P2 mechanism is highly robust and truly symmetric, potentially paving the way for novel implementations of coherent photonic Ising machines.

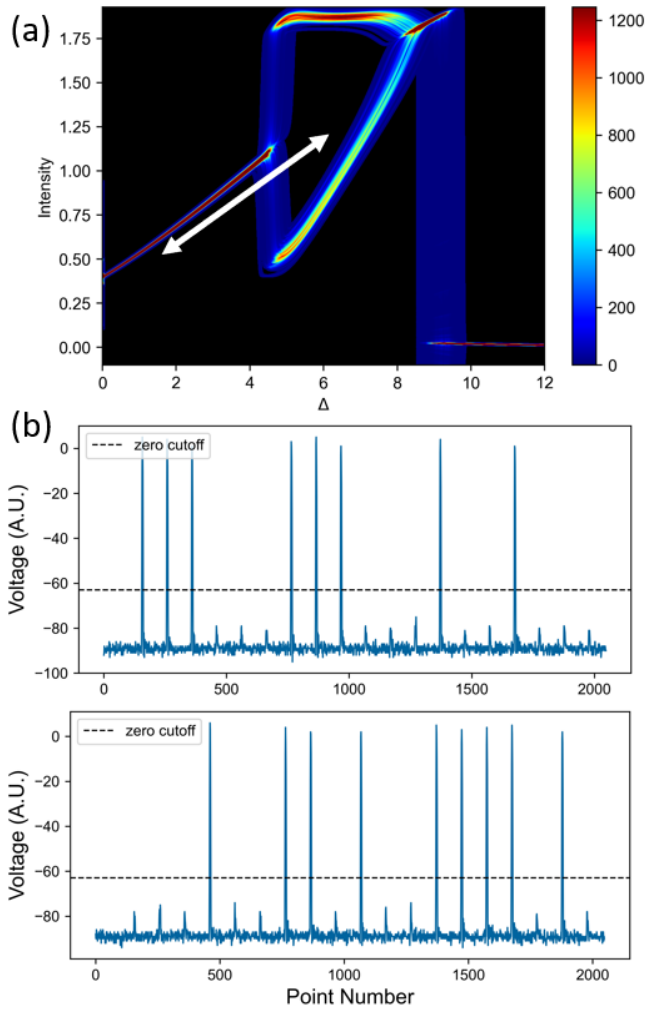

References:

1. J. Fatome, G. Xu, B. Garbin, N. Berti, G.-L. Oppo, S. G. Murdoch, M. Erkintalo, and S. Coen, *CLEO US, 2021*
2. B. Garbin, J. Fatome, G.-L. Oppo, M. Erkintalo, S. G. Murdoch, and S. Coen, *Physical Review Research, 2(2):023244, May 2020.*
3. Y. Okawachi, M. Yu, K. Luke, D. O. Carvalho, M. Lipson, and A. L. Gaeta, Optics Letters, 41(18):4194, Sept. 2016.
4. A. Rukhin, J. Soto, J. Nechvatal, E. Barker, S. Leigh, M. Levenson, D. Banks, A. Heckert, and J. Dray, *A Statistical Test Suite for Random and Pseudorandom Number Generators for Cryptographic Applications.*

Catching quantum jumps through heterodyne monitoring of a thermal drive

G. Hennin Arencibia and H. J. Carmichael
The Dodd-Walls Centre for Photonic and Quantum Technologies, Department of physics, University of Auckland, Private Bag 92019, Auckland, New Zealand
email: geraud.arencibia@auckland.ac.nz

Abstract: *The coherence of an atomic quantum jump triggered by a thermal drive is recovered by continuously monitoring the system emissions using heterodyne detection.*

Quantum jumps have been a controversial component of the Quantum Physics Theory since its foundation. They were conceived in 1913, as a consequence of the discrete energy levels introduced by Neils Bohr in his atomic model [1]. They were consolidated as being instantaneous and random and, despite their strangeness, these properties have found their place in both theoretical and experimental literature, without being replaced by any satisfactory alternative description.

It is only recently that the nature of these events has been questioned. It was reported in [5] that quantum jumps may take time, be continuous, coherent, and deterministic. The conclusion was raised after the authors managed to predict and reverse a quantum jump between two atomic levels. The experimental setup followed the lead of experiments with trapped ions [2]-[4], in which a continuously monitored strong transition is used to track the jumps affecting a so-called weak transition that is driven coherently (See Fig. 1). The results display a beautiful simplicity: the quantum jump can be described as a fixed path on the Bloch Sphere in the $|G\rangle - |D\rangle$ sub system, as shown in Fig 2.a.

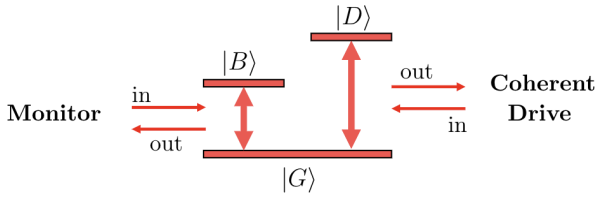

Figure 1: Sketch of the tree-level setup underlying the experiment of [5]. The monitored G-B transition tracks up-jumps on the coherently driven G-D transition.

In this talk, we aim to put the results from [5] into a broader context and develop how they can be generalised. This is done by replacing the coherent excitation by a thermal drive, which is to be continuously monitored using heterodyne detection. For fundamental reasons, this modification precludes achieving the same results as [5] (See Fig. 1), however, we show how the heterodyne current can be used to calculate the phase of the jump and therefore, allows to describe it as a deterministic path in the surface on a rotated Bloch Sphere. Different regimes and their experimental feasibility are discussed.

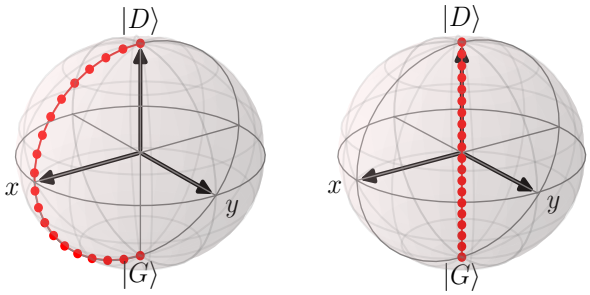

Figure 2: Representation of a quantum jump on the Bloch Sphere. On the left, the transition is represented as reported in [5], revealing the coherent nature of the excitation. On the right, the traditional representation of an incoherent atomic transition.

References

[1] N. Bohr, *Phil. Mag.* **26**, 1–25 (1913).

[2] W. Nagourney, J. Sandberg, H. Dehmelt, *Phys. Rev. Lett.* **56**, 2797–2799 (1986).

[3] T. Sauter, W. Neuhauser, R. Blatt, P. E. Toschek, *Phys. Rev. Lett.* **57**, 1696 (1986).

[4] J. C. Bergquist, R. G. Hulet, W. M. Itano, D. J. Wineland, *Phys. Rev. Lett.* **57**, 1699–1702 (1986).

[5] Z. K. Minev, S. O. Mundhada, S. Shankar, P. Reinhold, R. Gutiérrez Jáuregui, R. J. Schoelkopf, M. Mirrahimi, H. J. Carmichael, and M. H. Devoret, *Nature* **507**, 200–204 (2017).

Revisiting plasmonic sensors: a non-Hermitian perspective

Alessandro Tuniz[1,2] and Boris. T. Kuhlmey[1,2]

[1]Institute of Photonics and Optical Science (IPOS), School of Physics, The University of Sydney, NSW 2006, Australia
[2]The University of Sydney Nano Institute (Sydney Nano), The University of Sydney, NSW 2006, Australia
email: alessandro.tuniz@sydney.edu.au

***Abstract**: We evaluate the sensing properties of plasmonic waveguide sensors by calculating their resonant transmission spectra in different regions of the non-Hermitian Eigenmode space. Plasmonic cutoff wavelengths yield the best proxy for sensitivity. Directional coupling, rather than loss peaks, provide optimal detection limits.*

Surface plasmon polariton (SSP) resonant sensors have found wide-ranging applications, particularly for bio-sensing, where they allow optical detection of binding events between molecules [1]. Plasmonic structures adjacent to conventional waveguides (e.g., cylindrical fibers [2] and planar circuits [3]), provide smaller sensors where SSP can easily be coupled to via directional [4] or quasi-adiabatic [3] coupling, using connectorized sources. Such lossy, non-Hermitian systems have been identified as a platform for accessing exceptional points, with the debated promise of increased sensitivity [5]. The inset of Fig. 1(a) shows such a system in one of its canonical forms: a dielectric waveguide (blue) coated by a gold nanofilm (yellow) surrounded by an analyte (green) whose index is to be measured. The excitation and interference of the lossy hybrid dielectric-plasmonic modes leads to a transmission spectrum with a resonant dip. Its wavelength λ_R and spectral width $\delta\lambda$ change as the analyte index changes, and in turn depends on the sensing region length L [5]. Comparisons between experiment and simulation often rely on mode calculations alone [2], which fail to reproduce many subtle features, instead requiring full propagation calculations: Due to finite length interference and the role of losses, simple modal considerations do *not* provide the exact wavelength of the transmission dip observed in experiments, providing misleading sensitivity and detection limits.
Here we show, via a simple model consisting of 1D modes undergoing 2D propagation, that full transmission characteristics of plasmonic waveguide sensors can be reproduced with a simple eigenmode model [3] as long as finite propagation and resulting interferences are taken into account. We validate our results by full vector finite element (COMSOL) calculations of field propagation. Our model enables computation of the transmission spectrum, Fig.1(a), extinction ratio, resonance width, and sensitivity, as a function of all key parameters, including wavelength, interaction length, and analyte index, as summarized in Fig 1(b)-(d). We compare the device sensitivity from the resonant wavelength λ_R, which would be obtained from measurement, with the sensitivity inferred from more conventional modal analysis of such devices such as those derived from phase matching wavelength (λ_{PM}), loss-matching wavelength (λ_{LM}), plasmonic cutoff wavelength (λ_{cutoff}), and the wavelength at which the beat length is maximum (λ_B^{max}). We find that the cutoff wavelength of the uncoupled plasmonic mode is the best proxy for the sensitivity of the full (coupled) dielectric-plasmonic waveguide sensor. The lowest detection limit δn occurs in regions where directional coupling is supported, rather than where transmission dips are due to propagation losses of a single mode, yielding narrow 3-dB width small $\delta\lambda$ depending on both the analyte index and the device length, as shown in Fig.1(d). These approaches can be immediately adapted to more realistic systems formed by 2D modes undergoing 3D propagation, and would find use in non-Hermitian systems whose mode topology varies with externally tunable parameters [5].

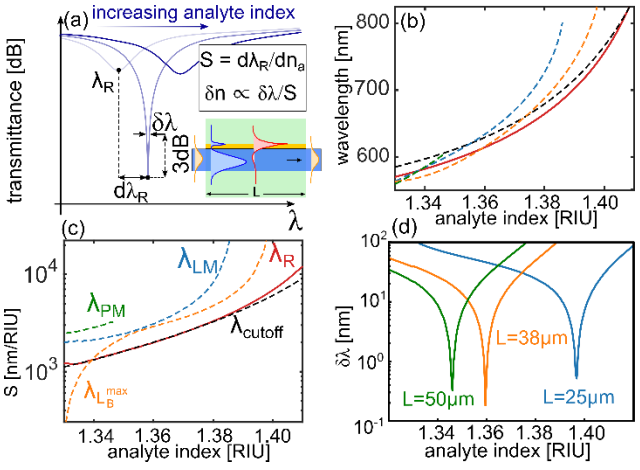

Figure 1: (a) Example transmission spectrum, geometry, and parameters. (b) Wavelength shift and (c) associated sensitivity, obtained when considering different parameters as labelled. (d) $\delta\lambda$ vs. analyte index for different lengths L of the analyte region.

References:

1. C. Caucheteur et al., Anal. Bioanal. Chem., **407**, 3883 (2105)
2.T. Wieduwilt et al., Sci. Rep. 5, 17060 (2015)
3. A. Tuniz et al., Nature Commun. **11**, 2413 (2020)
4. A. Tuniz et al., Opt. Express **24**, 7507 (2016)
5. A Tuniz et al., Phys. Rev. Lett., **123**, 213903 (2019)

Magnetic Tuning of Liquid Crystal Metasurfaces

Y. Izdebskaya, Z. Yang, M. Liu, D.-Y. Choi, A. Komar, D. Neshev, and I. Shadrivov

ARC Centre of Excellence for Transformative Meta-Optical Systems (TMOS), Research School of Physics, Australia National University, Acton, ACT 2601, Australia
email: yana.izdebskaya@anu.edu.au

***Abstract**: We demonstrate active magnetic tuning of the spectral response of a Mie-resonant dielectric metasurfaces infiltrated with liquid crystals. Our results open important opportunities for a new family of tunable devices without the usual limitations of other tuning methods.*

All-dielectric metasurfaces hold an exceptional potential for the next generation tunable optical systems that are promising for applications in sensing, ranging and imaging. Infiltration of dielectric metasurfaces with nematic liquid crystals (NLCs) is an especially attractive direction for achieving tunability, mainly because of the large tunability that can be achieved. To date, tuning of NLC-integrated metasurfaces have been demonstrated using temperature [1] or voltage [2], or their combination. While all these methods achieve tuning of an optical response of metasurfaces, they have several drawbacks, including limited control of NLC orientation as well as fixed boundary conditions induced by molecular pre-alignment that cannot be changed.

Here, we demonstrate a novel dynamic control of the spectral response of Mie-resonant all-dielectric metasurfaces using external magnetic field that induces reorientation of the anisotropic NLC. This approach has significant advantages over other methods, since it does not require pre-alignment or electrodes, and there is no limitation on the metasurface geometry and thickness of LC cells.

In our work, we use an all-dielectric Huygens' metasurface composed of zigzag arrays of silicon elliptical-cylinders that working at the near-infrared wavelengths around 1500 nm [see inset in Fig.1] [3]. The fabricated metasurface is then covered by the NLC (6CHBT) [see Fig.1]. The thickness of the LC cell was up to 1 mm and it was chosen to minimize the influence of Fabry-Perot oscillations within the optical cavity formed by the LC cell on the optical spectra of the metasurface.

In order to control the orientation of the NLC molecules, we use a magnetic field **B** [4]. We utilize a block permanent neodymium magnet (24mm x 24mm x 10mm) mounted on a three-dimensional mechanical stage and place it at a distance of 4 mm from the metasurface. Considering that the magnet size is relatively large in comparison with the distance between the magnet and the metasurface, the magnetic field across the sample can be assumed uniform.

Next, using a white-light spectroscopy setup, we measured the linear-optical transmittance spectra of the metasurface integrated into the LC cell. The active magnetic tuning of the metasurface for *x*-polarized incident beam is shown in Fig. 1. When the magnetic field **B** is applied parallel to *x*, we observe two resonances at wavelengths $\lambda_1 \approx 1.53$ μm and $\lambda_2 \approx 1.57$ μm [Fig.1 (a)]. When, the magnetic field is applied parallel to *y* [Fig.1 (b)], the resonances of move closer towards each other and finally, we clearly observe one resonance at $\lambda_3 \approx 1.55$ μm.

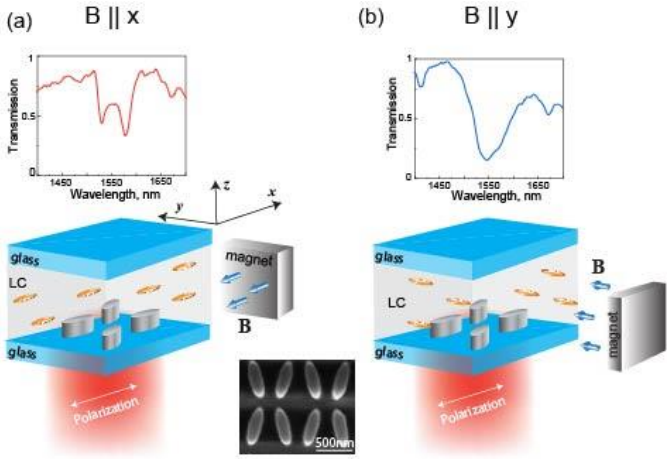

Figure 1: Magnetic tuning of Mie-resonant silicon metasurface integrated into the NLC cell for the cases when B||x (a) and B||y (b).

In summary, we demonstrate a novel dynamic control of the spectral response of dielectric metasurfaces using external magnetic field that induces reorientation of the anisotropic NLCs. Our results entail a new approach to the tuning of dielectric metasurfaces with no pre-alignment or electrodes required.

References:

1. J. Sautter, et al., *ACS nano* **9**, 4308 (2015).
2. A. Komar, et al., *Appl. Phys. Lett.* **110**, 071109 (2017).
3. M. Liu and D.Y. Choi, *Nano Lett.* **18**, 8062 (2018).
4. Y. Izdebskaya, et al., *Nat. Commun.* **8**, 1 (2017).

Coupling spin defects in a layered material to nanoscale plasmonic cavities

Ritika Ritika[1,2], Noah Mendelson[1], Mehran Kianinia[1,2], John Scott[1,2], Sejeong Kim[3], Johannes E. Fröch[1], Licheng Xiao[4, 5], Seyed Sepehr Mohajerani[4, 5], Stefan Strauf[4, 5], Igor Aharonovich[1,2*] and Zai-Quan Xu[1*]

[1]*School of Mathematical and Physical Sciences, University of Technology Sydney, Ultimo, New South Wales 2007, Australia*
[2]*ARC Centre of Excellence for Transformative Meta-Optical Systems (TMOS), University of Technology Sydney, Ultimo, New South Wales 2007, Australia*
[3]*Department of Electrical and Electronic Engineering, University of Melbourne, Victoria 3010, Australia*
[4]*Department of Physics, Stevens Institute of Technology, Hoboken, New Jersey 07030, USA*
[5]*Center for Quantum Science and Engineering, Stevens Institute of Technology, Hoboken, New Jersey 07030, USA*
E-mail: igor.aharonovich@uts.edu.au and zaiquan.xu@uts.edu.au.

***Abstract**: Spin defects in hexagonal boron nitride (hBN) are emerging candidates for quantum sensing. However, the VB suffers from low quantum efficiency and as a result exhibits weak photoluminescence. In this work, we demonstrate a scalable approach to dramatically enhance the VB emission by coupling to a plasmonic gap cavity. The plasmonic cavity is composed of a flat gold surface and a silver cube, with few-layer hBN flakes positioned in between. Employing these plasmonic cavities, we extracted a PL enhancement of 265, a maximum Purcell factor of 500 and a corresponding 2-fold enhancement in optically detected magnetic resonance (ODMR) contrast. The work will be pivotal to progress in quantum sensing using 2D materials, and realisation of nanophotonic devices with spin defects in hBN.*

Hexagonal boron nitride (hBN) has recently emerged as an attractive layered material for nano-photonics. Some of its unique features include strong confinement of phonon polaritons and a wide bandgap that facilitates a range of deep fluorescent defects that act as single photon emitters. The negatively charged boron vacancy (VB^-) is of particular interest because of its recently discovered spin properties.

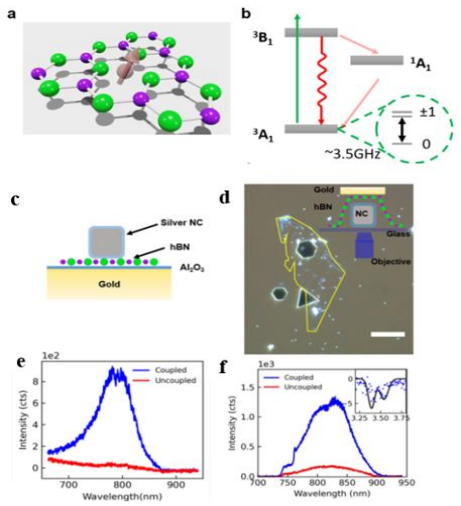

Figure 1. (a) 3D illustration of the boron vacancy (VB) in hBN, with boron and nitrogen presented as purple and green spheres, respectively. (b) Level structure of the VB^-. (c) A side-view of the conventional gap plasmonic sample structure used. (d) Dark field optical image of the fabricate hBN in gap plasmonic structures. The hBN flake is transferred onto a glass cover slip and outlined in yellow. The black triangle and hexagons are the ultra-flat gold crystals. The white dots are the silver nano-cubes. Inset: a side-view of the inverted sample structure used.

A schematic of a VB^- defect in hBN is shown in Fig1a. It has a triplet ground state (Fig.1b), and a microwave field can be used to promote an electron in the m_s= 0 state to the m_s= +/- 1 states. An electron excited from the m_s= +/- 1 spin states can decay non-radiatively from the $^3B^1$ excited state via the $^1A_1$ metastable state, causing a significant reduction in PL intensity. Hence, Zeeman splitting of the triplet ground state, achieved using an applied magnetic field, leads to a dependence in PL intensity on microwave frequency (ODMR contrast). A limitation of VB^- defects is a low brightness that originates from a high intrinsic non-radiative decay rate. Quantum spin system of VB^- can be controlled and read out optically by ODMR and holds great potential for real-world applications. Comprehensive studies were performed to compare the emission from uncoupled (as-fabricated) VB^- ensembles to those integrated in gap cavities. A side view of the sample is presented in Fig 3c, PL spectra from structure is plotted in Fig 3e (coupled: blue) and compared with a spectrum from the uncoupled VB^- emission (red) taken from the same flake. The peak height is ~17 times greater when the VB - ensemble is coupled to the cavity. A schematic illustration of the sample structure is shown as an inset in Fig 3d with dark-field optical microscope image of the sample. PL spectra recorded from the uncoupled (red) and coupled (blue) VB - ensembles are shown in Fig 3f. The peak height is enhanced by ~7 times while the peak position remains nearly identical.

References:

1. Luo, Y., Shepard, G.D., Ardelean, J.V., Rhodes, D.A., Kim, B., Barmak, K., Hone, J.C. and Strauf, S., 2018. Deterministic coupling of site-controlled quantum emitters in monolayer WSe 2 to plasmonic nanocavities. *Nature nanotechnology*, *13*(12), pp.1137-1142.
2. Reimers, J.R., Shen, J., Kianinia, M., Bradac, C., Aharonovich, I., Ford, M.J. and Piecuch, P., 2020. Photoluminescence, photophysics, and photochemistry of the V B− defect in hexagonal boron nitride. *Physical Review B*, *102*(14), p.144105.

Classical ghost phase imaging using optical metasurfaces

S. B. Sulejman, L. Wesemann and A. Roberts

ARC Centre of Excellence for Transformative Meta-Optical Systems, School of Physics, The University of Melbourne, Victoria 3010, Australia
email: ssulejman@student.unimelb.edu.au

***Abstract**: Ghost Imaging is a novel technique made possible by statistical correlations in electromagnetic fields and single-pixel detection. The power of this modality permits imaging at wavelengths ordinarily inaccessible to silicon cameras and the transfer of complexity from detection to illumination. As with conventional cameras, the method exhibits no inherent sensitivity to properties of the imaged object beyond its amplitude information. Here we present a novel configuration incorporating an optical metasurface that can be used in conjunction with ghost imaging to permit visualisation of phase variations in an optical field. We anticipate applications including biomedical imaging of unstained cells and wavefront sensing in various regions of the spectrum.*

Ghost Imaging (GI) is an indirect technique for constructing images of an object without physically accessing its image plane, using a detector that lacks spatial resolution [1]. The process involves sequentially illuminating the object with an ensemble of N spatially incoherent light patterns that span the image space, and collecting all transmitted (or reflected) light with a single-pixel detector, or *bucket detector* (BD) [2]. A classical *ghost image* is obtained via the second-order spatial correlation function between the single-pixel measurement and its corresponding illumination pattern [3]

$$\Gamma_{\mathrm{br}}^{(2)}(x,y) \equiv \langle \mathcal{B} \cdot I_r(x,y) \rangle = \frac{1}{N}\sum_{k=1}^{N} \mathcal{B}^{(k)} I_r^{(k)}(x,y) \quad (1)$$

where $I_r(x,y)$ is the intensity distribution in the input plane of the object, or the *reference plane; and* $\mathcal{B}$ is the integrated intensity distribution in the input plane of the BD, or the *bucket signal*, given by

$$\mathcal{B} \equiv \int_{\mathcal{A}_b} dxdy I_b(x,y) \approx \int_{-\infty}^{\infty} dxdy I_b(x,y)\,. \quad (2)$$

Since Eq. (1) involves only intensities and quantities derived thereof, the ghost image is a phase-insensitive reconstruction of the object. This motivates the introduction of other optical elements, in this case optical metasurfaces, into the GI configuration to capture phase information.

Wesemann *et al.* (2021) [4] demonstrated a resonant waveguide grating that converted phase information contained in an optical field into intensity variations that can be readily captured using a conventional camera. The structure, shown in Fig. 1, is tailored such that it exhibits an approximately linear optical transfer function when tilted by a few degrees. This is a consequence of the excitation of guided modes in a thin high refractive index layer. This means that the spatial frequency content of an incident field is filtered, resulting in a modified output field. More specifically, a linear transfer function corresponds to spatial differentiation of the input field, converting phase gradients into amplitude terms in Eq. (2).

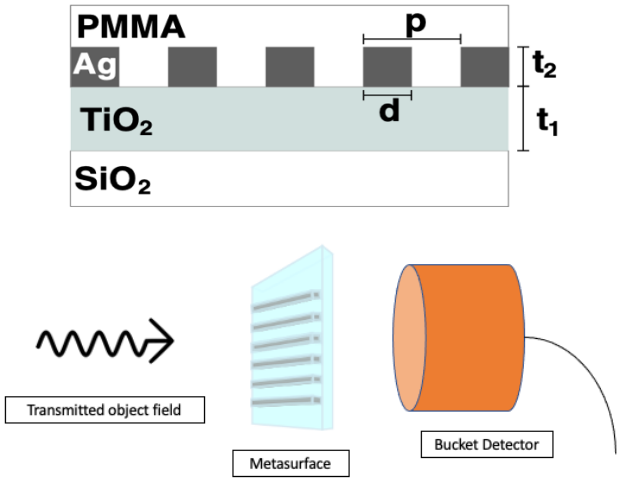

Fig. 1: NEC metasurface design [4] (top), and depiction of an angle-sensitive pixel (bottom).

Inserting this structure into the input plane of the BD effectively creates an angle-sensitive pixel. It enhances performance to discriminate spatial frequencies and detects phase variations in the incident field. As a result, we can perform Ghost Phase Imaging to reveal local refractive index or thickness variations in an object. It offers the potential to enhance biomedical imaging and diagnostics, particularly at wavelengths that cannot be accessed using conventional techniques.

References:

1. H.-C. Liu *et al.*, *Science Advances* **3**, e1701477 (2017).
2. J. H. Shapiro, *Phys. Rev. A* **78**, 061802 (2008).
3. T. Kuusela, *Am. J. of Phys.*, **87**, 846 (2019).
4. L. Wesemann *et al.*, *Light: Sci. & Appl.* **10**, 98 (2021).

Morphology of femtosecond laser inscribed point-by-point Bragg gratings

S. Bhardwaj, T. T. Fernandez, S. Gross, M. J. Withford and M. J. Steel

Macquarie University, Sydney, NSW 2109, Australia

email: saurabh.bhardwaj@students.mq.edu.au

***Abstract**: The morphology of femtosecond laser-written point-by-point gratings was investigated with several characterization techniques. Comparison of results from different characterization techniques suggests the creation of an increased refractive index region around the center of the void is due to contribution from both densification and the formation of highly polarizable non-bridging oxygen bonds.*

The unique morphology of femtosecond laser-inscribed point-by-point (PbP) gratings provides useful properties such as strong coupling to cladding modes [1] and high thermal stability. Knowledge of the grating morphology and index change is important to engineer mode coupling in few-mode fibre and to design gratings with optimum functionality. Here we discuss the underlying structural changes of PbP gratings inscribed in fused silica fiber with the help of Raman and photo-luminescence studies [2] and provide a directly measured refractive index profile with micro-reflectivity measurements.

Second order PbP gratings at 1550 nm with a period of 1.06 μm were inscribed inside OFS two-mode graded index fiber using an 800 nm femtosecond laser emitting 120 fs long pulses at 100 Hz repetition rate with pulse energy of 210 nJ. To expose and characterize the buried PbP gratings, the fibre was polished (at a shallow angle) with colloidal silica. A back-scattered electron (BSE) image of the polished fibre core and the PbP grating planes is shown in Fig. 1(a). More material has been removed by the polishing on the left side of the image than on the right and the brightness is indicative of density. Individual grating elements consist of an array of voids (dark spheroids) along the confocal direction (*z* axis). The first visible structure from the left (marked 4 in Fig. 1(a)) and the visible brighter regions in between the voids confirm the existence of a densified shell region encapsulating each discrete void.

A map of refractive index (spatially averaged by the 0.6 μm resolution) is shown in Fig. 1(b). The index increase of the positive index shell reaches as high as 0.039 in the region around the void of the grating element 8. Next, to map the structural changes Raman spectra were recorded confocally using 532 nm excitation. A map of the Raman D_2 (605 cm^{-1}) peak intensity (Fig. 1(c)) spatially overlapped with the BSE image and suggests the D_2 band increase in the shell regions. The D_2 band increase indicates densification and hence an increase in the refractive index.

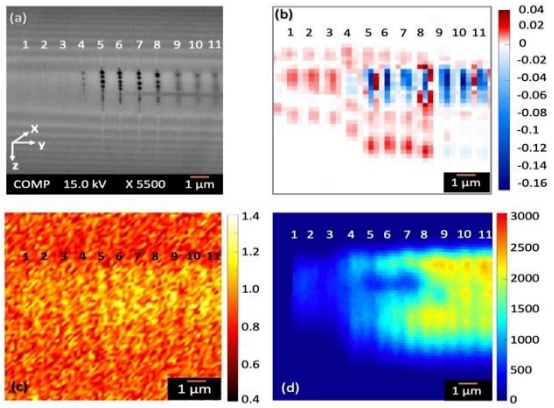

Figure 1: PbP gratings (a) Backscattered electron image (b) Refractive index profile (c) D2 peak intensity map and (d) PL spatial map at 653 nm indicating NBOHC distribution (1-11 represent individual grating elements).

Using mass conservation and the Lorenz-Lorentz model [3] we estimate a density-induced index change of 0.0073 in the region surrounding the void. This is a relatively small fraction of the total measured index change of 0.0390, suggesting an additional form of material modification must be present to account for the remaining 0.032 index change. This additional mechanism is associated with the polarizability of the non-bridging oxygen hole center (NBOHC) in the lattice. The presence of NBOHC is confirmed with photo-luminescence (PL). PL mapping was carried out confocally using a 633 nm excitation wavelength. The observed PL (Fig. 1(d)) was broad and centered at 653 nm which is assigned to the NBOHC. The maximum PL intensities were found at the positive index regions.

From this analysis we conclude that the positive index change is dominated by non-bridging oxygen polarizability, with the previously recognized density effects taking a secondary role.

References:

1. J. U. Thomas et al., *Opt. Express* **20**, 21434 (2012).
2. K. Mishchik et al., *J. Appl. Phys.* **114**, 133502 (2013).
3. S. Juodkazis et al., *Appl. Phys. Lett.* **114**, 201909(2006).

GaAsSb nanowire array based filter-free wavelength-selective photodetectors

Z.Y. Li[1], S. Trendafilov[2], F. Zhang[1,3], M. S. Allen[2], J. W. Allen[2], S. U. Dev[2], W. Pan[4], Y. Yu[1], Q. Gao[1], X. Yuan[5], I. Yang[1,6], Y. Zhu[1,3], A. Bhat[1,3], S. X. Peng[1], W. Lei[4], H. H. Tan[1,3], C. Jagadish[1,3], and L. Fu[1,3]

[1]*Department of Electronic Materials Engineering, Research School of Physics, The Australian National University, Canberra, ACT 2601, Australia*
[2]*Air Force Research Laboratory, Munitions Directorate, Eglin AFB, FL 32542, USA*
[3]*Australian Research Council Centre of Excellence for Transformative Meta-Optical Systems, Department of Electronic Materials Engineering, Research School of Physics, The Australian National University, Canberra, ACT 2601, Australia*
[4]*Department of Electrical, Electronic and Computer Engineering, The University of Western Australia, 35 Stirling Highway, Perth, WA 6009, Australia*
[5]*Hunan Key Laboratory of Nanophotonics and Devices, School of Physics and Electronics, Central South University, 932 South Lushan Road, Changsha, Hunan 410083, P. R. China*
[6]*Advanced LED Development Group, Device Solutions, Samsung Electronics Co. Ltd., Yongin-si, Gyeonggi-do 17113, Republic of Korea*
email: ziyuan.li@anu.edu.au; lan.fu@anu.edu.au

***Abstract**: In this work, we demonstrate room-temperature high-performance wavelength-selective photodetectors based on GaAsSb nanowire arrays grown by metalorganic vapor phase epitaxy, providing broadband photodetection covering both visible and near-infrared ranges without using any optical filters. They are promising candidates for the development of future highly compact, filter-free multispectral imagers that have important applications in biological imaging, face recognition and remote sensing.*

III-V semiconductors have attracted intensive attentions as ideal materials for photodetector applications due to their direct and tunable bandgap, as well as excellent carrier transport properties. In particular, III-V ternary semiconductor nanowires (NWs) such as GaAsSb NWs have been demonstrated as high-performance broadband infrared photodetectors at room temperature, [1, 2] with a wide photodetection range extending up to 1700 nm (GaSb). [3] Moreover, they present tunable spectral response at selective wavelengths originating from the strong and tunable resonance modes that are supported in the GaAsSb array NWs due to their nanoscale size and one-dimensional geometry.

Therefore, in this work, we synthesized ordered GaAsSb NW arrays on a (111)A-oriented GaAs substrate by employing a pre-patterned SiO_2 mask to define the gold seed particles' size and position as well as to facilitate NW growth via vapor-liquid-solid mechanism along the [111]A direction. Through such growth control to ensure uniform diameter, length, and ordered position, we demonstrate multi-pixel GaAsSb NW array photodetectors with broad photoresponse with tunable peak wavelength ranging from visible to near infrared (i.e., 470 to 828 nm) by engineering the NW diameter from 54 to 129 nm, as shown in Figure 1. A high responsivity and detectivity (up to 44.9 A/W and 1.2×10^{12} cm$\sqrt{\text{Hz}}$/W @ 1 V, respectively) have also been obtained, indicating a high conductivity gain in the GaAsSb NWs. We further realize high-resolution RGB color imaging by applying a GaAsSb NW array based single pixel imager, [4] indicating their potential for next-generation high performance and miniaturized multispectral photodetection systems.

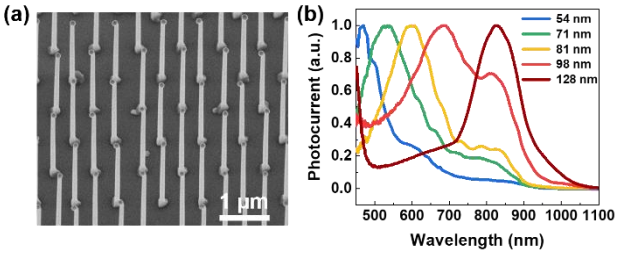

Figure 1: (a) Scanning electron microscopy image of a GaAsSb NW array with NW tip diameter of 81 nm and pitch of 800 nm. (b) Photocurrent spectra of multi-pixel GaAsSb NW array photodetectors with NW tip diameter ranging from 54 to 128 nm.

Acknowledgments:

The authors would like to acknowledge the financial support from the Air Force Office of Scientific Research and the Australian Research Council, and facility support from the Australian National Fabrication Facility, ACT node and the National Computational Infrastructure.

References:

1. Z. Li et al, *Nanotechnology* **26**, 445202 (2015).
2. Z. Li et al, *Nanotechnology* **31**, 244002 (2020).
3. J. Sun et al, *Nano Res.* (2021).
4. W. Pan et al, *Nano Res.* (2021).

Independent absorption and extrinsic scatter measurements in low loss glasses

S.K. Muusse[1,2], S.W.S. Ng[1,2], E.P. Schartner[1,3], A.K.L. Ng[1,3], H.T. Cao[1,2], C. Ingram[1,2], H. Ebendorff-Heidepriem[1,3], A. Hemming[5] and P.J. Veitch[1,2]

[1]*School of Physical Sciences, The University of Adelaide, SA 5005, Australia*
[2] *ARC Centre of Excellence for Gravitational Wave Discovery, The University of Adelaide, SA 5005, Australia*
[3]*Institute for Photonics and Advanced Sensing, The University of Adelaide, SA 5005, Australia*
[4]*Commonwealth Scientific and Industrial Research Organisation, 5005, Australia*
[5]*Defence Science and Technology Group, Edinburgh SA 5111, Australia*

Abstract: *The development of new materials for ultra-low loss optical fibres requires an independent quantification of extrinsic absorption and scatter losses. We describe a photothermal technique that can measure optical absorption with 1 ppm/cm sensitivity and present the measurement of absorption in ZBLAN at 2 μm for future telecommunication networks.*

Ultra-low attenuation due to extrinsic absorption and scatter in SWIR-transparent materials is critical for a variety of high-performance optical systems, including next-generation gravitational wave detectors and long-haul optical fibre communication systems.

ZBLAN glass is predicted to have an intrinsic loss at 2 μm as low as 0.001 dB/km (2.3 ppb/cm), which is about three orders of magnitude less than that of fused silica at 1.5 μm [1]. However, this ultra-low level of loss has not been demonstrated due to excess extrinsic absorption and scatter.

This scatter in ZBLAN is due to crystallites formed during manufacture and fibre drawing. These crystals are formed by convection currents in the molten glass during cooling. To prevent this crystal formation and reduce scatter loss, ZBLAN fibres are currently being fabricated in microgravity aboard the international space station [2].

Achieving the ultra-low loss in ZBLAN glass requires a detailed understanding of crystal formation. However, this relies on the rapid and independent quantification of absorption and scattering losses.

We report the development of a differential photo-thermal technique that is sensitive to the optical absorption only. The scatter loss can then be inferred from a measurement of total loss.

To quantify absorption a continuous-wave laser beam is transmitted through a ZBLAN fibre preform. The resulting temperature increase is probed using an ultra-sensitive differential Hartmann wavefront sensor with a low power probe beam [3]. The absorption coefficient is determined by comparing the observed wavefront change in the probe wavefront with that predicted by a finite-element model (FEM). This includes both the thermo-optic effect within the bulk and thermo-elastic distortion of the entrance and exit faces. An off-axis probe beam is used to enable separation of surface and bulk absorption, and to exclude the effect of absorption in other components.

For an initial test, we used a 7.4W heating beam at 2 μm and a 23 mm thick preform. The resulting wavefront change is shown in Figure 1. Comparison with the FEM yields an absorption coefficient of 82 ± 1 ppm/cm. The accuracy of this value is determined primarily by the accuracy of the power meter used to measure the incident power.

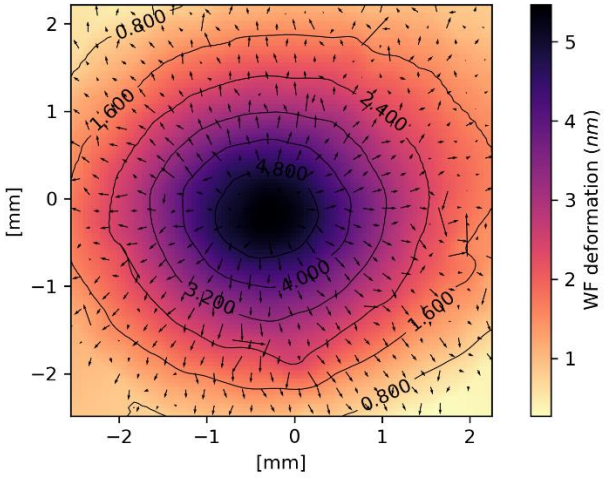

Figure 1: Example of the differential wavefront deformation of the probe beam due to optical absorption at 2 μm in ZBLAN.

In this presentation we shall describe the measurement system, present latest ZBLAN absorption coefficients and discuss the development of ZBLAN glasses with reduced scatter loss.

References:

1. D.S. Tucker et al., *Proc. SPIE* **2809**, 23 (1996)
2. A. Torres et al., *J. Mater. Sci.* **49**, 7770 (2014)
3. A.F. Brooks et al., *Opt. Express* **15,** 10370 (2007)

Particle size characterisation using a multimoded fibre

Lu Peng[1,2,3*], Linh Viet Nguyen[1,2], Jiawen Li[2,3,4], Nicolas Riesen[2,5], Mengke Han[1,2,3], Heike Ebendorff-Heidepriem[1,2,3] and Stephen C. Warren-Smith[1,2,3,5]

[1]*School of Physical Sciences, The University of Adelaide, Adelaide, SA, 5005, Australia.*
[2]*Institute for Photonics and Advanced Sensing, The University of Adelaide, Adelaide, SA 5005, Australia*
[3]*Australian Research Council Centre of Excellence for Nanoscale Biophotonics, The University of Adelaide, Adelaide, SA 5005, Australia*
[4]*Adelaide Medical School, The University of Adelaide, Adelaide, SA 5005, Australia*
[5]*Future Industries Institute, University of South Australia, Mawson Lakes, SA 5095, Australia*
**E-mail: lu.peng@adelaide.edu.au*

***Abstract**: Particle size characterisation is demonstrated using machine learning analysis on the optical frequency domain reflectometry signal from a multimode exposed core microstructured fibre. This method has potential biological applications such as detecting cells.*

The detection of small particles such as biological cells, viruses and proteins, is important to life science [1]. Many techniques have been proposed to detect them based on microscopes, microfluidic chips or fibre-based approaches [2-4]. Fibre-based methods, which can be portable and achieve remote sensing, offer an ideal candidate for in-vivo studies, but demonstrations to-date either rely on bulky external optics to collect signals or fragile tapered fibres with limited sensing region. Here, for the first time, we propose a distributed sensing approach to not only detect the spatial positions of particles but also classify their size characteristics. Through machine learning analysis of optical frequency domain reflectometry (OFDR) signals from a multimode fibre, the particles' axial positions and size could be determined.

Polystyrene spheres with average diameters of 10 and 20 μm were deposited on the exposed core fibre (ECF) as sensing targets. The interface reflection from the input end of the ECF acts as the reference light to interfere with the scattering from each polystyrene sphere in a reflection detection mode. Particles' axial positions along the ECF were acquired using Fast Fourier Transform (FFT) to resolve the interferences [5]. By changing the launching conditions, different superpositions of modes are launched into the ECF, and the FFT signals from the polystyrene spheres vary due to different overlapping evanescent field interactions. The large spheres have wider FFT peaks compared with that of the small spheres. One of the reasons is that the large scattering cross-sections from large spheres can overlap and interact more with guided modes of the ECF. Another is the observation of whispering gallery modes (WGMs) resonances from spheres under some launching conditions.

While WGMs can be used to detect particle size in the specific case of spherical particles, we show here a generalisable method based on machine learning. The FFT peak associated with each particle and each mode launching condition show high variability but are difficult to interpret directly. We first visualise the FFT data using t-SNE as displayed in Fig. 1. We then apply K-means clustering, a machine learning algorithm to classify unlabelled data into known groups (two groups here), which is shown by colour in Fig. 1. The K-means clustering can correctly classify more than 95% of the particle sizes. We will present further results including supervised learning methods such as K-nearest neighbours and discuss pathways towards further generalisation.

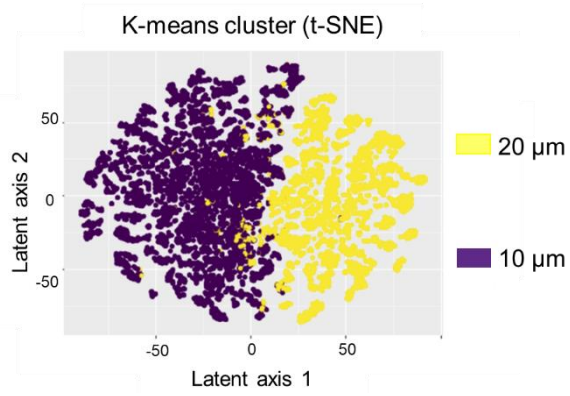

Figure 1. K-means clustering used to group particle size into two groups, visualised using t-SNE.

References:

1. H. Shen, L. J. Tauzin, R. Baiyasi, W. Wang, N. Moringo, B. Shuang, and C. F. Landes, Chem. Rev., 2017, 117, 7331.
2. R. Förster, S. Weidlich, M. Nissen, T. Wieduwilt, J. Kobelke, A. M. Goldfain, T. K. Chiang, R. F. Garmann, V. N. Manoharan, and Y. Lahini, ACS Sens., 2020, 5, 879.
3. S. Faez, Y. Lahini, S. Weidlich, R. F. Garmann, K. Wondraczek, M. Zeisberger, M. A. Schmidt, M. Orrit, and V. N. Manoharan, ACS Nano, 2015, 9, 12349.
4. X. C. Yu, B. B. Li, P. Wang, L. Tong, X. F. Jiang, Y. Li, Q. Gong, and Y. F. Xiao, Adv. Mater., 2014, 26, 7462.
5. L. Peng, J. Li, R. A. McLaughlin, H. Ebendorff-Heidepriem, and S. C. Warren-Smith, Sens. Actuator A Phys., 2020, 303, 111762.

Spectrally resolved point-spread-function engineering using scattering media

M. Mounaix[1], A. Boniface[2], B. Blochet[3], H. B. de Aguiar[2], F. Quéré[4], and S. Gigan[2]

[1]School of ITEE, University of Queensland, Brisbane, QLD 4072, Australia
[2]Laboratoire Kastler Brossel, ENS-Université PSL, CNRS, Sorbonne Université, Collège de France, 24 rue Lhomond, 75005 Paris, France
[3]Department of Electrical Engineering, California Institute of Technology, Pasadena, CA 91125, USA
[4]Université Paris-Saclay, CEA, CNRS, LIDYL, 91191, Gif-sur-Yvette, France

email: m.mounaix@uq.edu.au

***Abstract**: We show how to engineer the point-spread function of a light beam both spatially and spectrally by exploiting the inherent spatio-spectral coupling of light's properties offered by multiple scattering media.*

The ability to control both the spatial and the spectral/temporal properties of light has opened a myriad of applications, such as the control of light propagation and the ability to deliver accurate foci for multiphoton imaging. Such control is usually achieved by combining a spatial light modulator (SLM) with a diffractive element, such as a grating, that offers spatial and spectral coupling of the light's properties.

However, such approach collapses when light travels in scattering materials, such as white paint, fog or biological tissues. Indeed, when a coherent ultrashort pulse of light propagates through a complex medium, its optical wavefront gets spatially distorted and forms a speckle pattern, which is a very complex interference pattern. This speckle also depends on the incident wavelength. Although this additional spatio-spectral coupling induced by the scattering medium itself seems detrimental, it is a linear and deterministic process, and thus controllable using an SLM. Over the past decade, different techniques have been proposed to control the spatio-spectral scattered field [1] among which measuring the multi-spectral transmission matrix (MSTM) of the scattering material [2].

In this work, we demonstrate how to perform spatio-spectral point-spread-function (PSF) engineering, by harnessing the spatio-spectral coupling offered by the scattering material. We first measure the MSTM of a thick scattering sample (ZnO), which relates the output spatio-spectral speckle field to the input field controlled by the SLM. Prior to exploiting the MSTM for spatio-spectral focusing of the light through the medium (by phase conjugating each spectral transmission matrix as in [2]), we present an operator built from the MSTM that enables to engineer the multi-spectral PSF of the transmitted light in Figure 1a. We compute the spatial Fourier transform of the measured output fields ((k_x,k_y) are the spatial frequencies), for all the input modes and all the spectral components. We then apply a numerical filter with a spectrally dependent mask M (k_x,k_y,λ), with λ the wavelength, where both the amplitude and the phase of the mask can be controlled. We then compute the inverse Fourier transform of the filtered MSTM: we now have a new operator MSTM^{filt} with which we can focus light through the scattering medium with any arbitrary spatio-spectral PSF.

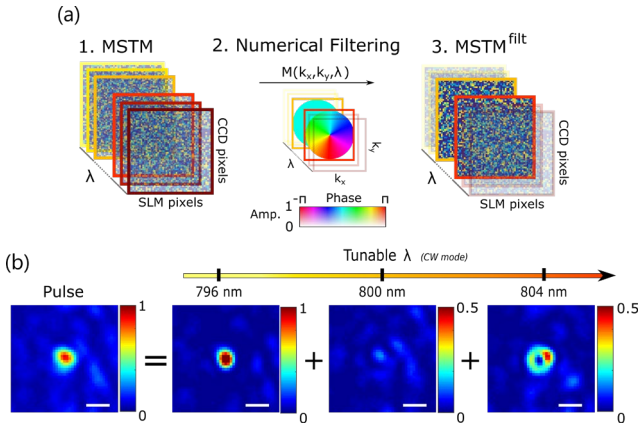

Figure 1: (a) Numerical Fourier filtering of the MSTM with a spectrally-dependent mask. (b) Experimental focusing at two spectral components with two different PSFs. Scale bars 20 μm. [3].

We demonstrate a proof-of-concept experiment in Figure 1b. We filter two transmission matrices with a flat (λ_1=796nm) and a spiral (λ_2=804nm) phase mask M. We then focus light by phase conjugating the MSTM^{filt}. This shaping enables to focus the transmitted pulse on the camera. A scan in wavelength shows a diffraction-limited focus at λ_1 a donut-like shape at λ_2, and a speckle field for the other uncontrolled wavelengths, in agreement with the masks applied in the spatial Fourier space of the corresponding matrices. Our approach could benefit different fields that require an accurate control of the PSF, such as microscopy and coherent control.

References:

1. S. Rotter and S.Gigan *Rev. Mod. Phys.* **89**, 015005 (2017)
2. M. Mounaix et al. *Phys. Rev. Lett.* **116**, 253901 (2016)
3. A. Boniface et al. *Opt. Exp.* **29**, 8985 (2021)

Heterodyne Brillouin microscopy for biomechanical imaging

Michael A. Taylor, Amanda W. Kijas, Zhao Wang, Jan Lauko and Alan E. Rowan

Australian Institute for Bioengineering and Nanotechnology, The University of Queensland, Australia
email: m.taylor@sbs.uq.edu.au

***Abstract**: Microscopic variations in material stiffness play an important role in cellular scale biomechanics, but are difficult to measure in a natural 3D environment. Brillouin microscopy is a promising technology for such applications which provides non-contact label-free measurement of mechanical properties at microscopic resolution. Here we develop heterodyne detection to measure Brillouin scattering signals in a confocal microscope setup, providing sensitive detection with excellent frequency resolution and robust operation in the presence of stray light. The functionality of the microscope is characterized and validated, and the imaging capability demonstrated by imaging structure within both a fibrin fiber network and live cells.*

Brillouin microscopy is a new approach for biomechanical imaging which allows noncontact elastography by characterizing light which has scattered from sound waves in the sample. Brillouin microscopy provides optical resolution, non-contact sampling of viscoelasticity, and allows mechanical imaging in otherwise inaccessible regions such as the interior of cells or within the cornea of intact eyes [1,2]. Since sound is always propagating, light which scatters from it has its frequency shifted due to the Doppler effect. Measuring the frequency shift of the scattered light allows measurement of the local speed of sound in the material, thereby achieving diffraction limited 3D elastography.

The two approaches which have been previously used are tandem Fabry-Perot interferometers (TFPI), which act as a narrow band-pass filter that is scanned over the spectral range, and virtually imaged phase array (VIPA) spectrometers which act as a dispersive element separating the range of frequencies onto different pixels of a camera [3]. TFPI offer superior spectral resolution and isolation of stray background light, while VIPA operate at far higher speed and require less total light flux due to the parallel simultaneous measurement of all frequencies [3].

We have constructed a Brillouin microscope that instead uses heterodyne detection to provide far greater frequency resolution, and insensitivity to stray light. The microscope has been used for some proof-of-principle biological experiments. These include measurement of the local Brillouin shifts within filaments of a fibrin gel, and subcellular imaging of a live cell.

The characteristics of Brillouin detection will be explained, and the relative advantages of different detection methods.

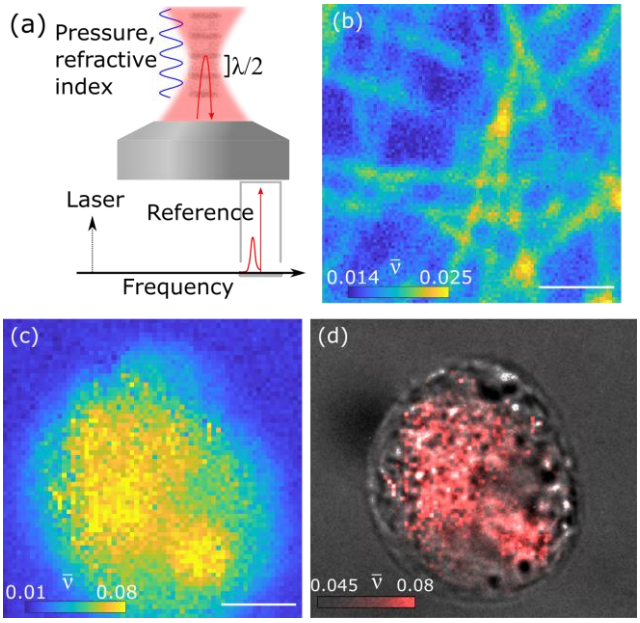

Figure 1: (a) Concept. Acoustic vibrations cause a periodic modulation of pressure and refractive index, which causes Brillouin scattering of light when its period is half the optical wavelength. The scattered frequency is determined by the longitudinal modulus, providing non-contact mechanical information. Heterodyne detection measures the beat between a reference and the Brillouin scattered light. (b) Spatially mapped Brillouin shift for a fibrin hydrogel, for which we can resolve the individual fibers. (c, d) Brillouin shift for a single live HeLa cell. Scale bars 5 μm.

References:

1. G. Scarcelli *et al.*, *Nat. Methods* **12**, 1132. (2015).
2. G. Antonacci *et al.*, *Biophys. Rev.* **12**, 615 (2020).
3. Z. Coker *et al.*, *Opt Express* **26**, 2400-2409 (2018).

Detection-loophole-free quantum steering with vector vortex states

D. J. Joch[1], S. Slussarenko[1], N. Tischler[1], F. Ghafari[1], L. K. Shalm[2], V. B. Verma[2], S. W. Nam[2], and G. J. Pryde[1]

[1]*Centre for Quantum Dynamics and Centre for Quantum Computation and Communication Technology, Griffith University, Brisbane, Queensland 4111, Australia.*

[2]*National Institute of Standards and Technology, 325 Broadway, Boulder, Colorado 80305, USA.*
email: g.pryde@griffith.edu.au

***Abstract**: We demonstrate a detection-loophole-free realization of the quantum steering test where a transmitted photon in encoded in a vector vortex state. Previously, inefficiencies in generating vortex entanglement—or converting between encodings–has limited detection-loophole free tests to polarization or which-way entanglement only. Here we overcome this limitation, and also demonstrate the robustness of the vector vortex encoding to errors in the angular orientation of the receiver.*

Quantum nonlocality is a resource that enables secure quantum information tasks, such as device-independent-type (DI-type) quantum communication and certified randomness. Rigorous verification of nonlocality requires the closure of loopholes to minimize the reliance on assumptions that may not hold or permit eavesdroppers to spoof nonlocality. Strong-loophole-free nonlocality has been demonstrated with photons entangled in polarization but has yet to be observed using other degrees of freedom in the photonic platform. Here we show detection-loophole-free quantum (or Einstein-Podolsky-Rosen) steering [1], using a vector vortex state encoding for one qubit, formed by a combination of orbital angular momentum and polarization. Steering nonlocality is interesting for one-side device-independent protocols in situations where one party is in a secure location and another remote party is not [2]. Physical encodings other than polarization can provide unique advantages such as better noise tolerance, access to qudits, or, as in our case, rotational invariance.

The detection loophole is the most difficult to close experimentally as it requires both high photon transmission and detection efficiencies to rule out the statistics being corrupted by cheating strategies concealed as loss [3]. Most methods to encode information in degrees of freedom besides polarization are limited in state quality and efficiency, hence the loophole has yet to be closed with other photon degrees of freedom. To overcome this limitation, we achieve a total throughput and detection efficiency of ~0.39-0.48 in conversion to vortex states, transmission, and analysis, allowing us to close the detection loophole in a steering test. Our measured steering parameter shows violation of an inequality at the level of 15 standard deviations on average. Finally, we observe that that encoding in a vortex state, which is predicted to be invariant to rotations of the observer around the transmission axis, allows for violations of a steering inequality over the whole rotation range, while a rotation-sensitive polarization encoding quickly fails, as expected. This represents a key step in the ability to apply physical encodings, beyond conventional polarization qubits, to demanding DI-type protocols.

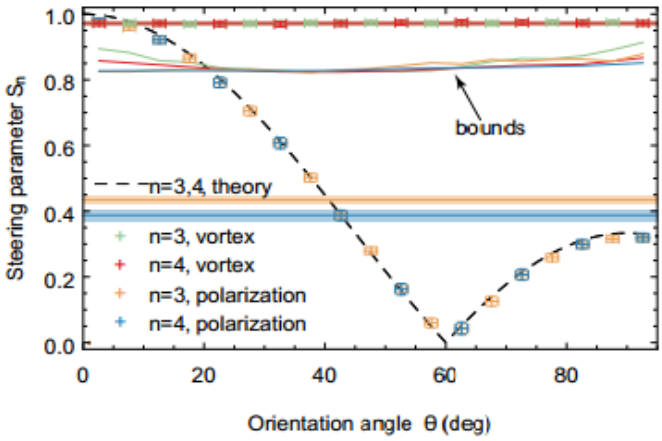

Figure 1: Demonstration of the resilience of the vortex encoding to noise in the orientation of the receiver. The orientation angle represents rotation of the receiver's measurement apparatus about the direction of propagation. With a polarization encoding, the degradation in steering correlations with angle is apparent. With a cortex encoding, the data beats the corresponding steering bound across the full angular range. [1].

References:

1. S. Slussarenko, et al., arXiv:2009.03918 (2020).

2. C. Branciard et al., Phys. Rev. A 85, 010301(2012).

3. A. J. Bennet et al., Phys. Rev. X 2, 031003 (2012).

Single-shot characterization of two-photon distinguishability with dielectric metasurfaces

Jihua Zhang, Jinyong Ma, Neuton Li, Andrey A. Sukhorukov

ARC Centre of Excellence for Transformative Meta-Optical Systems (TMOS), Research School of Physics, The Australian National University, Canberra, ACT 2601, Australia
email: jhzhanghust@gmail.com, andrey.sukhorukov@anu.edu.au

***Abstract**: We show that a static dielectric metasurface can enable single-shot characterization of the distinguishability between two photons in all degrees of freedom including time, spectrum, and polarization.*

Photons are superb quantum information carriers, due to their long propagation distance, long coherence time, room-temperature stability, easy manipulation and light-speed signal transmission. In quantum photonics, the indistinguishability between photons is the key feature absent in classical optics. Therefore, characterizing the distinguishability of photons accurately and reliably is an essential task in many quantum photonic applications.

The distinguishability of two photons, which forms the most studied quantum optical states, is typically determined through the Hong-Ou-Mandel (HOM) interference [1] by comparing the output photon correlations with different time delays. Whereas traditionally HOM is performed with bulky beam splitters, the multiphoton interference was recently demonstrated with metasurfaces containing a thin layer of subwavelength nanostructures [2,3]. Importantly, multiple transformations can be encoded in a single metasurface, allowing for parallel measurements and full characterization of quantum states. However, the potential of metasurfaces for characterization of photon distinguishability remains unexplored.

In this work, we propose a concept for characterization of two-photon distinguishability in several degrees of freedom including time, spectrum, and polarization using a specially developed dielectric metasurface, without a need for multiple measurements at different time delays. As shown in Fig. 1a, the metasurface grating is designed to interfere photons from two inputs in the three outputs. The measurements of distinct two-photon correlations between the output ports provide complete information for reconstruction of the input two-photon split state reduced density matrix, in which two independent elements quantify the photon distinguishability. By utilizing a topology optimization algorithm, we numerically designed free-form silicon metasurfaces (600nm thickness) on a sapphire substrate (Fig. 1b) that simultaneously satisfy three requirements: low sensitivity of the scheme to measurement noise, polarization independence except for a global phase, and high total transmission for all polarizations. As a result, the optimized condition number of the characterization is lower than 2 and the total transmission is over 90%, indicating a high robustness to noise and a prominent efficiency, respectively. The design parameters are suitable for nanofabrication, which is currently in progress.

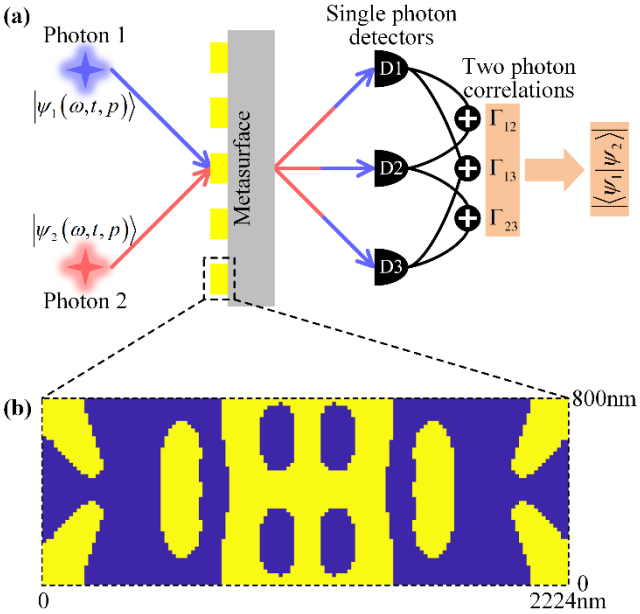

Figure 1: (a) Schematic of the metasurface-enabled single-shot characterization of two-photon distinguishability. (b) Top view of one unit cell of the designed metasurface by topology optimization. The yellow and blue areas represent silicon and air, respectively.

We anticipate that the metasurface design can be further tailored for multi-photon states and additional degrees of freedom associated with spatial modalities, providing versatile and ultracompact quantum optical elements for various applications.

References:

1. C. K. Hong, Z. Y. Ou, and L. Mandel, *Phys. Rev. Lett.* **59**, 2044 (1987).
2. K. Wang, J. Titchener, S. Kruk, L. Xu, H. Chung, M. Parry, I. Kravchenko, Y. Chen, A. Solntsev, Y. Kivshar, D. N. Neshev, A. A. Sukhorukov, *Science* **361**, 1104 (2018).
3. Q. W. Li, W. Bao, Z. Y. Nie, et al, *Nat. Photon.* **15**, 267 (2021).

Experimental quantum channel correction via heralded amplification

S. Slussarenko[1,2], M.M. Weston[1,2], L.K. Shalm[3], V.B. Verma[3], S.W. Nam[3], S. Kocsis[1,2], T.C. Ralph[4,2] and G.J. Pryde[1,2]

[1] *Centre for Quantum Dynamics, Brisbane, Queensland 4111, Australia.*
[2] *Centre for Quantum Computation and Communication Technology (Australian Research Council).*
[3] *National Institute of Standards and Technology, Boulder, Colorado 80305, USA.*
[4] *School of Mathematics and Physics, University of Queensland, Brisbane 4072, Australia.*
email: s.slussarenko@griffith.edu.au

***Abstract**: We present here a realization of an error-corrected quantum channel, where an entangled state, affected by a large amount of loss, is purified using heralded amplification and used as a resource for quantum state teleportation over the so-improved channel. We demonstrate improved performance of the error-corrected channel over direct transmission through loss, without relying on postselection.*

Quantum information science will revolutionize modern computation and communication technology. Many quantum information science applications, such as quantum internet, or distributed quantum computing and sensing, require long-distance transmission of quantum states [1]. In this process, quantum optical states are necessarily subject to photonic loss, due material loss in optical fibre, free-space diffraction, and so on. The inevitable presence of loss leads to errors in transmitted quantum information and degradation of distributed quantum entanglement. These effects prevent the realization of the most sophisticated quantum protocols such as device-independent communication or distributed quantum metrology. Development and testing of quantum optical schemes that can correct for loss-induced errors are thus of paramount importance for future quantum technologies.

The most straightforward way to negate the effect of loss is to use postselection. In experiments that rely on postselection, failed transmission events are discarded and only successful trials are taken into consideration. Postselection, however, has very limited applicability and cannot be used for example in the most advanced quantum communication schemes, such as device-independent protocols.

It is possible to reduce the effect of loss on a quantum state using heralded (or noiseless linear) amplification [2,3]. This procedure can probabilistically amplify the state affected by loss. It also provides an independent heralding signal that can be used to identify successful events without involving postselection. The downside is that heralded amplification destroys the input state in cases when it fails and thus cannot be used, by itself, to implement a genuine quantum communication channel.

What we present here is a realization of an error-corrected quantum channel, where we first prepare a purified copy of entanglement using heralded amplification. Upon success over the purification operation, the entangled state can then be used as a resource to implement quantum state teleportation over the so-improved channel. We test our channel by using it to teleport entanglement via entanglement swapping [4] through a large amount of loss and demonstrate improved performance over direct transmission, see Fig. 1, without relying on postselection.

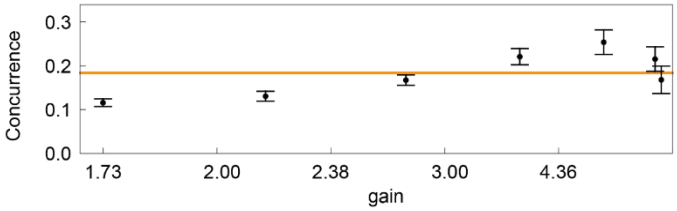

Figure 1 Amount of measured entanglement, characterized by concurrence, distributed directly through loss (line) and through the error-corrected quantum channel (dots) with different settings of the amplification gain. The amount of added loss on the channel is ≈90%

References:

1. S. Slussarenko and G. J. Pryde, *Appl. Phys. Rev.* **6**, 041303 (2019).
2. T.C. Ralph and A.P. Lund, *AIP Conference proceedings*, (ed. A. Lvovsky), 155 (2009).
3. G.Y. Xiang, T.C. Ralph, A.P. Lund, N. Walk and G.J. Pryde, *Nat. Photon.* **4**, 316 (2010).
4. J.-W. Pan, D. Bouwmeester, H. Weinfurter and A. Zeilinger, *Phys. Rev. Lett.* **80**, 3891 (1998).

Conditional quantum states of macroscopic objects at room temperature

S. Khademi[1], C. Meng[1], J. S. Bennett[1], E. Bridge[1], and W. P. Bowen[1]

[1]*Australian Research Council Centre of Excellence for Engineered Quantum Systems, School of Mathematics and Physics, University of Queensland, St Lucia, Queensland 4072, Australia*
email: s.khademi@uqconnect.edu.au

***Abstract**: Given the photocurrent produced by continuously measuring the position of a macroscopic object with a laser beam probe, one can find the conditional state of the object. We show that, in some systems, this conditional state can be 'quantum' even when the object is in touch with a room-temperature thermal bath.*

Quantum systems can be monitored continuously. For example, we can measure the position of a micro-mechanical oscillator or a micrometer-sized silica sphere by a continuous-wave (cw) laser beam. Using photodetectors, the output of the measurement mixed with different kinds of noise form a photocurrent $i(t)$. In case of linear Gaussian quantum systems, we can use special type of classical filters in order to discard the noise to a good level and find the state of the system conditioned to $i(t)$ [1].

Let's consider a micromechanical oscillator interacting with an optical cavity via radiation pressure with the time rate g. The oscillator is in thermal equilibrium with its room-temperature environment (the substrate, the air molecules, etc.) and, as a result, a thermal noise is introduced to it while its energy dissipates with the time rate Γ. The optical cavity is coupled to a cw laser beam while dissipating its energy with the time rate κ. Meanwhile, the photons enter the cavity and, after a while, leave that with the position of the oscillator imprinted on the phase of the output field [2]. We can measure the phase by doing optical homodyne detection [2].

Traditionally, it was believed that the conditional state of the mechanical oscillator in such a system is either a thermal state or a coherent state. And the latter is achievable for large mechanical resonance frequencies and large values of cooperativity – the cooperativity C equals $4g^2/(\kappa\Gamma)$ and is a comparative measure of the optomechanical interaction strength. Recently my colleagues employed a more accurate model [3] and showed that it is possible for the oscillator to find a quantum squeezed state in the system described above. Furthermore, a highly impure quantum squeezed state is achievable at small mechanical resonance frequencies and pretty small values of cooperativity. To fabricate such an optomechanical system is an ongoing task.

Our numerical calculations on a similar system with two, rather than one, mechanical oscillators interacting with the same optical cavity show that the conditional state of the oscillator can be an entangled state. An interesting room-temperature regime is the case that the two oscillators are sufficiently different – see Figure 1 where logarithmic negativity has been used as the measure of entanglement.

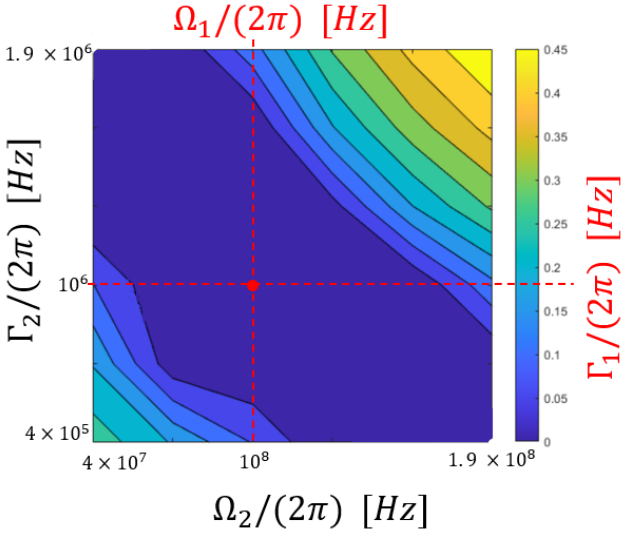

Figure 1: (colorful) While the resonance frequency Ω_1.and the mechanical decay rate Γ_1 of the first mode are fixed (the red dot), those of the second mode are swept. There is no entanglement until the two modes are sufficiently different. The entanglement has been quantified using logarithmic negativity. The cooperativities are equal ($C_1 = C_2 = 10^8$) and the thermal bath temperature is 300 K.

The conditioning technique can be used in optical tweezers too. Our preliminary calculations for the position of a silica microsphere, which is in water and trapped by high-power optical tweezers, suggest that its conditional state can be a thermal state with an average phonon number of less than fifty. This is a significant reduction compared to the unconditional state which has about 10^8 phonons.

References:

1. H. M. Wiseman, and G. J. Milburn. *Quantum measurement and control*. Cambridge university press (2009).

2. W. P. Bowen, and G. J. Milburn. *Quantum optomechanics*. CRC press (2015).

3. Meng, Chao, et al. *Physical Review Letters* 125.4 043604 (2020).

Zeeman Sub-level Raman Sideband Cooling with $^{171}Yb^{+}$

J. Scarabel[1], K. Shimizu[1], M. Ghadimi[1], M. Lobino[1,2] and E. Streed[1,3]

[1] *Centre for Quantum Dynamics, Griffith University, Nathan QLD 4111, Australia*
[2] *Queensland Micro- and Nanotechnology Centre, Griffith University, Nathan 4111, Australia*
[3] *Institute for Glycomics, Griffith University, Southport 4215, Australia*
email: j.scarabel@griffith.edu.au

***Abstract**: Raman sideband cooling with $^{171}Yb^{+}$ across the $6^2S_{1/2}$ F=1 Zeeman sub-levels and $6^2P_{1/2}$ F=0 excited state rather is observed. We infer sub-Doppler cooling from measurements of Raman spectra pre- and post-cooling. Raman laser frequencies are easier to produce than 12.6 GHz hyperfine schemes.*

Precise and deterministic quantum operations can be engineered with trapped ion qubits in their motional ground state. Trapped ions can be cooled to their motional ground state by Raman sideband cooling (RSC)[1]. Raman sideband cooling (RSC) requires two ground states with a shared excited state. In $^{171}Yb^{+}$ the 12.6 GHz split $^2S_{1/2}$ hyperfine ground states are typically used as ground states in a Raman transition[2] however having phase locked laser frequencies split by 12.6 GHz can be costly or technically difficult. Instead, the $^2S_{1/2}$ F=1 ground state Zeeman sub-levels can be used as the ground states of a Raman transition. The laser frequency splitting required can be achieved using a single continuous wave laser and acousto-optic modulators. RSC across Zeeman transitions is typically only done in even-isotope ions because of their lack of hyperfine structure.

We achieve Raman transitions across $^2S_{1/2}$ F=1, m_F=0 → m_F=+1 ($|\uparrow\rangle$) and $^2P_{1/2}$ F=0, m_F=0 excited state. Raman beams were detuned from resonance by -1 GHz and split by at most 6.5 MHz using two 180 MHz acousto-optic modulators. A continuous cooling scheme was used where a $\sigma^{\pm}$ resonant reset beam was used simultaneously with the Raman beams. An unwanted resonant Raman transition also occurs across the the $^2S_{1/2}$ F=1, m_F=0 → m_F=-1 Zeeman sub-levels and $^2P_{1/2}$ F=1, m_F=-1 excited state driving opposite sidebands to the main Raman transition. With -2.1 GHz extra detuning its Rabi rate is slower than the main transition. Cooling is currently limited by line broadening of the centre transition over the -570 kHz z-mode red sideband.

Red sidebands for the three motional modes, -[1.58, 1.33, 0.57] MHz, of the Raman spectrum were suppressed after RSC. Reduction in Rabi oscillation damping was also observed on the $\Delta n_{x,y,z}$=[0,0,0] Raman transition after RSC due to lower energy thermal states. Simultaneous fits to the spectra and Rabi oscillations give thermal states with $\bar{n}_{x,y,z}$=[29(2), 36(16), 16.2(5)] and [0.07(7), 2.0(1.2), 5.6(2)] before and after RSC respectively.

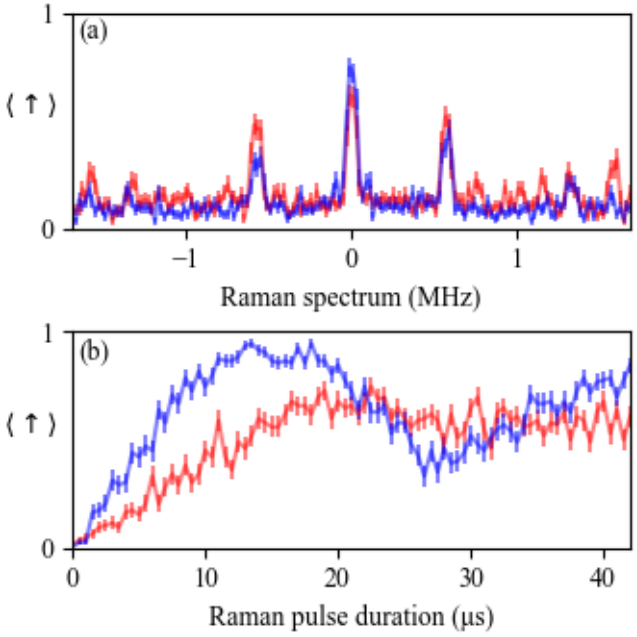

Figure 1: Comparison of the Raman motion spectrum (a) and Rabi oscillations of the center resonance(b) with 0 ms (red) and 6 ms (blue) of RSC.

References:

[1] C. Monroe *et al.*, "Resolved-sideband Raman cooling of a bound atom to the 3D zero-point energy," *Phys. Rev. Lett.*, vol. 75, no. 22, pp. 4011–4014, Nov. 1995, doi: 10.1103/PhysRevLett.75.4011.

[2] D. Hayes *et al.*, "Entanglement of Atomic Qubits Using an Optical Frequency Comb," *Phys. Rev. Lett.*, vol. 104, no. 14, p. 140501, Apr. 2010, doi: 10.1103/PhysRevLett.104.140501.

Ultrafast coherent excitation of an Ytterbium ion with single laser pulses

K. Shimizu[1], J. Scarabel[1], M. Lobino[1,2] and E. Streed[1,3]

[1]*Centre for Quantum Dynamics, Griffith University, Brisbane, 4111 QLD, Australia*
[2]*Queensland Micro and Nanotechnology Centre, Griffith University, Brisbane, QLD 4111, Australia*
[3]*Glycomics, Griffith University, Gold Coast, QLD 4222, Australia*

Email: kenji.shimizu@griffithuni.edu.au

***Abstract**: Fast entangling gate with ultrafast resonant optical pulses can significantly increase the gate speed and fidelity in trapped-ion quantum computing. One of the most important requirements for the implementation of the fast two-qubit phase gates is to realize π-pulse with a single pulse. Here we demonstrate ultrafast coherent excitation of a $^{171}Yb^{+}$ ion across the $^{2}S_{1/2}$-$^{2}P_{1/2}$ transition at 369.53 nm using 1.5 ps single near-resonant pulses with maximum population transfer of 95.0±2.9%.*

Trapped-ion qubits are a leading candidate for the realization of a full-scale quantum computer thanks to their long coherence time, great isolation from the environment, and scalability [1,2]. Although high fidelity qubit gates have been demonstrated in these platforms, these gates typically require near ground-state motional cooling to address their spectroscopically-resolved motional sidebands, necessarily limiting their gate speeds below the secular frequency of trapped ions and practical implementations to microseconds [3].

An alternative approach to overcome this speed limit is a fast entangling phase gate with ultrafast pulsed lasers [4]. This approach is based on the idea of shining a sequence of counter-propagating π-pulse pairs onto the trapped ions, which give the ions state-dependent optical momentum kicks to acquire a relative phase shift through the pulse sequence.

The aim of this research is to demonstrate the coherent excitation of $^{171}Yb^{+}$ across $^{2}S_{1/2}$-$^{2}P_{1/2}$ transition with single pulses to validate that the pulsed laser can work as π-pulses. The pulsed laser used has a repetition rate of 300.0000 MHz and its center frequency is tunable around atomic resonance of $^{171}Yb^{+}$ and measured using a home-built high-resolution spectrometer with a resolution of 3.6±2 GHz.

First, the center frequency of the pulsed laser is tuned to the atomic resonance of $^{171}Yb^{+}$ and a single $^{171}Yb^{+}$ is trapped in a quadrupole Paul trap. We then performed a single shot measurement where the ion in $^{2}S_{1/2}$ F=0 state is excited by a single pulse and the excitation probability P_{ex} was measured by a collection of ion's fluorescence by PMT. The measurements were performed with different pulse powers and we expected the result to follow the Rabi oscillation equation,

$$P_{ex} = \frac{\Omega^2}{\Omega^2 + \Delta^2} \sin^2\left(\frac{\sqrt{\Omega^2 + \Delta^2}}{2} t_{eff}\right) \qquad (1)$$

where, Δ is the frequency detuning, t_{eff} is the effective pulse width and Ω is the Rabi frequency.

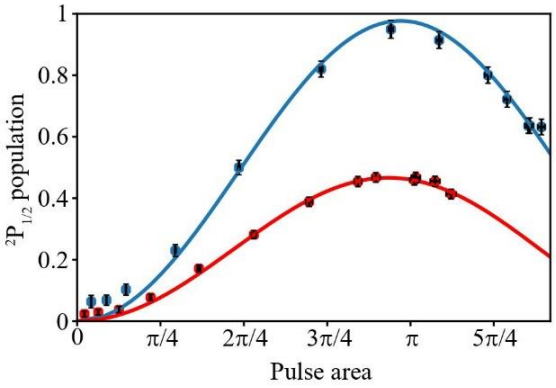

Figure 1: Excitation probability of the $^{171}Yb^{+}$ to $^{2}P_{1/2}$ state as a function of pulse area. The experimental data are shown with dots and blue and red curves are theoretical fittings with conditions of laser detuning being 33.4±6.8 GHz and 189.89±6.9 GHz, respectively.

The experimental result is shown in Fig. 1 and indicates the maximum population transfer of 95.0±2.9% was achieved when the detuning of the pulse laser is 33.4±6.8 GHz. The population transfer can be improved by minimizing the detuning of the pulsed laser more accurately. This result will pave the way to demonstrate counter-propagating π-pulse scheme, which is a fundamental requirement for the demonstration the fast entangling gate.

References:

1. C. D. Bruzewicz, et al, Applied Physics Reviews6, 021314 (2019).
2. A. Bermudez, et al, Phys. Rev. X7, 041061 (2017).
3. F. Schmidt-Kaler, et al, Nature422, 408–411(2003).
4. J. J. García-Ripoll, et al, Phys. Rev. Lett.91, 157901 (2003)

A better method for calculating filtered photon correlations

J. P. K. Ngaha[1, 2] and H. J. Carmichael[1, 2]

[1] *University of Auckland, Private Bag 92019, Auckland, New Zealand*

[2] *The Dodd-Walls Centre for Photonic and Quantum Technologies, Department of Physics, email: j.ngaha@auckland.ac.nz*

***Abstract**: Fluorescence from a resonantly driven two-level system is coupled into an array of single-mode cavities whose outputs are combined to calculate frequency filtered photon-correlations. Coupled operator moment equations form the basis of the calculations, providing a natural and efficient way to calculate second-order correlation functions.*

Fluorescence and correlation filtering is a field with a rich history and, with the advent of quantum dots, continues to be studied [1-3]. In this work we develop an efficient theoretical approach to better filter fluorescence from a driven system. To demonstrate this, we model a resonantly driven two-level system coupled as a cascaded system into an array of tunable single-mode filter cavities. This allows us to derive a set of moment equations for the two-level system and cavity mode operators, building upon the uncoupled Maxwell-Bloch equations:

$$\frac{\mathrm{d}}{\mathrm{d}t}\langle\hat{\boldsymbol{\sigma}}\rangle = \boldsymbol{M}\langle\hat{\boldsymbol{\sigma}}\rangle + \boldsymbol{b}, \tag{1}$$

where $\langle\hat{\boldsymbol{\sigma}}\rangle$ is the set of Pauli operator expectation values, $\langle\hat{\sigma}_{\pm}\rangle$ and $\langle\hat{\sigma}_z\rangle$, $\boldsymbol{M}$ is a matrix governing the evolution of the operator moments, and $\boldsymbol{b}$ is the non-homogeneous vector establishing a non-trivial steady state. The Pauli operator moments act as the progenitor source terms for all of the system's dynamics, and feed in to the higher order moments, as depicted in Fig. 1, where $\hat{a}_j$ and $\hat{a}_j^\dagger$ are the photon annihilation and creation operators for the j^{th} filter mode.

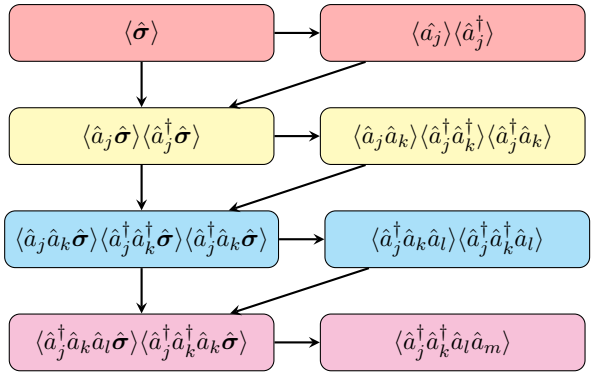

Figure 1: The operator moments have couple in a cascaded scheme, where lower-order moments can be solved independently from the higher-order moments.

In this work we will discuss how the structure of these coupled equations gives us a natural path to computing frequency filtered second-order photon-photon auto-correlations and cross-correlations. When solving the Lindblad master equation, computations could take up to 30 hours. With the moment equations, however, we cut the computation time down to less than a second. This allows us to perform much larger calculations, such as scanning for regions of anti-bunching with two multi-mode filters, as shown in Fig. 2.

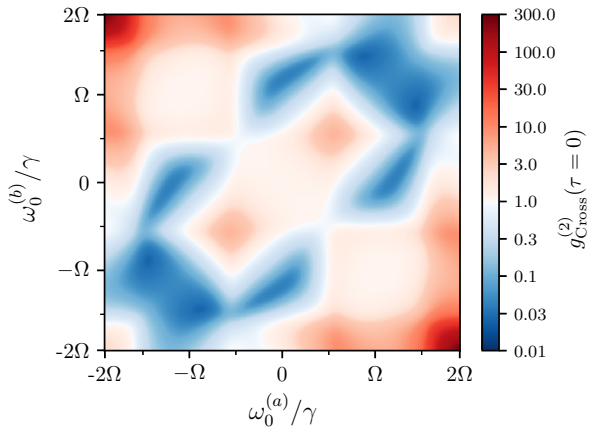

Figure 2: Initial photon correlation value for two tunable multi-mode array filters centered at the frequencies $\omega_0^{(a)}/\gamma$ and $\omega_0^{(b)}/\gamma$, where γ is the emitter linewidth.

References

[1] Aspect, A., Roger, G., Reynaud, S., Dalibard, J. & Cohen-Tannoudji, C. *Phys. Rev. Lett.* **45**, 617–620 (1980).

[2] Apanasevich, P. A., Kilin, S. Ya., & Fedorov, A. F. *J. Phys. B: At. Mol. Opt. Phys.* **18**, L55 (1985)

[3] Ulhaq, A., Weiler, S., Ulrich, M., Roßbach, R., Jetter, M. *Nature Photonics*, 238 (2012).

[4] Nieves, Y., and Muller, A. *Phys. Rev. B* **102**, 155418 (2020).

Creation and properties of spin-bearing defects in hBN

M. Kianinia[1], S.White[1], J. E. Froch[1], C. Bradac[2] and I. Aharanovich[1]

[1]University of Technology Sydney, NSW 2007, Australia
[2]Trent University, Ontario, Canada
email: Mehran.kianinia@uts.edu.au

***Abstract**: Optical control over spin properties of an electron in a point defect in solids is a promising tool for realization of quantum technologies. In this work we have demonstrated a fabrication technique for generation of negatively charged boron vacancy (V_B^-) defects in hexagonal boron nitride (hBN). We show that these centres can be engineered using a variety of focused ion beams with high resolution. The spin properties of these defects were confirmed by applying a microwave energy of 3.46 GHz equivalent to the zero field splitting of the ground state of V_B^- defects in hBN. In addition, we performed cryogenic and photoluminescence excitation spectroscopy measurement to shed light on the properties of these defects. Out result are important for advanced quantum and nanophotonic realizations involving manipulation and readout of spin-bearing defects in hBN.*

Two dimensional hexagonal boron nitride offers intriguing opportunities for advanced studies of light-matter interaction at nanoscale specifically for realization of quantum nanophotonics and scalable quantum information technologies[1,2]. Significant effort has been devoted to engineering, characterization and control of spin defects in diamond[3], silicon carbide[4] and rare earth materials[5]. The success of these defects are, arguably marked by the ability to initialize, manipulate and optically read out of individual spins with long coherence times. However, the challenge in these materials systems remains on the ability to engineer quantum emitters that besides exhibiting spin-dependent photon emission, also display high photon extraction rates and ease of integrability with other (hybrid) nanoscale systems.

In this context, two-dimensional materials specifically hexagonal boron nitride (hBN) have recently emerged as promising platform for integrated nanophotonics[6]. More recently, discovery of spin defect in hBN has burst the interest of researchers for application of this materials for spin-based sensing applications and quantum information technologies[7,8,9].

Here we have deterministically created boron-vacancy (V_B^-) defects as shown in figure 1a using ion implantation process in a commercially available focused ion beam (FIB) system[10]. Both arrays of spots and boxes were implanted. The implanted regions are clearly visible both in the optical and photoluminescence images in the latter case. The implanted areas exhibit strong photoluminescence (PL) emission under excitation of 532nm laser, centered, spectrally, at ~820 nm. The observed emission is characteristic of V_B^- centers and confirms the selective creation of V_B^-defects in hBN by focused ion patterning. To verify that the created defects are V_B^- centers, we performed optically detected magnetic resonance (ODMR) measurement, at room temperature.

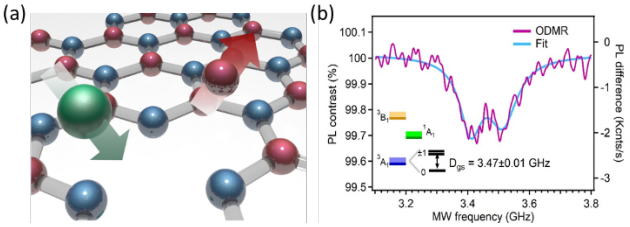

Figure 1. (a) Schematic of ion implantation process. (b). ODMR measurement from created defects in hBN.

The results are shown in Figure 1d. The V_B^- defect has a triplet (S = 1) ground state with a zero-field splitting of 3.47 GHz which is also observed in our ODMR measurement, confirming the created defects are indeed V_B^-. We measured the maximum absorption for these defects to be ~2.6 eV. Although the emission gets marginally narrower at cryogenic temperatures, we could not unequivocally identify the zero-phonon line emission energy. Our results are an important step toward the controlled engineering of spin defects in hBN. It may prove van der Waals materials as a possible platform, in addition to established ones such as diamond and silicon-carbide, for the realization of spin-based applications in quantum information and quantum sensing.

References:

1. J. H. Bodey, et al, npj Quantum Information 5 (1), 95T (2019).
2. D.D. Awschalom, et al, Nat. Photonics 12 (9), 516– 527 (2018).
3. N. Calb, et al, Science 356 (6341), 928– 932 (2017).
4. S. Whiteley, et al, Nat. Phys., 15 (5), 490– 495 (2019).
5. M. Zhong, et al, Nature, 517 (7533), 177– 180 (2015).
6. J. D. Cladwell, et al, Nat. Rev. Mater. 4 (8), 552– 567 (2019).
7. A. Gottscholl, et al, Nat. Mater. 19, 540– 545 (2020).
8. A. Gottscholl, et al, Nat Commun 12, 4480 (2021).
9. X. Gao, et al, ACS Photonics 8, 994–1000 (2021).
10. M. Kianinia, et al ACS Photonics 7, 8, 2147–2152 (2020).

Developing a Space-Based Quantum-Secure Time Transfer System

S. L. Slimani[1], B. M. Sparkes[2], F. Baynes[3], K. J. Grant[2], K. A. Mudge[2], B. A. Clare[2], A.N. Luiten[1,3] and J.Q. Quach[1]

[1]*Institute for Photonics and Advanced Sensing (IPAS) and School of Physical Sciences, The University of Adelaide, Adelaide SA 5005, Australia.*
[2]*Defence Science and Technology Group, Edinburgh SA 5111, Australia.*
[3]*QuantX Labs, Lot Fourteen, Adelaide SA 5000, Australia.*
email: sabrina.slimani@adelaide.edu.au

***Abstract**: Secure time transfer for space-based applications using current techniques is limited by security and Relativistic effects. We aim to develop a novel hybrid-quantum clock synchronisation protocol to overcome these limitations.*

Accurate clock synchronisation is vital in maintaining correct location and time data for Global Positioning System (GPS) satellites. The two current classical methods for clock synchronisation, the Einstein method and the Eddington method, are limited by Relativistic effects and the requirement that the light propagation path is the same in both directions, both of which are significant issues for space-based time transfer. An additional requirement of space-based time transfer is security from attacks. Transmission of radio signals via the GPS satellites is not secure. Jamming of the GPS signal occurs via the introduction of noise such that the signal is no longer detected by a receiver. Furthermore, the GPS signal can be spoofed whereby false time and location information is sent to a receiver.

Quantum clock synchronisation protocols have been proposed as a means of overcoming some of the limitations associated with the classical protocols in addition to some quantum protocols providing secure time transfer. In 2020, work involving the Micius satellite showed for the first time that it could be possible to use quantum time transfer protocols for secure time transfer [1].

We will present our latest results investigating one-way, two-way (i.e., distance-independent) and quantum-secure time-transfer over a free-space channel of up to 100 m. Figure 1(a) shows our current correlated photon generation system, with the corresponding coincidence peak shown in Figure 1(b). We are using this system, along with another off-the-shelf correlated photon source and a White Rabbit classical time-transfer system to develop a quantum-classical hybrid clock synchronisation protocol. We will also present our results investigating the effect of turbulence and loss across the free-space channel.

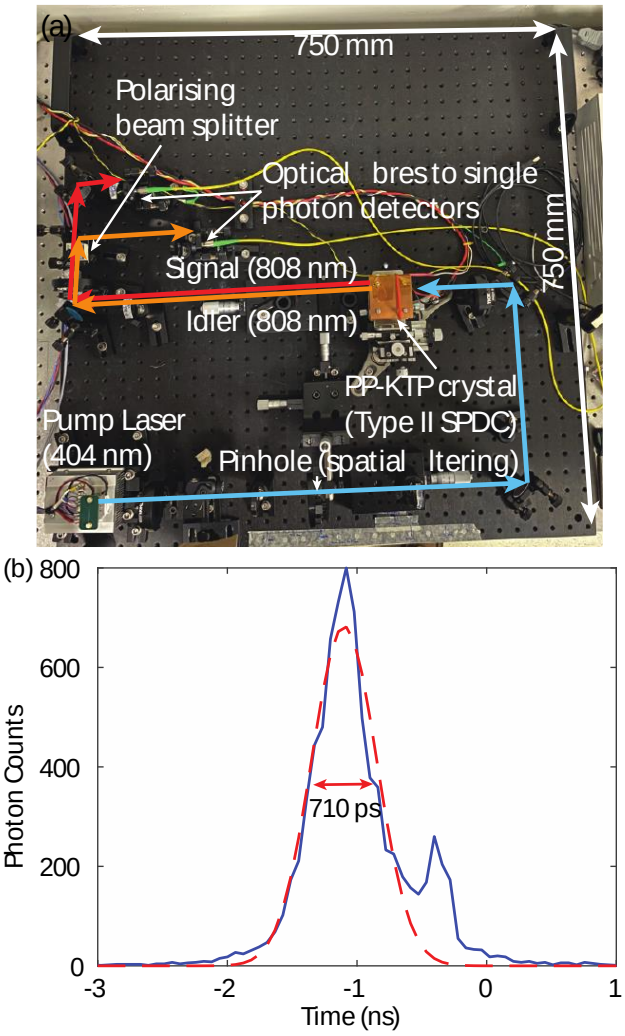

Figure 1(a) Correlated photon source system. (b) Correlation peak. Full-width-at-half-maximum of the correlation histogram represents the precision of clock synchronisation.

References:

1. H. Dai, Q. Shen, C.-Z. Wang *et al.* Nat. Phys. **16**, 8 (2020).

Towards a compact ytterbium magneto optical trap for use in precision timekeeping applications

B. R. White[1], B. M. Sparkes[2], R. F. Offer[1], A. P. Hilton[1], X. Sun[3], W. D. A. Rickard[3], C. N. Ironside[3], and A. N. Luiten[1]

[1]*Institute for Photonics and Advanced Sensing (IPAS) and School of Physical Sciences, University of Adelaide, 5005 South Australia, Australia.*
[2]*Defence Science and Technology Group, Edinburgh, 5111 South Australia, Australia.*
[3]*John De Laeter Centre, Curtin University, Bentley, 6102 Western Australia, Australia.*
email: benjamin.white@adelaide.edu.au

***Abstract**: We report on the development of a portable ytterbium atom trap system to compliment a compact ytterbium thermal beam clock.*

High performance atomic timing systems are essential components in modern technology, with applications ranging from navigation and geodesy to tests of the fundamental theories of physics [1]. Current commercial timing systems are based on microwave technology, which is now over half a century old. State-of-the-art atomic clocks (Figure 1. TOP) are based on optical transitions, but due to their size and complexity these are mostly confined the laboratory.

To realise the step change in performance that optical clocks will provide, we must reduce their size weight and power (SWaP), making them compact, portable, and robust. Motivated by this need, at the University of Adelaide we are developing a compact thermal Ytterbium beam clock. While this clock is predicted to have high precision on short and medium time scales, its output may drift over time. To overcome this, we are investigating using a miniature cold atom trap-based clock to provide both long term stability and fundamental accuracy.

We will present our latest results towards the development and characterisation of a compact ytterbium Magneto-Optical Trap (MOT). This includes efforts towards fabricating an efficient diffraction optic to create grating MOTs (gMOTs) [2] using a focused ion beam (FIB) system (Figure 1. BOTTOM), to operate at the fast 399 nm cooling transition. This development will drastically reduce the SWaP and complexity of the cold atom system, making it possible to use in a field-deployable device. By achieving this result, we will have demonstrated three key performance metrics: long term stability, accuracy, and reproducibility.

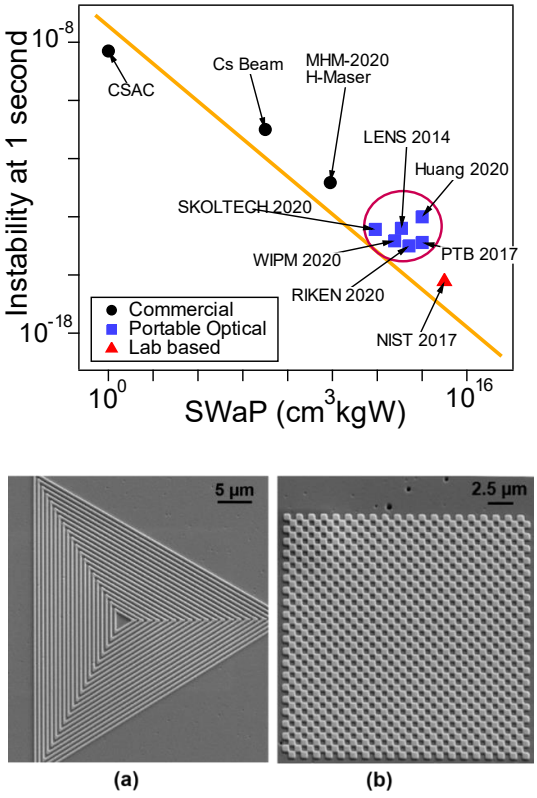

Figure 1. TOP: Current high performance portable clock technology. BOTTOM: Example of tetrahedral (a), and chess-board gMOTs (b) created [3].

References:

[1] 1. Ludlow, A. D. *et al.*, *Rev. Mod. Phys.* **87,** 637 (2015).

[2] Nshii, C. C. *et al.*, *Nature Nanotech.* **8,** 321 (2013).

[3] 3. Sun, X. *et al.*, *in prep.* (2021).

Determining the Advantage of Quantum Lidar

Z. Koumi[1], B. M. Sparkes[2], B. Smith[2], K. Grant[2] and D. Ottaway[1]

[1]*Institute for Photonics and Advanced Sensing (IPAS) and School of Physical Sciences, University of Adelaide, Adelaide SA 5005, Australia*
[2]*Defence Science & Technology Group, Edinburgh SA 5111, Australia*
email: Zachary.koumi@adelaide.edu.au

***Abstract**: Through modelling and experimentation we are providing an estimate of the true quantum advantage of a quantum-based lidar system.*

In recent years there have been a number of claims made about the potential of quantum-based technologies to significantly enhance standoff imaging and ranging ("quantum radar"). Motivated by the potential improvements there have been multiple experimental demonstrations since 2019, in both the optical and microwave domains, all claiming some form of quantum enhancement over classical radars using a number of different metrics.

For instance, using correlated photon pairs in the optical domain England *et al.* [1] suggests an improvement of 60-fold in the signal-to-noise ratio while, using a similar experimental system, Liu *et al.* [2] claim a 1,000-fold increase in the Fischer information. In both cases the comparison is between classical and quantum radars with the same transmitted power. Meanwhile, theory suggests that at most a factor of 4 improvement is possible over an optimal classical radar [3]. This highlights a key question relating to quantum radar: *how can we translate the results from one experiment to another to allow a reasonable comparison?*

Here we present our work on developing a model that will be able to predict the outcome of quantum illumination experiments. For instance, Figure 1(a) shows receiver-operator characteristic (ROC) curves simulated for the works presented in Refs [1,2], allowing us to analyse their performance using a metric more familiar to radar scientists. We will also discuss current experimental efforts to compare an optical quantum radar system with similar classical radar systems, such as pulsed lidar or heterodyne (Figure 1(b)). Through both our modelling and experimental work we will be able to provide an estimate of the quantum advantage provided by a quantum-based radar and identify where it could find practical applications going forward.

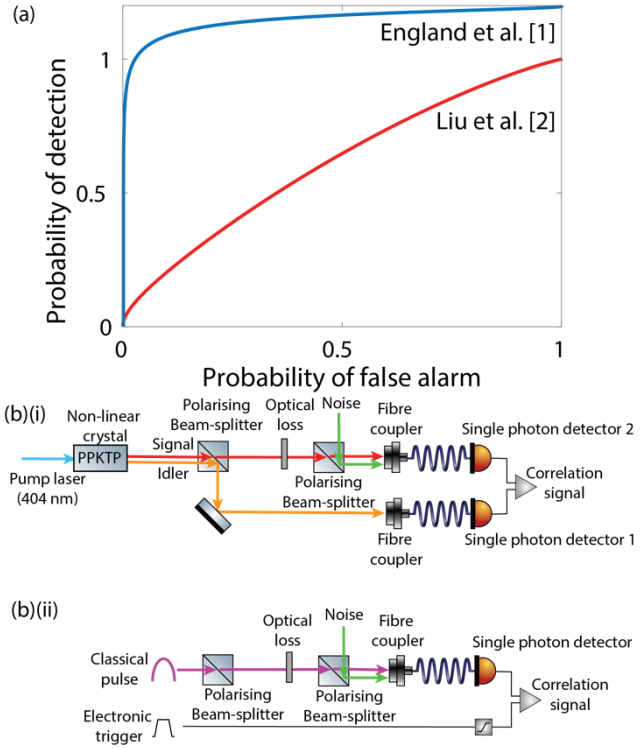

Figure 1: (a) Receiver-operator characteristic curves for Refs. [1,2]. (b) Experimental set-up for comparing the performance of (i) a quantum lidar system using correlated photons and (ii) a pulsed lidar system with the same average transmitted power.

References:

1. D. England, B. Balaji, and B. Sussman, *Phys. Rev. A* **99**, 023828 (2019).

2. H. Liu *et al.*, *Optica* **6**, 1349 (2019).

3. B. De Marco and D. S. Jin, Phys. Rev. A 58, R4267 (1998).

Low bandgap Janus semiconductors from carbon and nitrogen family of elements – property analysis through Density Functional Theory

Sri Kasi Matta[1#], Ting Liao[2], Salvy P Russo[1]**

[1] ARC Centre of Excellence in Exciton Science, School of Science, RMIT University, Melbourne 3000, Australia

* salvy.russo@rmit.edu.au

srikasi.qut@gmail.com

[2]School of Mech., Medical & Process Engineering, Queensland University of Technology, Gardens Point Campus, Brisbane, Queensland, Australia.

* t3.liao@qut.edu.au

Abstract

Two-dimensional (2D) nano materials have shown excellent electronic properties that can be used in many electronic devices, photovoltaics, and solar energy applications as well to meet the global energy demands. With an optical device usage in mind, our study here is focused on 2D materials designed from the groups 14 and 15 of periodic table. We have designed a few new two-dimensional Janus semiconductors having low bandgap with elements from these groups and computationally analyzed their electronic and optical properties. The density functional theory (DFT) analysis revealed many interesting properties. Based on the results, we propose a low-band gap semiconductor for optoelectronic and thermoelectric devices applications. Vienna Ab initio Simulation Package (VASP) is used conduct our computational study with supporting post-processing software. The essential band structure, bandgap, optical properties were analyzed to systematically segregate the materials according to their potential uses. The results are qualified with hybrid exchange correlation functional (HSE06/Wannier90 functions) for analysis of electronic properties. The structure stability is ascertained with the phonon spectrum studies. All the results will be presented in methodical way to appraise the importance of computational analysis for prediction and design of new materials for modern applications.

***

Quantum engineering the effective optomechanical coupling

M.K. Schmidt[1], G. Brennen[1], D. Burgarth[1], C.G. Poulton,[2] and M.J. Steel[1]

[1]*Macquarie University Research Centre in Quantum Engineering (MQCQE), MQ Photonics Research Centre, Department of Physics and Astronomy, Macquarie University, NSW 2109, Australia*
[2]*School of Mathematical and Physical Sciences, University of Technology Sydney, NSW 2007, Australia*
email: mikolaj.schmidt@mq.edu.au

***Abstract**: We show how the optomechanical coupling between optical and acoustic modes of a diamond microresonator can be mediated by an ensemble of nitrogen vacancies coupled to the strain and the electromagnetic fields of the resonator's acoustic and optical modes. We compare this effective coupling to other mechanisms of optomechanical coupling in subwavelength optoacoustics cavities, and show that out quantum-engineered material response can become the dominant coupling mechanism in realistic experimental systems.*

Optomechanical interaction in nano- and microresonators can couple their optical and acoustic modes. This effect offers avenues to translate the toolbox of quantum optics towards the physics of single acoustic phonons, develop macroscopic quantum-mechanical systems in a new range of frequencies, and implement transducers and new types of memories for hybrid quantum devices [1]. The optomechanical coupling is a result of several well-understood mechanisms, predominantly radiation pressure and photoelasticity, both explicitly non-resonant and dependent on the intrinsic response of the material, optimized by careful engineering of the optical and acoustic modes in the resonators [2].

However, some materials can support alternative, and possibly much more efficient coupling mechanisms, mediated by the strong optical and acoustic response of the embedded atomic defects [3]. For example, in diamond, ensembles of nitrogen- and silicon-vacancies (NVs and SiVs) can both exhibit strong resonant coupling to the dynamic strain [1,4] and electromagnetic fields induced in the material.

In this work we harness these effects and discuss the possibility of achieving an effective optomechanical coupling between the acoustic and optical modes of diamond micro- and nanoresonators [5]. Our theoretical framework is developed using the 3rd order projection operator method, which adiabatically removes the NV degrees of freedom, and allows us to explicitly account for the collective dynamics of a large ensemble of the NVs [3]. We also show that this approach describes both the dispersive *and* dissipative optomechanical coupling.

We analyze the dependence of the optomechanical coupling on the critical parameters of the NV ensemble – its density, and the inhomogeneous broadening due to internal static strain in diamond, as well as on the several proposed designs of the diamond resonator. In particular, we propose effective models which relate the overall optoacoustic coupling to the effective volumes of the optical and acoustic modes. We then compare this optimized defect-induced coupling with that achieved by the material response of the resonators: its intrinsic photoelastic response, and the radiation pressure effects.

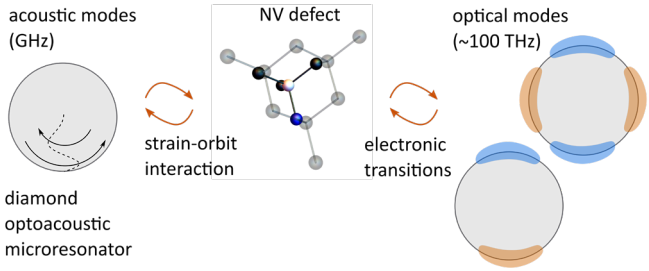

Figure 1: Nitrogen-vacancies in diamond can couple to both the strain, and electromagnetic fields. Harnessing these interactions, we can engineer an effective photoelastic interaction between acoustic and optical modes of diamond nanoparticles.

References:

1. D. Lee, K.W. Lee, J.V. Cady, P. Ovartchaiyapong, and A.C.B. Jayich, J. Opt.19, 033001 (2017).
2. A.H. Safavi-Naeini, P.T.M. Alegre, M. Winger, and O. Painter, Appl. Phys. Lett. 97(18), 181106 (2010).
3. S. Schutz, J. Schachenmayer, D. Hagenmuller, G.K. Brennen, T. Volz, V. Sandoghdar, T.W. Ebbesen, C. Genes, and G. Pupillo, Phys. Rev. Lett. 124, 113602 (2020).
4. M.K. Schmidt, C.G. Poulton, and M.J. Steel, Phys. Rev. Research 2, 033153 (2020).
5. M.K. Schmidt, G. Brennen, D. Burgarth, C.G. Poulton, and M.J. Steel, in preparation.

Mapping the geometry of quantum correlation microscopy: Voronoi cells in the Hanbury Brown and Twiss experiment

Jaret Vasquez-Lozano[1], Shuo Li[1], D. W. Drumm[2], and Andrew D. Greentree[1]

[1]*ARC Centre of Excellence for Nanoscale Biophotonics, RMIT University, Melbourne 3001, Australia*
email: jaret.vaslo@gmail.com

[2]*Physics, School of Science, RMIT University, Melbourne 3001, Australia*

***Abstract**: Quantum correlation microscopy provides an interesting and new approach to super resolution imaging and localisation. These quantum techniques use changes in the detected photon arrival statistics to extract information about the number and relative brightness of emitters as a function of space. Here we explore a new technique for quantum correlation microscopy, where we map out Voronoi cells of the photon correlation signal (Hanbury Brown and Twiss experiment). Using Voronoi cells provides a useful geometrical basis to localise the emitters and combine data from the entire image. We show modelling that determines the diffraction unlimited localisation precision as a function of noise for a field of four emitters and provide estimates for the efficiency and scaling of our approach.*

Hanbury Brown and Twiss measurements (HBT) [1] are a quantum-based measurement that can improve upon the resolution of classical measurements [2, 3, 4]. Higher order correlations allow the effective point-spread function (PSF) for imaging to be raised to the corresponding power of the correlation function, reducing the width of the point-spread function and thereby improving resolution.

The second-order correlation function from HBT measurements at zero time delay ($g^{(2)}(0)$) for N emitters is

$$g_N^{(2)}(0) = \frac{2\,\Sigma_{i=1}^{N-1}\Sigma_{j=i+1}^{N} P_i P_j}{\Sigma_{i=1}^{N}\Sigma_{j=1}^{N} P_i P_j} \qquad (1)$$

where N is the number of emitters, and P_i, is the probability of detecting a photon from emitter i [4].

It is possible to account for weak background emitters using the $g^{(2)}(0)$ equation by introducing terms for the correlation of emitters P_i, and $\mathcal{N}$ number of weak background emitters with detection probability P_{bg} [4]. We can represent the case of 2 emitters with background using the expression

$$g_{2+bg}^{(2)}(0) = \frac{2(P_1P_2+(P_1+P_2)\mathcal{N}P_{bg}+\frac{(\mathcal{N}P_{bg})^2}{2})}{(P_1+P_2)^2+2(P_1+P_2)\mathcal{N}P_{bg}+(\mathcal{N}P_{bg})^2} \qquad (2)$$

By exploring $g_N^{(2)}(0)$ as a function of space, we are able to develop a new approach to the localisation of emitters. Mapping the second-order correlation function for emitters of equal brightness results in a diagram that can be fitted with a Voronoi tessellation. A Voronoi tessellation is comprised of cells, where each cell contains a Voronoi site. The space enclosed within a cell is closest to its respective site, and no other.

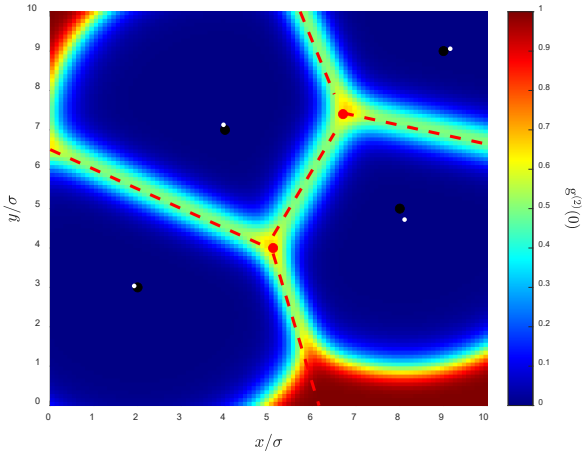

Figure 1. $g^{(2)}(0)$ plot (colour) generated from synthetic data for $N = 4$ equal brightness emitters with PSF standard deviation $\sigma = 10$, and background of $10^{-4}/\sqrt{(2\pi\sigma^2)}$. The black dots are the positions of the emitters, and the white are the estimated positions.

Voronoi tessellations offer a new method for quantum superresolution imaging that also accounts for classical data, and is well suited to the localisation of multiple equal brightness emitters. Our results show the localisation precision as a function of both background noise and finite measurement time.

Acknowledgements: This work was funded by the Air Force Office of Scientific Research (FA9550-20-1-0276). ADG also acknowledges funding from the Australian Research Council (CE140100003 and FT160100357).

References:

1. Hanbury Brown, R. and R.Q. Twiss, Nature, 1956. **177**(4497): p. 27-29.
2. Gatto Monticone, D., *et al.*, Physical Review Letters, 2014. **113**(14): p. 143602.
3. Schwartz, O., *et al.*, Nano Letters, 2013. **13**(12): p. 5832-5836.
4. Worboys, J.G., D.W. Drumm, and A.D. Greentree, Physical Review A, 2020. **101**(1): p. 013810.

Photon-pair generation enhanced by extended resonances in metasurfaces

Jinyong Ma [a], Jihua Zhang [a], Matthew Parry [a], Marcus Cai [a], Rocio Camacho Morales [a], Lei Xu [a,b]
Dragomir N. Neshev [a], Andrey A. Sukhorukov [a]

[a] *ARC Centre of Excellence for Transformative Meta-Optical Systems (TMOS), Research School of Physics, The Australian National University, Canberra, ACT 2601, Australia*
[b] *Advanced Optics and Photonics Laboratory, Department of Engineering, School of Science and Technology, Nottingham Trent University, Nottingham, NG11 8NS, UK*
email: jinyong.ma@anu.edu.au, andrey.sukhorukov@anu.edu.au

***Abstract**: We predict and observe experimentally enhanced generation of photon pairs via spontaneous parametric down conversion from a metasurface supporting extended resonances at the photon wavelengths.*

Nanofabricated structures with subwavelength thickness, known as metasurfaces, can facilitate the development of miniaturized and robust quantum photonic devices [1]. Metasurfaces made of nonlinear materials enable the generation of quantum-correlated photons through the spontaneous frequency mixing, and an enhancement through optical resonances of nanostructures was demonstrated [2].

We predict and observe experimentally that the photon-pair generation via spontaneous parametric down conversion (SPDC) can be significantly enhanced through extended lattice resonances in a nonlinear metasurface, which is the foundation for the preparation of strongly entangled quantum states with a much higher spectral brightness compared to localized resonances [3]. We designed and fabricated a 1D dielectric grating on top of an *x*-cut lithium niobate film of 300 nm thickness, supporting guided mode resonances at 1570 nm with a high-quality factor of Q~1,000. As the film thickness is much shorter than the coherence length of the SPDC, longitudinal phase-matching limitations are relaxed, allowing for the efficient generation of photons across the metasurface resonance. The experimental setup is shown in Fig. 1(a). The metasurface is pumped with a continuous-wave laser at 785 nm. A short-pass filter at 850 nm before the metasurface and a long-pass filter at 1100 nm after metasurface suppress the fluorescence produced by the metasurface and other optics. The correlation of photon pairs generated at the metasurface is analysed with a Hanbury Brown-Twiss setup, using a 50:50 beam splitter and two single-photon detectors based on InGaAs/InP avalanche photodiodes.

We find that the measured coincidence-to-accidental ratio is larger than the classical bound, confirming the generation of non-classical photon pairs. We show in Fig. 1(b) that the real coincidence is strongly dependent on the pump polarization. The coincidence rate is maximised when both the pump and emitted photon pairs are polarized along the *z*-axis of the film, in agreement with the theoretical predictions. These results pave the way towards the generation of spatially and polarization entangled photon states in nonlinear metasurfaces with the properties tailored to various applications.

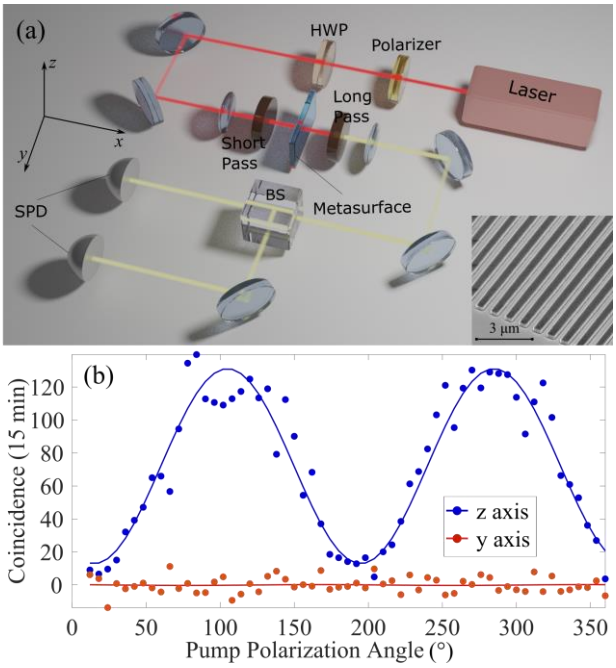

Fig. 1 (a) Experimental setup. A laser beam with a wavelength at 785 nm is focused on a lithium niobate film patterned with metasurface to produce photon pairs. The photon pairs pass through a 50:50 beam splitter, and their coincidence is then registered by two single-photon detectors. The inset shows the SEM image of the Metasurface. (b) Real coincidence as a function of pump polarization. Points and lines are experimental results and theoretical fitting, respectively, for the photon-pair polarization along the *z* or *y* axis of the film as indicated in the inset.

References:

1. A. S. Solntsev, G. S. Agarwal, and Yu. S. Kivshar, *Nat. Photonics* **15**, 327 (2021).
2. T. Santiago-Cruz, et al., *Nano Lett.* **21**, 4423 (2021).
3. M. Parry, A. Mazzanti, A. Poddubny, G. Della Valle, D. N. Neshev, A. A. Sukhorukov, arXiv:2104.07299 (2021).

Scalable and Deterministic Fabrication of hBN Quantum Emitter Arrays

Chi Li[1], Noah Mendelson[1], Zaiquan Xu[1], Milos Toth[1,2] and Igor Aharonovich[1,2]

[1]*School of Mathematical and Physical Sciences, Faculty of Science, University of Technology Sydney, Ultimo, New South Wales 2007, Australia*
[2]*ARC Centre of Excellence for Transformative Meta-Optical Systems (TMOS), University of Technology Sydney, Ultimo, New South Wales 2007, Australia*
email: Chi.li@student.uts.edu.au

***Abstract**: We demonstrate the fabrication of large-scale arrays of single photon emitters in hexagonal boron nitride. Bottom-up growth of hBN onto nanoscale arrays of dielectric pillars yields corresponding arrays of hBN emitters at the pillar sites. Statistical analysis shows that the pillar diameter is critical for isolating single defects, and diameters of ~250 nm produce a near-unity yield of a single emitter at each pillar site.*

Solid-state single photon emitters (SPEs) lie at the heart of a wide range of emerging quantum technologies, such as quantum memories, quantum communications, and quantum sensing. In recent years, SPEs originating from defects in hexagonal boron nitride (hBN) have been intensively investigated as they display outstanding optical properties at room temperature, including high brightness, linear polarization, and access to spin states.[1] These emitters can occur in commercially-available hBN, or can be engineered by employing various growth techniques. Specifically, Chemical vapor deposition (CVD) methods are attractive due to their low cost, simple experimental setups, short growth times, and the ability to grow hBN over large areas. As a result, hBN CVD protocols have been developed to control material properties such as SPE density and the spectral distribution of SPE zero phonon lines (ZPLs).[2]

In parallel, numerous attempts have been carried out to control the spatial location of SPEs in hBN with high fidelity. This is of paramount importance for SPE-based quantum technologies as it enables practical and scalable integration of quantum emitters with nanophotonic components. While some evidence of SPE localization was observed in most cases, deterministic site-specific generation of narrow-band SPEs and large-scale SPE arrays with a high success rate has remained elusive.

Here we address this challenge by growing hBN directly onto dielectric nanopillars, and show conclusively that under specific conditions, a near-unity yield of SPEs is achieved at the pillar sites. Specifically, we focus on the generation of large-scale emitter arrays through CVD growth onto SiO_2. Some data were demonstrated in figure 1.[3] In summary, we have demonstrated the deterministic formation of quantum emitters with spatial control by growing hBN directly onto SiO_2 pillars. The pillars diameter is critical for isolating a single emitter per pillar, and diameters of ~250 nm yield a near-unity success rate of emitter creation; specifically, ~80% of the pillars exhibit a $g^{(2)}(0)$ value of less than 0.5, characteristic of single photon emission. Our results constitute an advance in the controlled engineering of arrays of solid-state quantum light sources, and specifically quantum emitters in hexagonal boron nitride. These techniques provide a vital step towards integration of these sources with nanophotonic devices.

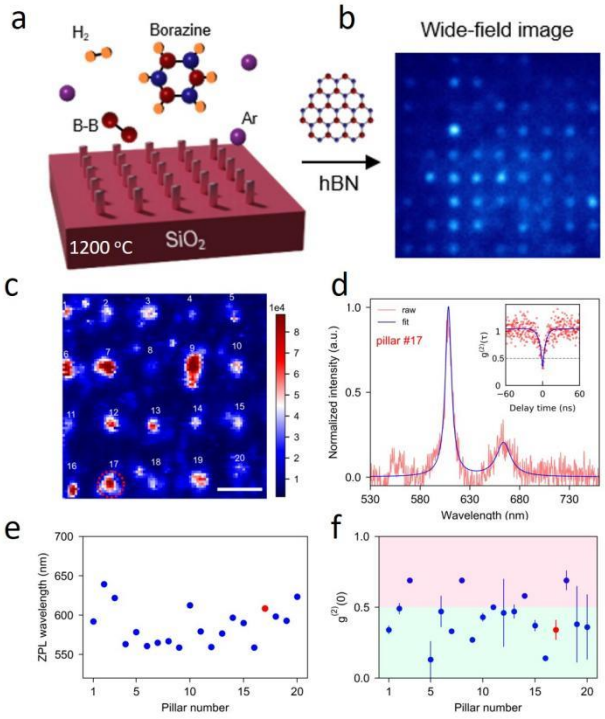

Figure 1: (a) Schematics of growing hBN on SiO_2 pillar array. (b)Wide-field image of the emitter array.(c) Confocal mapping of the array. (d) one emitter spectrum from pillar number 17. (e) and (f) emitter ZPL and $g^{(2)}(0)$ values from the above pillar array.

References:

1. J. D. Caldwell, et al. *Nat Rev Mater* **4**, 8 (2019).

2. N. Mendelson, et al. *ACS nano*, **13**, 3 (2019).

3. C. Li, et al. *Nano Letters* **21**, 8. (2021)

Quantum states of light generated from a single atom through cavity-assisted Raman transitions

A. E. J. Elliott[1, 2] and A. S. Parkins[1, 2]

[1] *Department of Physics, University of Auckland, Private Bag 92019, Auckland, New Zealand*

[2] *The Dodd-Walls Centre for Photonic and Quantum Technologies, New Zealand*

email: aell060@aucklanduni.ac.nz

***Abstract**: The states of light generated from an atom undergoing cavity-assisted Raman transitions are investigated. Wigner distributions taking on negative values, and strong squeezing are predicted to be available through this system.*

Generating states of light with negative-valued Wigner function representations is a necessary step in the pursuit of optical-based quantum information technologies [1]. Heralded sources of photons are promising but inherently probabilistic [2, 3]. Deterministic generation of negative Wigner states has been proposed in temporal modes from pulsed systems [4]. In this work, we put forward a cavity QED system which is capable of generating Wigner-negative light deterministically and in steady-state. In another regime, the same system also generates quadrature-squeezed states of light.

Raman transitions between hyperfine sublevels of an atom offer the possibility to engineer interesting and novel atom-light interactions [5]. In this work, adjacent sublevels are coupled via such transitions, which facilitate exchange of a photon with the cavity at an effective rate g. Another transition is driven by secondary laser fields, off-resonant with the cavity field, which cause a $m_F \to m_F \pm 2$ change of the atomic sub-level at a rate Ω. This system (Fig. 1) can be described by the Hamiltonian

$$\hat{H} = g(\hat{a}^\dagger \hat{S}_- + \hat{S}_+ \hat{a}) - i\Omega(\hat{S}_+^2 - \hat{S}_-^2), \qquad (1)$$

where $\hat{a}$ ($\hat{a}^\dagger$) is the cavity annihilation (creation) operator, and $\hat{S}_-$ ($\hat{S}_+$) is the spin-S atomic lowering (raising) operator.

Rabi oscillations between states can be limited by appropriately tuning the relative interaction rates of this open quantum system. In a limit where the cavity decay rate κ exceeds the cavity coupling rate, and $g \gg \Omega$, the system undergoes a cycle of transitions. To preserve quantum features of the light coupled into the cavity from the atom, the cavity is chosen to be effectively one-sided by making one mirror far more reflective than the other. Under these conditions, the system behaves as a steady state source of even numbers of photons through the "bad" mirror output channel.

The characteristic time of emissions can be quantified by the cavity field amplitude correlation function $g^{(1)}(\tau) = \langle \hat{a}^\dagger(\tau)\hat{a}(0)\rangle_{ss}$, which is used to define a temporal envelope for the output field mode $\hat{a}_f$. In an appropriate coupling regime, the temporal mode quantum state displays negative values in the Wigner distribution, as shown in Fig.1 for an effective spin-1 system, where the state produced is close to a superposition of 0 and 2 photons. By working with longer effective spin lengths, higher-order superpositions can be generated which also display negative-valued Wigner distributions.

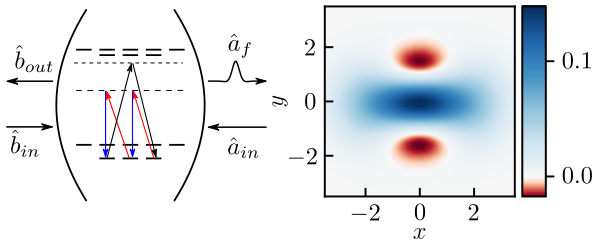

Figure 1: (Left) Cavity-assisted Raman transitions within the hyperfine sublevels of the Rb-87 D1 line. (Right) Wigner distribution in a temporal mode of the output field, with $\{\kappa/g, \Omega/g\} = \{2, 0.1\}$.

Even superpositions of photons are associated with squeezed light, which can also be generated from this system. As the spin length and superposition becomes larger, so does the magnitude of squeezing. Compared to a coherent state, an 85% reduction in quadrature variance is attainable from for an effective spin-4 system in the $6S_{1/2}$ $F = 4$ state of Cs-133.

References

[1] A. Mari and J. Eisert, *Phys. Rev. Lett.* **109**, 230503 (2012).

[2] S. Barz, G. Cronenberg, A. Zeilinger, and P. Walther, *Nature Photon* **4**, 553–556 (2010).

[3] Y-S. Ra, C. Jacquard, A. Dufour, C. Fabre, and N. Treps, *Phys. Rev. X*, **7**, 031012 (2017).

[4] C. Groiseau, A.E.J. Elliott, S.J. Masson, A. S. Parkins, *Phys. Rev. Lett.*, **127**, 033602 (2021).

[5] E.J. Davis, G. Bentsen, L. Homeier, T. Li, and M.H. Schleier-Smith, *Phys. Rev. Lett.* **122**, 010405 (2019).

Coupling Spin Defects in Hexagonal Boron Nitride to Monolithic Bullseye Cavities

Johannes E. Fröch[1,*], Lesley Spencer[1,2,*], Mehran Kianinia[1,2], Daniel Totonjian[1], Minh Nguyen[1], Andreas Gottscholl, Vladimir Dyakonov[3], Milos Toth[1,2],Sejeong Kim[4], Igor Aharonovich[1,2]

[1]*School of Mathematical and Physical Sciences, University of Technology Sydney, Ultimo, New South Wales 2007, Australia*
[2]*ARC Centre of Excellence for Transformative Meta-Optical Systems (TMOS), University of Technology Sydney, Ultimo, New South Wales 2007, Australia*
[3]*Experimental Physics 6 and Würzburg-Dresden Cluster of Excellence ct.qmat, Julius Maximilian University of Würzburg, 97074 Würzburg, Germany.*
[4]*Department of Electrical and Electronic Engineering, University of Melbourne, Victoria, 3010, Australia*
**These Authors contributed equally*

email: lesley.p.spencer@student.uts.edu.au

***Abstract**:* The integration of spin centers in hexagonal boron nitride (hBN) with photonic resonators demonstrates significant progress towards their implementation as a scalable spin-photon interface. This work is a step towards that, demonstrating the efficient coupling of boron vacancy spin defects to monolithic hBN bullseye cavities. This coupling resulted in emission enhancement of the defect by an order of magnitude. It also exhibited better contrast and improved signal to noise ratio for optically detected magnetic resonance measurements. Additionally, through comparison to finite-difference time-domain modelling, our results shed light on the dipole orientation of the emission.

Phonon dephasing and spectral diffusion of quantum emitters in hexagonal Boron Nitride

Simon White[1], Connor Stewart[1], Alexander S. Solntsev[1], Chi Li[1], Milos Toth[1,2], Mehran Kianinia[1, 2, *] and Igor Aharonovich[1, 2]

1. School of Mathematical and Physical Sciences, Faculty of Science, University of Technology Sydney, Ultimo, New South Wales 2007, Australia

2. ARC Centre of Excellence for Transformative Meta-Optical Systems (TMOS), University of Technology Sydney, Ultimo, New South Wales 2007, Australia

email: Mehran.kianinia@uts.edu.au

***Abstract**: Quantum emitters in hexagonal boron nitride (hBN) are emerging as bright and robust sources of single photons for applications in quantum optics. Here we study the limiting factors to achieve Fourier Transform limited spectral lines. Specifically, we study phonon dephasing and spectral diffusion of quantum emitters in hBN via resonant excitation spectroscopy at cryogenic temperatures. We show that the linewidths of hBN quantum emitters are phonon broadened, even at 5K. We also show spectral diffusion is dependent on excitation power and can be minimized by working well below saturation power. Our results are important for future utilization of quantum emitters in hBN for quantum interference experiments.*

Solid state quantum light sources are emerging as promising candidates for many applications in quantum technologies [1]. Among these sources, optically active point defects in hexagonal boron nitride (hBN) are attracting considerable attention due to their extreme brightness, and high proportion of emission into the zero-phonon line (ZPL); as opposed to the phonon sideband (PSB). For practical implementation of such emitters, it is important to understand the broadening mechanisms that affect photon coherence. In solid state emitters the dominant broadening mechanisms are coupling to vibrational modes (phonon dephasing) and local charge fluctuations (spectral diffusion), depicted schematically in Fig 1(a).

To study these broadening mechanisms in hBN single photon emitters, we employ resonant photoluminescence excitation (PLE) where the excitation energy matches that of the ZPL (in this work ~578 nm). We find that the resonant linewidth for a single SPE is dominated, even at cryogenic temperatures, by phonon broadening and results in linewidths ~ 1 GHz (bottom PLE spectra Fig 1(b)). We measure homogeneously broadened linewidth as a function of temperature and find the model that best describes the observed data indicates that degenerate electronic states and strong strain do not play a significant role in phonon dephasing [2-4].

We also measure the effects of excitation power on spectral diffusion and show it can be minimized by employing excitation powers well below saturation (Figure not shown).

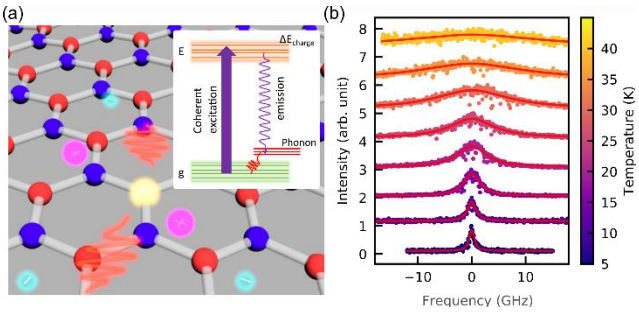

Figure 1: (a) *Schematic representation of the hBN lattice with a point defect (yellow sphere)*, and inset showing SPE broadening due to local field fluctuations and phonon coupling. (b) Phonon broadening of the ZPL as a function of SPE temperature.

In summary, we characterize the significant broadening mechanisms in hBN SPE. We find phonon dephasing persists at 5K, signifying further cooling should enable narrow linewidths. We also find inhomogeneous spectral diffusion is power dependent such that minimization of local field fluctuations should significantly improve resonant excitation efficiency. This study will help guide the development of hBN emitter stabilization for applications toward quantum interference and in demand indistinguishable photons.

References:

1. I. Aharonovich, D. Englund & M. Toth. *Nat. Photonics* 10, 631-641, (2016).
2. K. D. Jahnke, et al. *New J. Phys.* 17, 043011, (2015).
3. E. Neu, et al. *New J. Phys.* 15, 043005, (2013).
4. V. Hizhnyakov, et al. *The Journal of chemical physics* 119.12 (2003): 6290-6295.

Enhanced spin readout in hBN via Coupling to Nanoscale Plasmonic Cavities

Zai-Quan Xu[1], Noah Mendelson[1], Ritika Ritika[1], Mehran Kianinia[1,2], John Scott[1,2], Sejeong Kim[3], Johannes E. Fröch[1], Stefan Strauf[4, 5], Milos Toth[1,2] and Igor Aharonovich[1,2]

[1]School of Mathematical and Physical Sciences, University of Technology Sydney, Ultimo, New South Wales 2007, Australia

[2]ARC Centre of Excellence for Transformative Meta-Optical Systems (TMOS), University of Technology Sydney, Ultimo, New South Wales 2007, Australia

[3]Department of Electrical and Electronic Engineering, University of Melbourne, Victoria 3010, Australia

[4]Department of Physics, Stevens Institute of Technology, Hoboken, New Jersey 07030, USA

[5]Center for Quantum Science and Engineering, Stevens Institute of Technology, Hoboken, New Jersey 07030, USA

E-mail: zaiquan.xu@uts.edu.au.

Abstract:

The atomic defects in van der Waals materials are emerging because of their fascinating optical properties and potential applications in quantum sensing and quantum information systems. The negatively charged boron vacancy (V_B^-) in atomically thin hexagonal boron nitride has the long-term sought after spin properties, i.e., optically detectable magnetic resonance (ODMR), which is the foundation of a plethora of quantum sensing applications such magnetic and electric fields, temperature and strain down to atomic scale. However, the low quantum yield of the V_B^- system hinders the real-world applications.

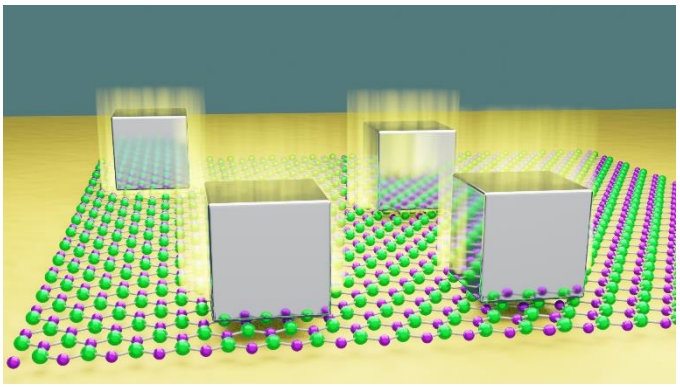

Fig. 1. Integration of V_B^- emitters in a plasmonic gap cavity. Schematic illustration of a nanocube-on-mirror plasmonic gap cavity. FIB irradiated hBN flakes are placed inside the gap to spatially match the cavity hot spot.

In this work, we solve this long-standing issue. We report for the first time the successful integration of V_B^- in hBN with plasmonic gap nanocavities, which leads to PL intensity enhanced by up to~100 times, together with a Purcell factor of ~480. The enhanced emission improve the ODMR contrast of V_B^- by a factor of 2. Our findings constitute an important basis for further studies of plasmon coupling to defects in 2D materials and will benefit future development of scalable rapid quantum sensing using this quantum spin system.

References:

1. *Nature Materials* **2020,** 19, (5), 540-545.
2. *ACS Photonics* **2020,** 7, (8), 2147-2152.
3. *Nano Letters* **2017,** 17, (4), 2634-2639.
4. *Nature Nanotechnology* **2018,** 13, (12), 1137-1142.
5. *Nature* **2016,** 535, (7610), 127-130.

Delay-Limited Phaselocking for Stable Narrow-Linewidth Laser Diodes

Z. J. Holmes[1], S. W. S. Ng[1], J. S. Pease[2] and D. J. Ottaway[1]

[1] *ARC Centre of Excellence for Gravitational Wave Discovery, The University of Adelaide, SA 5005, Australia*
[2] *Institute for Photonics and Advanced Sensing, The University of Adelaide, SA 5005, Australia*
email: zachary.holmes@adelaide.edu.au

***Abstract**: The next generation of gravitational wave detectors will operate at a different wavelength to current installations. Laser sources are needed at a variety of wavelengths to test subsystems and research interferometer configurations. Laser diodes offer inexpensive, robust, wavelength tuneable sources, exhibiting high bandwidths for actuation. We present a high bandwidth phaselock capable of delay-limited bandwidths in the MHz range using a broadband electro-optic phase modulator aided by frequency division.*

Stable narrow-linewidth laser sources are essential for remote sensing, nonlinear frequency generation quantum information applications, and interferometric gravitational wave detection. The next generation of gravitational wave detectors will require greater laser power and change operating wavelength from 1 um to a wavelength in the 1.3-2.1 um band. Rigorous testing of materials and interferometer subsystems is necessary before committing to a wavelength; as such, inexpensive and low noise laser sources are needed across the prospective wavelength band.

Phaselocking establishes a transfer of coherence between sources, enabling stable narrow-linewidth lasers to be derived from inexpensive yet higher noise single-frequency laser diodes. Achieving coherence between sources is critical to coherent beam combination, which allows for power scaling beyond the nonlinear thresholds of a single source. Coherent combination of multiple sources is under investigation to solve power requirements and long-term stability challenges in the laser sources of current gravitational wave detectors. Phaselocking and beam combination methods are a pathway towards stable, high power, low noise sources at a variety of wavelengths.

We present a laser frequency stabilisation technique to establish stable, narrow-linewidth laser sources for interferometric gravitational wave detector research. The demonstration is a wavelength-independent, all-fibre, high bandwidth phaselock utilising an electro-optic phase modulator to achieve time delay-limited locking bandwidths in noisy single-section laser diodes to improve suppression in the gravitational wave detection band of 10 Hz – 10 kHz.

A noisy Distributed Feedback (DFB) single frequency laser diode of 10 MHz linewidth is phaselocked to an External Cavity Diode Laser (ECDL) master of 100 kHz linewidth. The heterodyne phaselock is capable of offset-locking at >15 GHz using frequency dividers. The dividers offer high nonlinear gain against cycle-slipping while attaining comparable residual phase errors to microwave synthesisers without incurring penalties to cost, footprint, and power consumption[1].

The sum of the laser linewidths is a heuristic for phaselock bandwidth requirements, suggesting a 10 MHz bandwidth would be necessary to suppress any noise of significance in the system. Single-section laser diodes exhibit a phase reversal in their frequency modulation response after several MHz, which necessitates the use of lead filters in the laser servo or external modulators operating in parallel to maximise performance to the time delay limit.

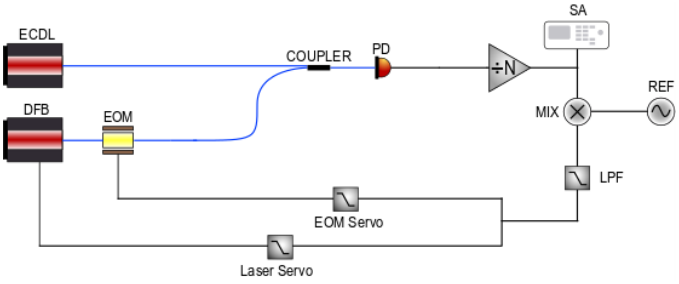

Figure 1: PD, Photodetector; SA, Spectrum Analyser; MIX, Mixer; REF, Reference; LPF, Low Pass Filter; EOM, Electro-Optic Modulator

The laser servo is a proportional-integral controller with an integrator operating to 1 MHz. A phase lead of 12° between 2-3 MHz is introduced to extend the laser servo bandwidth to a maximum of 2.5 MHz with 12 dB of peaking. A broadband fibre phase modulator with a 200 MHz bandwidth amplifier extends the locking bandwidth until the delay limit is reached. The phase modulator servo is a bandpass filter with a low pass corner of 2.6 MHz to attenuate the response at the gain crossover and avoid instability due to time delay. Delay manifests as phase lag and a 10 m optical delay line has shown the overall servo to be delay-limited by introducing approximately 50 ns of delay.

The all-fibre, delay-limited phaselock demonstrates the feasibility of establishing stable, narrow-linewidth laser sources from low cost, single-section, single-frequency laser diodes.

References:

1. E. N. Ivanov, F.-X. Esnault, and E. A. Donley, *Rev. Sci. Instrum.* **82**, 083110 (2011)

Single-frequency 1950nm, 1980nm, and 2035nm thulium-doped fiber lasers

G. N. Bolingbroke[1,2], M. Oermann[3], S.W.S. Ng[1,2], A. Hemming[3], D. Stepanov[3], J. Munch[1,2] and P. Veitch[1,2]

[1]*ARC Centre of Excellence for Gravitational Wave Discovery, Australia*
[2]*University of Adelaide, SA 5005, Australia*
[3]*Defence Science and Technology Group, SA 5111, Australia*
email: georgia.bolingbroke@adelaide.edu.au

***Abstract**: Thulium-doped silica lasers have a broad tuning range near 2*μm*, making it an attractive gain medium for laser sources for next-generation cryogenic silicon gravitational wave detectors. We demonstrate single frequency thulium-doped distributed-Bragg-reflector fiber lasers at 1950nm, 1980nm, and 2035nm with single-longitudinal-mode operation and output powers of up to 180mW.*

Current ground-based laser-interferometer gravitational wave observatories have detected almost 50 signals from the mergers of binary-black-hole systems binary-neutron-star (BNS) systems and black-hole and neutron-star binaries. Of these, only 2 BNS signals were detected. The international community is thus planning the next generation of detectors to increase detections, from more distant regions of the universe, with better fidelity from known and as-yet unknown sources.

To reach the required sensitivities, current detectors need to be upgraded and new longer-arm-length detectors must be developed. One proposed detector uses large single-crystal cryogenic silicon mirrors to reduce the effect of Brownian and thermo-elastic noise [1]. This change in material requires a change of laser wavelength to within the transmission window of silicon [1]. Thulium-doped silica sources are an ideal candidate, operating at around 2 μm, they meet this requirement and would exhibit minimal absorption in both the silicon mirror substrate and the amorphous-silicon mirror coatings [1, 2]. Additionally, thulium-doped fiber (TDF) lasers with kHz linewidths at high efficiency [3] and high output powers but with lower efficiencies [4, 5] have previously been reported. Thus, this abstract presents on the development and characterisation of a new 2 μm thulium doped silica fibre laser source, that has a high power, single-polarisation, single-frequency, diffraction-limited output with ultra-low intensity and frequency noise, for this application.

The sources presented here are TDF distributed-Bragg-reflector (DBR) lasers at 1950 nm, 1980 nm, and 2035 nm fabricated using the in-house direct writing fiber Bragg grating (FBG) setup [6]. These sources are able to be amplified to meet the power requirements of the next generation gravitational wave detectors.

A schematic of the TDF lasers is shown in Figure 1(a). They consist of a high-reflectance (HR) FBG through which the pump is injected, a short TDF fiber, and polarisation maintaining output coupler (OC) FBG. The 1950 nm laser featured a 30 mm TDF and cavity length, whereas, the 1980 nm and 2035 nm lasers consisted of a shorter 25 mm cavity. The short, heavily doped, cavities supported only a single longitudinal mode and provide adequate pump absorption and gain to overcome the DBR's intracavity losses. The reflectance peaks of the FBGs are matched using a combination of tension and thermal tuning. The thermal tuning was achieved using a two-stage temperature-controlled mount that isolates the TDF laser from the environment and independently controls the temperatures of the TDF and FBGs.

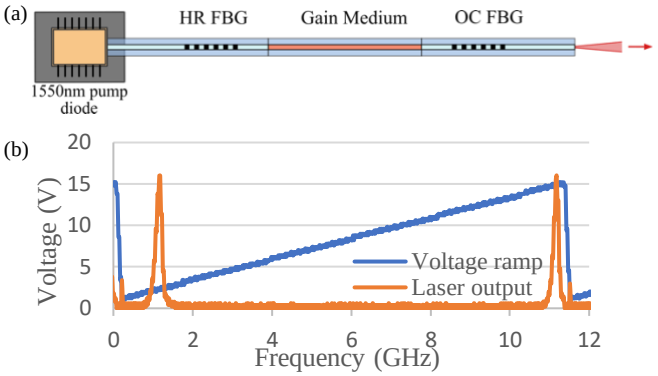

Figure 1(a): Schematic of the DBR fiber laser. (b) Scanning Fabry-Perot demonstrating the single-polarisation, single-mode output.

The lasers have been pumped using both a fiber-coupled 450 mW 1550 nm single-mode diode laser and a ErYb fiber amplifier that increased the pump power to 1.1 W. Initial testing demonstrated output powers of up to 50 mW with the direct diode pumping and 180 mW with the amplified pump.

The single-polarisation, single-frequency output from the lasers is illustrated in Figure 1(b) for the 1980 nm laser using a 10 GHz free spectral range scanning Fabry-Perot. This measurement was repeated for the other wavelengths along with measurements of the output spectrum, relative intensity noise, phase noise and output power. These results suggest that these lasers should be suitable for use as a master oscillator (MO) in the next-generation cryogenic-silicon gravitational wave detectors.

In this report, we shall present on the design and characterisation of the 1950 nm, 1980 nm, and 2035 nm single-frequency TDF lasers.

References:

1. R X Adhikari et al, *Class. Quantum Grav*. **37** 16 (2020)
2. J. Steinlechner et al, *Phys. Rev. Lett.* **120** 20 (2018)
3. J. Geng et al, *Opt. Lett.* **34** 22 (2009)
4. A Hemming et al, *Workshop on Specialty Optical Fibers and their Applications* (2013)
5. Z. Zhang et al, *IEEE Photonics Technol. Lett.*, **23** 7 (2011).
6. D. Stepanov et al., *Opt. Express*, **22** 22 (2014)

Optimisation of dispersion-compensation fiber length in a SESAM-Soliton hybrid mode-locked laser

A. Kolovinos[1], K. Boyd[1,2], D. McAfee[1,2], M. Ganija[1,2] and P. Veitch[1]

[1]*University of Adelaide, SA 5005, Australia*
[2]*Defence Science Technology Group, Edinburgh 5111, Australia*
email: alexandros.kolovinos@adelaide.edu.au

***Abstract**: The balancing of nonlinear effects with group dispersion is of key importance to ultrashort pulse shaping. We present the results of tuning the group dispersion with the use of varying lengths of dispersion compensating fibre.*

The advent of ultrashort pulsed mode-locked laser technology has opened many opportunities in medical imagery, surgery, and manufacturing [1]. The balancing of nonlinear self-phase modulation (SPM) and group velocity dispersion (GVD) of soliton-like pulses in optical cavities is a desirable method for mode-locking [2]. A semiconductor saturable absorber mirror (SESAM) both initiates mode-locking and stabilises the solitons [3]. Optimising the stability and pulse duration of the mode-locked pulse train from a laser cavity involves varying the amount of negative GVD. Incorporating different lengths of dispersion compensating fibre (DCF) is one method for tuning this parameter.

The SESAM-soliton hybrid mode-locked Ho-doped fibre laser is shown in Fig. 1(a). It is comprised of 10 m of SM2000 passive fibre, 1 m of custom SM active 0.5% wt Ho-doped active fibre [4], a 2100 nm broadband 75/25 output coupler and a PM circulator. The PM circulator both directs light toward the SESAM and acts as an artificial nonlinear polarisation-based SA [5]. The cavity incorporated 13 m of DCF and incident fluence on the SESAM was adjusted by moving a three-axis stage.

The length of the DCF fibre was gradually reduced from 13 m while the output was characterised using a 6 GHz-BW detector and oscilloscope, fringe-resolved autocorrelation (FRAC), radio frequency (RF) and optical spectra (OS), as shown in Fig. 1(b,c,e).

Pulse duration was minimised with 7.2 m of intra-cavity DCF. The temporal FWHM was 494 fs assuming a sech^2 shape (typical for soliton-like pulses) [6] with a 25nm spectral FWHM. Pulse trains were similar for all 3 DCF lengths, with amplitude fluctuations of ca. 20%. The RF spectrum showed a roll-off of only 3 dB across a 1 GHz span, indicating the stability of the pulse train at these DCF lengths.

At DCF lengths below ca. 5.6 m the laser would not produce stable continuous mode locking (CML), with Q-switching and multi-pulse instabilities dominating. CML operation was possible for DCF lengths above 8 m but the pulse duration increased with increasing DCF length.

All FRAC traces included satellite pulses located ca. 5 ps from the primary pulse. FRAC traces close to the 7.2 m DCF saw satellite pulses with only 1-5% of the primary pulse height, compared with around 20% for longer and shorter DCF lengths.

We have demonstrated that stable CML with ca. 450 fs soliton-like pulses can be produced by optimising the length of DCF fiber. Our results indicate that this length must be adjusted to within ca. 20 cm, or 3%.

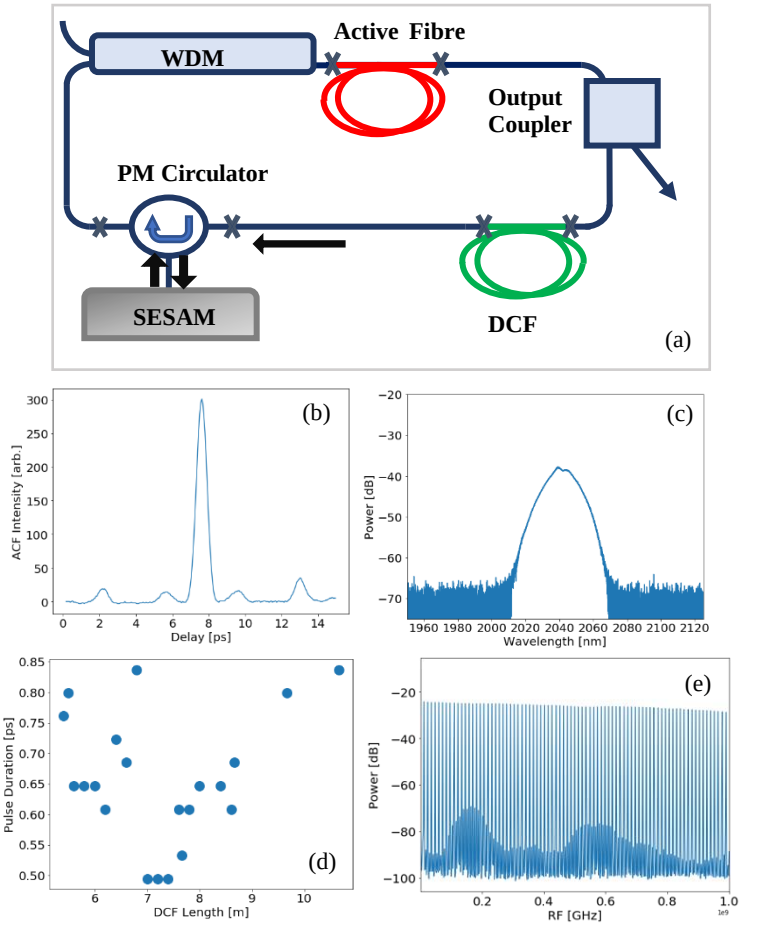

Figure 1: Characteristics of mode-locking pulses for a DCF length of 7.2 m: (b) optical spectrum, (c) FRAC, (d) FRAC FWHM vs. DCF length, (e) RF spectrum.

References:

1. B. Pal, *Frontiers in Guided Wave Optics and Optoelectronics*, IntechOpen (2010)
2. Martinez et. al., *Opt. Lett.*,**9**, 156 (1984)
3. J.N. Kutz, *SIAM Review* **48**, 629 (2016)
4. A. Hemming et. al, *CLEO*, paper SM3Q.5. (2016)
5. Wang et. al., Laser Phys. Lett. **13**, 55102 (2016)
6. R. Paschotta, *Field Guide to Laser Pulse Generation*, SPIE, Bellingham (2004)

Bottom-up Synthesis of Single-crystal Diamond Pyramids Containing Germanium Vacancy Centers

Milad Nonahal[1], Mehran Kianinia[1,2], Igor Aharonovich[1,2]

[1]School of Mathematical and Physical Sciences, Faculty of Science, University of Technology Sydney, Ultimo, New South Wales 2007, Australia

[2]ARC Centre of Excellence for Transformative Meta-Optical Systems (TMOS), University of Technology Sydney, Ultimo, New South Wales 2007, Australia

email: milad.nonahal@student.uts.edu.au

***Abstract**: In this work, we employ pattern growth method to engineer arrays of single-crystal diamond pyramid from a low-cost polycrystalline diamond substrate. Deterministic incorporation and enhanced emission from fabricated pyramid shaped single-crystal diamonds containing germanium vacancy (GeV) color centers is demonstrated.*

Diamond color centers have been at the center of many studies on quantum science and engineering and light matter interactions. To improve the optical emission of color centers, a wide array of approaches has been developed to fabricate nanostructured resonators and cavities. [1] These include top-down etching techniques using reactive ion etching (RIE), or bottom-up techniques such as chemical vapor deposition (CVD), both through a predefined pattern. In top-down techniques, color centers often introduced via ion implantation whereas bottom-up approach is promising for the incorporation of specific color-centers within the photonic structure during the diamond growth. This feature eliminates the damage occurring during ion implantation process, which requires a recovery process to bring back the crystal quality.

Moreover, the bottom-up approach shows potential to be utilized in the future to facilitate the growth of 3D structures that are inherently challenging to fabricate using top-down techniques. In addition to the host crystal quality, various color centers in diamond have been proposed for application in quantum technologies. Among these, IV color centers including the germanium vacancy (GeV), have attracted attention because of its desirable optical properties. The emission of GeV center consists of a strong zero photon line (ZPL) at 602 nm and a weak photon side band (PSB) with larger spin and orbit splitting in both ground and excited states. [2]

In the current work, we employ the bottom-up growth method to engineer arrays of single-crystal diamond structures from a polycrystalline substrate. We then purposely introduce germanium vacancy (GeV) color centers and investigate the photoluminescence enhancement within the pyramid shaped diamond. Data are briefly shown in figure 1. [3] In summary, we demonstrate emission enhancement from the pyramids compared to unpatterned overgrown substrate and linewidth of ~500 MHz and $g^{(2)}(0)$ value of less than 0.5 from these centers at cryogenic temperature.

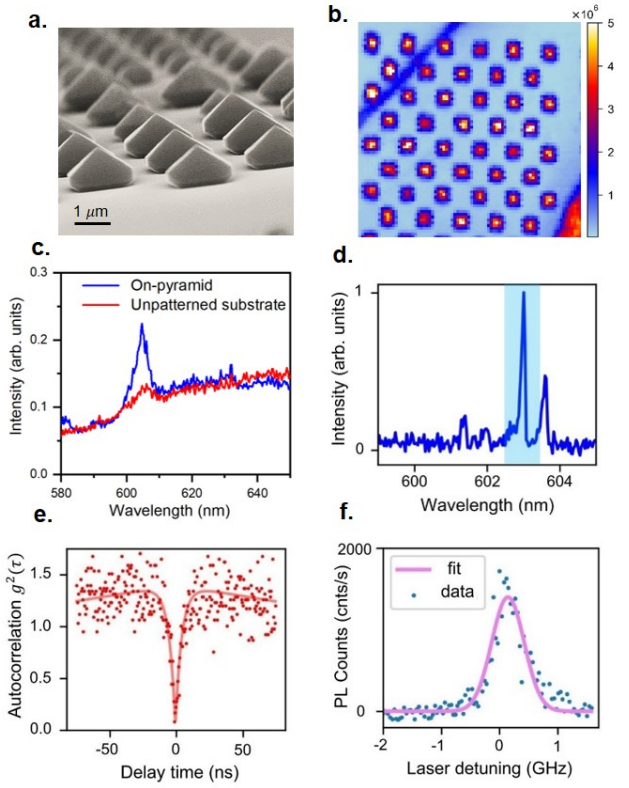

Figure 1: (a) SEM image of diamond pyramid arrays. (b) confocal mapping of the arrays. (c) room temperature spectra obtained from a pyramid and un-patterned substrate (d) cryogenic spectrum (4 K) from a pyramid (e) Autocorrelation measurement of resonantly driven GeV under 50 nW laser power (f) Resonant photoluminescence excitation of the highlighted peak in (d)

Reference:

1. S. Mi, et al. J. Phys. Photonics **2,** 4 (2020).

2. C. Bradac, et al. Nat. Commun. **10**, 1 (2019).

3. M. Nonahal, et al. Adv. Quantum Technol **4**, 7 (2021).

Investigating a titanium doped sapphire whispering-gallery mode resonator as a laser and amplifier

F. Azeem[1,2], L. S. Trainor[1,2], A. Gao[3,4], M. Isarov[1,2], D. V. Strekalov[1,2], and H. G. L. Schwefel[1,2]

[1]*The Dodd-Walls Centre for Photonic and Quantum Technologies, New Zealand*
[2]*Department of Physics, University of Otago, 730 Cumberland Street, Dunedin 9016, New Zealand*
[3]*MOE Key Laboratory of Weak-Light Nonlinear Photonics, TEDA Institute of Applied Physics and School of Physics, Nankai University, Tianjin, 300457, China*
[4]*State Key Laboratory for Artificial Microstructure and Mesoscopic Physics, School of Physics, Peking University, Beijing,100871,China*

email: harald.schwefel@otago.ac.nz

***Abstract**: The first titanium doped sapphire (Ti:sapphire) whispering-gallery laser (WGL) was successfully demonstrated and investigated. The lasing threshold was the record lowest reported for a Ti:sapphire laser. Furthermore, the WGL was explored as an optical amplifier inside the gain range of Ti:sapphire.*

Ti:sapphire has been one of the building blocks of the solid state laser industry since its invention in 1986 [1]. Its broad gain band, ranging from 650 nm up to 1100 nm, and peak absorption wavelengths between 514 nm and 532 nm made it the gain material of choice for a variety of lasers ranging from constant-wave lasers to femtosecond lasers. Moreover, Ti:sapphire lasers [2] have been used to demonstrate frequency combs and to study ultrafast dynamics of atomic, molecular, and condensed matter [3].

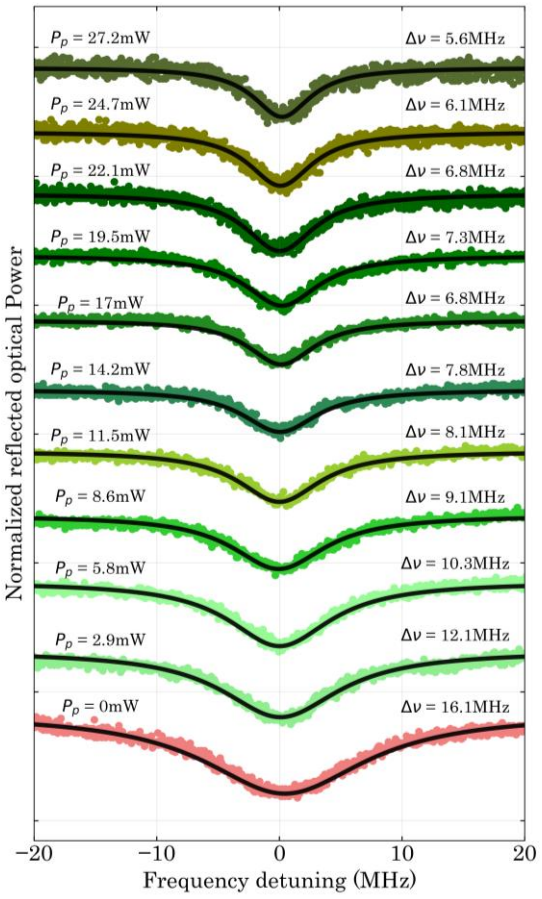

Figure 1: Decrease in linewidth (increase in Q-factor) of the same mode excited by the probe laser, due to the increase in power of pump laser.

Optical cavities are utilized in conjunction with gain media to compensate losses and enable lasing. The performance of a laser depends on the qualify factor (Q-factor) of the cavity. A larger Q-factor results in a longer cavity confinement time and leads to a lower lasing threshold, as well as to a lower frequency noise of the laser. Shaping a single Ti:sapphire crystal into a millimeter sized high quality whispering gallery mode resonator (Q-factor $\approx 10^8$) resulted in the lowest recorded lasing threshold of 14.2 mW and a high laser slope efficiency of 34%. The observed lasing can be either multi-mode or single-mode. This is the first demonstration of a Ti:sapphire WGL. Furthermore, an amplification experiment was realized based on a novel method. This method was implemented by introducing a tunable probe laser with a central wavelength of 795 nm, which is used to measure the linewidth of a whispering gallery mode (WGM). The purpose for this was to characterize gain inside the Ti:sapphire WGL in the near infrared region. The gain controlled by the optical pump power partially compensates the WGM loss and results in a decrease of the linewidth, as shown in Figure 1. The change in linewidth is explained using population inversion of a four-level laser system [4].

In conclusion, this study has opened the door for compact Ti:sapphire WGLs. This study can further lead to amplifiers based on the pump-probe method implemented in experiment. Further avenues can be explored in the existing experiment by employing Ti:sapphire WGM resonators of varying dimensions.

References:

1. P. F. Moulton, *JOSA B* **3**, 125 (1986).
2. L. Matos et al., *Opt. Lett.* **29**, 1683 (2004).
3. B. Frietsch et al., Rev. Sci. Instrum **84**, 075106 (2013).
4. F. Azeem et al., *arXiv:*2108.11171 (2021).

Nanorubies for multiplexed imaging of cells

A. Maleki[1,2], X. Yang[1,2,3], N. Lipey[1,4], X. Zheng[1], M. Santiago[1], M. Connor[1], V. Sreenivasan[5,6], Y. Lu[1], J. Dawes[1]*, A. Zvyagin[1,3]*

[1]*Macquarie University, Sydney, 2109 Australia*

[2.]*Northeastern University, Shenyang 110819, China*

[3] *Sechenov University, Moscow, 119991, Russia*

[4] *National Research Nuclear University, Moscow, 115409, Russia*

[5] *University of New South Wales, Sydney 2052, Australia*

[6] *University of Lübeck, 23568 Lübeck, Germany*

email: alireza.maleki@mq.edu.au

***Abstract**: Nanorubies with different photoluminescence lifetimes were used to label receptors to distinguish cells for background-free detection and imaging.*

Photoluminescence imaging using biomarker-labelled nanoparticles is a valuable tool for distinguishing cell populations [1]. Key challenges of implementing photoluminescence imaging are to eliminate the autofluorescence background due to other cell chromophores, and to separately identify the different labels. Spectral filtering is used to discriminate differently-labelled cell populations, but the different labels may overlap in the spectral domain, so time-gated imaging offers an alternative to separate the labelled cells. Here we demonstrate chemically-labelled, non-toxic nanorubies of distinct photoluminescence lifetimes, which are bound to specific cell receptors and are distinguished using a time-gated microscopy imaging system.

We fabricated different classes of nanorubies [3] with distinct emission lifetimes by separately crushing, grinding and ball-milling three bulk ruby crystals (0.2% Cr^{3+}, 0.6% Cr^{3+} and 0.8% Cr^{3+} doping) with different photoluminescence lifetimes. Increased Cr^{3+} concentration leads to quenching, and shorter emission lifetime. The nanorubies were centrifuged, acid-alkali-acid washed, and then coated in SiO_2 for bioconjugation with appropriate antibody biomarkers using click chemistry [4]. The target cells were incubated with the nanoruby suspensions and then washed and mounted for imaging. The lifetime imaging setup used a 525 nm LED focused on the sample using an objective (60×) and the emission light was collected by the same objective and reflected from a dichroic. The emission was gated by a chopper (to block the excitation) and focused on a camera. A set of time-gated images were recorded with increasing time delays, then these were reconstructed pixel by pixel to produce individual photoluminescence decay curves to which lifetimes were fitted.

Figure 1 shows the pseudo-colour-mapped lifetime images of nanoruby-labelled opioid (AtT20 MOR) receptors on mouse tumour cells acquired by lifetime imaging. The upper row represent lifetime images of labelled cells, while the lower row represent the measured photoluminescence lifetime, calculated from pixels corresponding to each sample in the lifetime image. The left column is 0.2% nanoruby labelled AtT20 MOR FLAG; the middle column is 0.6% ruby labelled AtT20 MOR HA; the right column (shortest lifetime) 0.8% ruby labelled AtT20 MOR HIS.

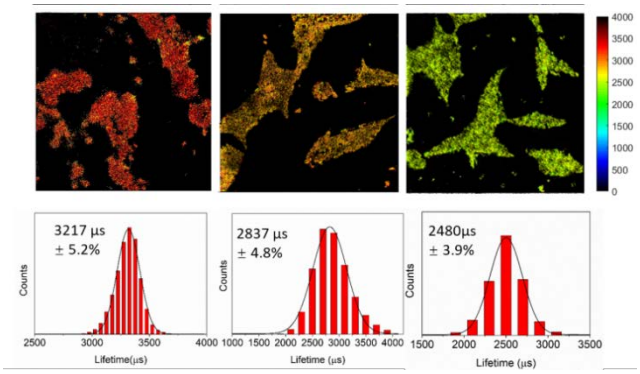

Figure 1: Pseudo-colour-mapped lifetime images of nanoruby labelled AtT20 MOR receptors acquired by lifetime imaging, with the photoluminescence lifetime, calculated from pixels corresponding to each sample in the lifetime image. After [4]

References:

1. F. Ritort, *J. Physics: Condensed Matter* **18,** R531-R583 *(*2006)
2. Y Fan, P Wang, Y. Lu, R. Wang, L. Zhou, X. Zheng, X. Li, J Piper, F. Zhang, *Nature Nanotech* **13,** 941. (2018)
3. A. Edmonds, M Sobhan, V Sreenivasan, E Grebenik, J Rabeau, E Goldys, AV Zvyagin, *Particle & Particle Systems Characterization***, 30** 506-513. **(**2013)
4. X. Yang, A. Maleki, N. Lipey, X. Zheng, M. Santiago, M. Connor, V. Sreenivasun, J. Dawes, Y. Lu, A. Zvyagin, *ACS Sensors* **6,** 1375-1383 (2021)

Terahertz topological meta-devices

Quanlong Yang[1], Dongyang Wang[2], Sergey Kruk[1], Mingkai Liu[1], Ivan Kravchenko[3], Yuri Kivshar[1], and Ilya Shadrivov[1]

[1]*Nonlinear Physics Center, School of Physics, Australian National University, Canberra ACT 2601, Australia*

[2]*Department of Physics, The Hong Kong University of Science and Technology, Clear Water Bay, Hong Kong 999077, China3*

[3]*Center for Nanophase Materials Sciences, Oak Ridge National Laboratory, TN 37831, USA*
email: quanlong.yang@anu.edu.au

***Abstract**: We introduce a range of topological meta-devices for on-chip terahertz photonics. We demonstrate the valley-locked energy flow in these topological meta-devices. The proposed devices include waveguides, splitters, couplers and resonators.*

Terahertz photonics is well known as a powerful and promising tool for bio-sensing, nondestructive imaging or detection, and next-generation communication technologies (6G and beyond). However, the existing terahertz devices are often bulky and lossy, and this limits their applicability in advanced technologies. Meta-optics offers pathways towards miniaturization and integration of photonic devices and systems. Meta-devices based on free-standing dielectric membrane at the subwavelength scale are of practical importance as they remove many limitations experienced by devices on substrates.[1, 2]

Recent discoveries of photonic topological insulators reveal that such materials may support robust edge states that are immune to disorder and sharp corners. Early approaches to the topological phases rely on an external magnetic field or a careful design which hinders the widespread implementation. Meanwhile, great efforts have been put into the study of valley-Hall photonics crystals (VHPCs), which support robust edge modes inside a photonic bandgap, but they do not require time-reversal symmetry breaking.[3, 4]

The combination of meta-optics and topological photonics offers pathways toward miniaturization and integration of terahertz photonics. We propose topological meta-devices for on-chip terahertz photonics and demonstrate valley-locked asymmetric energy flow and mode conversion of two types of domain walls. Our topological meta-devices leverage new on-chip integration of terahertz photonics inspired by valley-hall photonics crystals, and their characterization via terahertz near-field setup, which allows us to selectively excite individual domain walls, and map field distributions around them. Our topology-empowered meta-devices present additional degrees of freedom for topological edge state manipulation in comparison with conventional dielectric or surface plasmon waveguides, and it paves the way for the development of a robust and efficient platform for terahertz on-chip communication, sensing, and multiplexing systems.

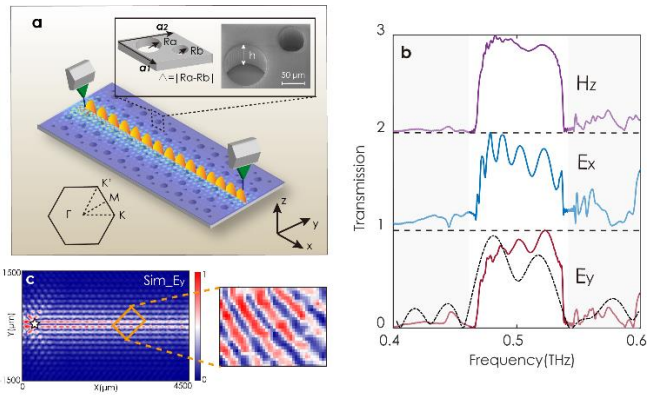

Figure 1: (a) Schematic of topological membrane meta-devices and terahertz near-field scanning microscope systems.(b) Calculated (solid line) and measured (dashed line) transmission curves of E_x, E_y and H_z for the topological straight waveguide.(c) Calculated in-plane E_y magnitude distribution for the straight topological waveguide at 0.5 THz. The inset is the measured E_y field distributions of topological waveguide.

Figure 1a illustrates the schematic design of topological meta-devices: a low-index (air) circular hole pairs are cut in a high-index (silicon) wafer. The meta-atoms are arranged in a rhombus lattice with spacing a = 170 μm, and thickness of the Si membrane is h = 90 μm. Here, we focus on the transverse-electric (TE)-like mode where the electric field lies in the x-y plane. This topological waveguide supports two counter-propagating edge modes with different valley-polarizations, for simplicity, only the forward propagating (along the positive x-direction) edge mode is considered here (σ+). Figure 2c shows the calculated transmission spectra of the topological waveguide (solid line), where an electric dipole is used

to excite the edge state in the simulation. A distinct transmission window from 0.46 THz to 0.54 THz can be clearly seen from the normalized transmission spectra for all the E_x, E_y and H_z components.

In the experiment, a terahertz near-field scanning spectroscopy is employed to characterize the performance of topological meta-device. The employed system includes a near-field excitation source and a near-field detection probe, as shown in Fig. 1a. Such configuration allows us to selectively excite individual waveguides, and map field distribution around them. The measured transmission spectra are shown in Fig. 1b as the dashed line for E_y polarization, and an excellent agreement is seen with the calculated results. The best experimental transmission efficiency reaches 94.7% at 0.48 THz over the distance of 0.5 mm.

In Figure 1c, we show the in-plane electric field (E_y) profile from simulation for 0.5 THz, where the TE-like field profile is presented. The edge modes are excited by the dipole source placed near the left edge of the sample and propagate along the x-direction, the field is confined to the straight waveguide, and it penetrates into each lattice by approximately five periods. The inset of Fig. 1c shows the experimentally measured electric field for the E_y component, a rectangle region as marked by the orange rectangle is selected for the detailed experimental scan. The measured field demonstrates a good agreement with simulation results.

In summarry, we have designed and demonstrated terahertz topological meta-devices based on VHPCs for integrated on-chip systems. Valley locked edge modes at discrete domain walls are utilized for mode coupling and conversion. The employment of a terahertz near-field spectroscopy system allows us to directly characterize and visualize the valley-locked edge state on our proposed topological devices. This demonstration opens a direct avenue towards terahertz topological on-chip photonic networks for next-generation wireless communications and quantum computing.

References:

1. Yang Q, et al. *Adv. Func. Mater*. **30**, 1906851 (2020).
2. Yang Q, et al. *Adv. Opt. Mater*. **8**, 2000555 (2020).
3. Yang Y, et al. *Nat. Photon*. **14**, 446-451 (2020).

Meta-optics for edge detection and enhanced phase contrast imaging

L. Wesemann[1], J. Rickett[2], J. Song[2], J. Lou[2], E. Hinde[2], T.J. Davis[2], and A. Roberts[1]

[1]*ARC Centre of Excellence for Transformative Meta-Optical Systems, School of Physics, The University of Melbourne, Victoria 3010, Australia*
[2] *School of Physics, The University of Melbourne, Victoria 3010, Australia*
email: ann.roberts@unimelb.edu.au

***Abstract**: Phase contrast imaging methods are widely used for studying weakly absorbing samples such as live cells, but conventional approaches involve either bulky optics or are computationally intensive. Here, the use of nanoscale resonant gratings and other thin film structures for enhancing images of both amplitude and phase objects is presented.*

The modification of images to enhance the appearance of edges, remove noise or enhance phase contrast is ubiquitous in contemporary image processing with applications in fields as diverse as machine vision, remote sensing and microscopy. The increasing amount of data required in many of these applications, however, is accompanied by corresponding increases in energy consumption, the time required to process images and the bandwidth necessary to transmit data from location to location. Furthermore, images obtained by conventional cameras do not capture information about phase variations within an optical field arising from transmission through transparent objects such as cells.

Prior to the advent of computational image processing, all-optical spatial filtering systems capable of real-time modification of both amplitude and phase images attracted widespread attention. The bulky nature of these systems is, however, generally incompatible with the miniaturisation of digital systems including cell phones and mobile platforms such as drones. The emergence of meta-optical and other nanophotonic systems provides an opportunity to develop compact all-optical systems capable of real-time image processing. This presentation discusses plasmonic approaches to enhancing the contrast of both amplitude and phase images with a particular focus on real-time imaging of transparent biological cells.

Conventional all-optical image processing requires the introduction of spatial filtering elements into the Fourier plane of an image accessed by a lens. A second lens recovers the processed image. These filters can modify the amplitude and/or phase of the angular spectrum of the image and typical systems have overall dimensions of the order of centimetres. Here we discuss the use of nanophotonic devices for performing 'object plane' filtering where the spatial frequency content of an image is modified directly by the device which can have thicknesses many orders of magnitude smaller. We have previously investigated reflection devices based on thin films [1] and the excitation of bound modes in the continuum [2,3] as well as transmission devices with both symmetric [4] and asymmetric [5] responses to spatial frequency.

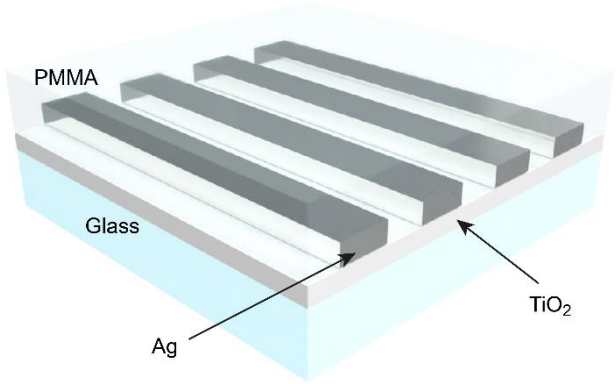

Figure 1: Resonant waveguide grating.

Here we discuss the use of resonant waveguide gratings consisting of an array of silver patches or gratings on a thin film of high index material (TiO_2) supported by a glass substrate and coated with PMMA (Fig. 1). The device composed of patches performs operations in two transverse dimensions, while the grating device responds to only spatial frequencies orthogonal to the grating lines. We demonstrate the application of these devices to the edge enhancement of images and the visualization of phase gradients produced by transparent objects including unstained biological cells [6].

References:

1. L. Wesemann, *et al.*, *APL Photonics* **4**, 100801 (2019).
2. L. Wesemann, *et al.*, *OSA Continuum* 1: 727-735, (2018).
3. L. Wesemann, *et al.*, *Proc. SPIE Micro+ Nano Materials, Devices, and Applications*, Melbourne, Australia, 112010F (2019).
4. F. Eftekhari, D. Gómez, and T. Davis, *Opt. Lett.* **39**, 2994 (2014).
5. T.J. Davis, *et al.*, *Phys. Rev. Lett.* **123**, 013901 (2019).
6. L. Wesemann, *et al.*, *Light: Sci. Appl*. **10**, 98 (2021).

Polarisation-independent gratings for high-reflectivity LCoS in near-infrared

Sangeeth S. Thandasseril[1], Alexander S. Solntsev[1], Mikhail Lapine[1], and Chistopher G. Poulton[1]

[1]School of Mathematical and Physical Sciences, University of Technology Sydney, *NSW* 2007, *Australia*
email: SangeethSoman.Thandasseril@student.uts.edu.au

***Abstract**: We have numerically optimised a reflectivity from cross-linked gratings to increase the efficiency of liquid crystal on silicon (LCoS) devices. For two different designs, we have observed the significant polarisation-independent increase in the reflectivity in telecommunication C-band and in 40nm wavelength range around 1.064 micron.*

HCG: High contrast grating LCoS: Liquid crystal on silicon

LCoS devices are known to suffer diffractive losses associated with a structure consisting of a two-dimensional array of individually addressable metallic pixels. Previous efforts to remove these losses employed Bragg reflector mirrors [1] and diffractive gratings [2,3]. A grating-based design is particularly elegant, since the effective cavity length is reduced compared to Bragg mirrors. In this work, we employ a cross-linked high-contrast grating (HCG) [4] to significantly increase the reflectivity of LCoS pixel structure in two broad wavelength ranges for both *s* and *p* polarisations.

The proposed structure consists of a cross-linked silicon HCG [Fig. 1(a)] with rectangular rod cross-section [Fig. 1(b)] on top of a bi-periodic aluminum pixel structure with dimensions typical for LCoS [2]. The 90° rotational symmetry of HCG provides the polarisation-independent reflectivity. The addition of HCG on top of the pixels of conventional LCoS increases the reflectivity of *p* and *s* reflectivity components from 92% to 100% at the wavelength of 1064 nm [Fig. 2(a)] and from 88% to 99.3% at the wavelength of 1550 nm [Fig. 2(b)]. For the simulation of the diffraction efficiency, we used rigorous coupled wave analysis (RCWA) using GD-Calc; the optimisation was performed using two dimensional grid optimisation.

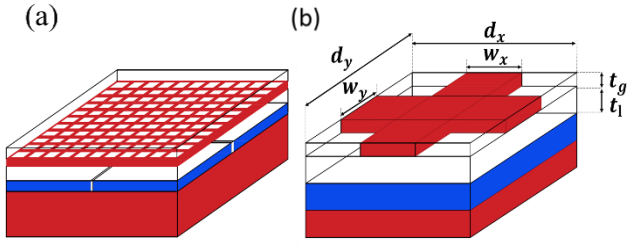

Figure 1: (a) schematic of high-contrast silicon grating on top of conventional LCoS pixels. (b) The unit cell of HCG.

In conclusion, we have optimised the design of cross-linked HCG to increase the performance of LCoS in two most highly though-after wavelength ranges in near-infrared

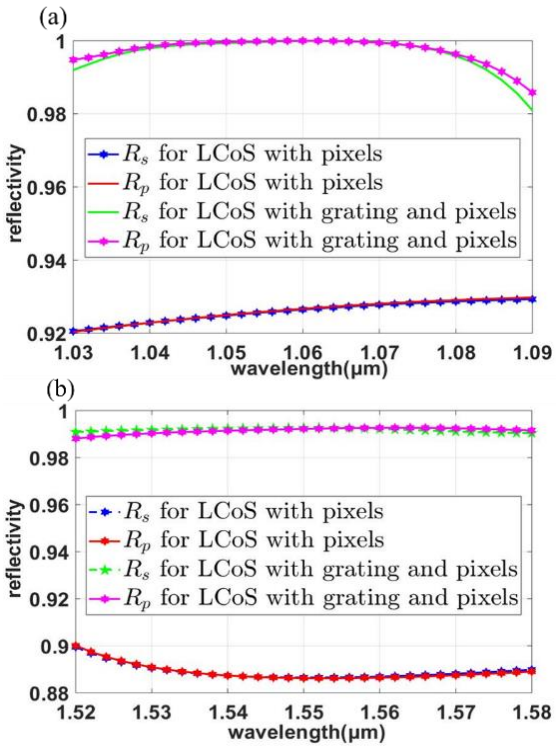

Figure 2: (a, b) The increase of R_s (pink) and R_p (green) reflectivity provided by the inclusion of the HCG with optimised parameters compared to R_s (red) and R_p (blue) for conventional LCoS at 1064 nm (a) and 1550 nm (b).

References:

1. H. Yang and D. Chu, "Digital phase-only liquid crystal on silicon device with enhanced optical efficiency," OSA Continuum 2, 2445-2459 (2019).
2. S. J. Frisken, Q. Wu, High reflectivity LCOS device, US10302995B2 (2015).
3. I.-S. Chung, V. Iakovlev, A. Sirbu, A. Mereuta, A. Caliman, E. Kapon, and J. Mørk, "Broadband MEMS-tunable highindex-contrast subwavelength grating long-wavelength VCSEL," IEEE J. Quantum Electron. 46, 1245–1253 (2010)
4. K. Ikeda, K. Takeuchi, K. Takayose, I. Chung, J. Mørk, and H. Kawaguchi, "Polarization-independent high-index contrast grating and its fabrication tolerances," Appl. Opt. 52, 1049-1053 (2013).

Tunable metasurfaces with electro-optic materials

Luyao Wang* and Ilya Shadrivov

ARC Centre of Excellence TMOS, Research School of Physics, Australian National University, Canberra, Australia
**Email: Luyao.wang2@anu.edu.au*

***Abstract**: We study all-dielectric optical metasurfaces containing lithium niobate. We explore several types of metasurfaces and study the tunability of transmission that can be achieved in the structures. Such tunability is of paramount importance for the development of fast ultra-thin electro-optical modulators.*

Metasurfaces are two-dimensional arrays composed of subwavelength elements (meta-atoms) that interact with the electric and magnetic fields of the incident electromagnetic waves, showing properties that are not found in nature. Metasurfaces can be used for beam forming, polarisation conversion and wavefront shaping. Properties of most metasurfaces, including operation frequency and bandwidth of wave-manipulation functionalities are fixed after fabrication, limiting their application in optical devices. There is a number of approaches that may allow creation of tunable devices, including the use of liquid crystals and MEMS structures [1]. One of the fastest known ways to modulate the properties of optical materials is by using electro-optic effect of lithium niobate (LN, $LiNbO_3$) whose properties change under applied external electric field. Here, we explore several metasurface structures containing LN.

When electric field is applied to LN, a linear electro-optic effect manifests in the change of the refractive index tensor [2]. The relationship between external electric field and refractive index is written as

$$\nabla\left(\frac{1}{n^2}\right) = \sum r_{ij}\overrightarrow{E_z} \qquad (1)$$

Where $\nabla\left(\frac{1}{n^2}\right)$ characterizes the changes of the relative permittivity (square of refractive index) caused by the applied electric field $\vec{E}$ along z direction, r_{ij} is the linear electric-optic coefficient tensor. The largest value of the tensor is r_{33} and by choosing appropriate crystalline axis of the LN we can maximize the electric-optic effect [3]. In our case, it is practical to use a z-cut film of the LN that will have the voltage applied to it at the top and bottom surfaces.

As an example, here we show a metasurface made of silicon disks placed on a surface of a z-cut LN substrate, see Fig. 1 (a). We use CST software to calculate light transmission properties of the structures. The thickness of the substrate is chosen to be 450 nm, the corresponding maximum applied voltage can reach 29 V before the electric breakdown occurs. Dependence of the transmission spectrum on wavelength and the disc radius is shown in Fig. 1 (b). We observe several resonances in the parameter range. To characterize these resonances, we performed multipole decomposition and analyzed the field structure at corresponding frequencies. Below the first resonance crossing, from left to right, these four resonances correspond to the magnetic dipole, electric dipole, guided mode of the LN substrate, and Fabry-Perot resonance in the substrate. We analyzed the achievable transmission amplitude and phase change that can be caused by applying voltage to the LN, and found that in this particular configuration, the strongest effects can be achieved by utilizing the guided mode.

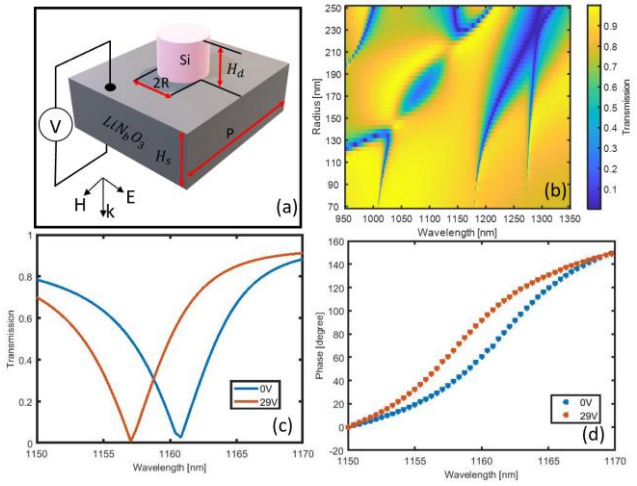

Figure 1: (a) Schematic of the unit cell. Silicon disk placed on the $LiNbO_3$ substrate. The thickness of the substrate H_s is 450 nm, the lattice constant P is 620 nm. R is the silicon disk radius, the height of the disk H_d is 200 nm. (b) Two-dimensional figure. When disks radius varies from 70 nm to 250 nm, their transmission spectra change simultaneously. (c) Guided mode transmission at 0 V (blue line) and 29 V (red line) when R is 126 nm. (d) The phase of guided mode at 0V (blue star line) and 29 V (red star line).

The results for the guided mode-induced tunability are shown in Fig 1 (c,d). There is 35 degrees phase difference between 0V and 29V external stimuli. We will further discuss other metasurfaces that can produce stronger effects using Mie resonances.

References

1. I.V. Shadrivov and D.N. Neshev, World Scientific Handbook of Metamaterials and Plasmonics, 387 (2017)
2. R.S. Weis, et al. Appl. Phys. A **37,** 191 (1985)

Direct Assembly of Single Nanocrystal Arrays

Heyou Zhang[1] and Paul Mulvaney[1]

[1] *ARC Centre of Excellence in Exciton Science, School of Chemistry, University of Melbourne, Parkville, Vic. 3010, Australia*
email: heyouz@student.unimelb.edu.au

***Abstract**: In this article, we introduce a universal method for assembling of single nanocrystal arrays. The method is based on the Electrophoretic Deposition. Nanocrystals with different sizes, shapes and species are all successfully assembly into single particle arrays.*

Nanocrystals have remarkable, size-dependent properties and their discovery has promoted the development of solar cells, displays, optics and new electronic architectures. To date, most nanocrystals have been made through wet chemical methods. However, there remains a fundamental challenge to incorporate these nanocrystals into solid-state devices. Directed assembly assembles pre-synthesised nanomaterials onto a pre-patterned substrate by application of an external force.

In this article, I will introduce Electrophoretic Deposition (EPD) assembly method, which, we believe, holds great potential as a universal assembly method for large scale fabrication with high controllability and nanometre precision. Our method is derived from the electrophoresis phenomenon of charged nanocrystals under the influence of external electric field. In combine with the lithography patterned substrate, the nanocrystals can be directly assembled from colloid onto a solid-state substrate. By tunning the parameters, such as applied electric field, electrolyte concentration and time, single particle level deposition with nanometre precision and perfect orientation control can be achieved through our EPD method.

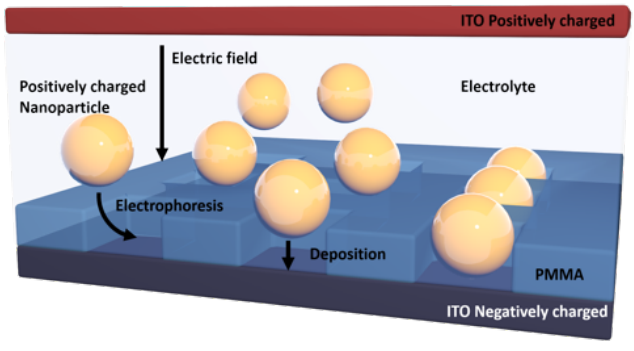

Figure 1. Schematic of the EPD process showing nanospheres deposited onto EBL fabricated ITO-PMMA template (dimensions not to scale).

Our EPD method has been carried out for a variety of nanocrystals including: gold particles with different morphologies, 9,10-bis(phenylethynyl) anthracene organic nanoparticles, Fe_3O_4 nanoparticles and quantum dot (QD) semiconductors, as shown in Figure 2. We discuss the role of the applied electric field, electrolyte concentration, the surface charge on the nanoparticle, and the template geometry. These data demonstrate that EPD assembly has the potential to be a universal method of nanoparticle fabrication.

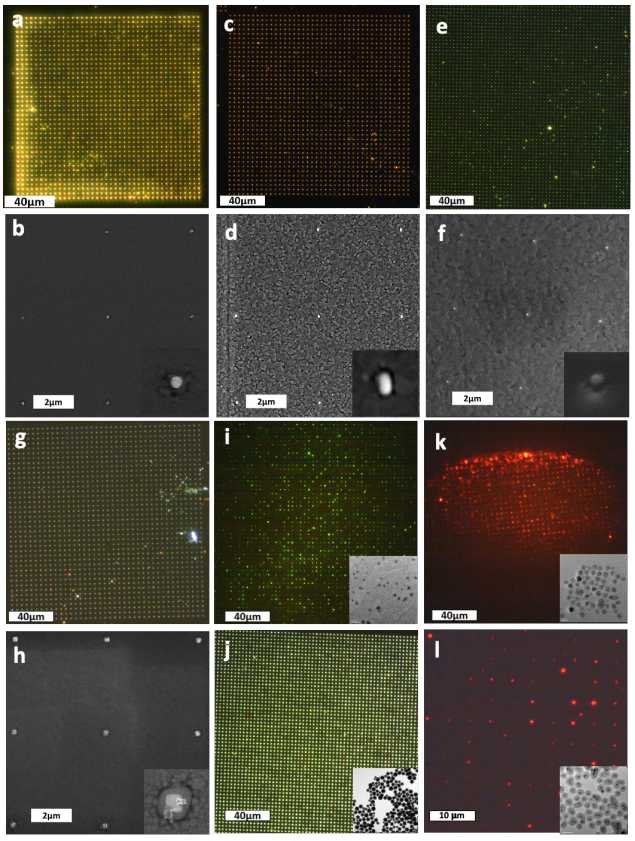

Figure 2. Results of EPD direct assembly. Gold nanocrystals with shape of spheres (a, b), rods (c, d), vertical rods (e. f), cubes (g, h), organic nanoparticles (i). Fe3O4 nanoparticles (j), QDs (k), and SiO2 coated QDs (l).

Reference:

1. H. Zhang, et al. Advanced. Materials. 2020, 32, 1904551.
2. H. Zhang, et al. ACS Nano 2018, 12 (8), 7529-7537.
3. H. Zhang, et al. Advanced Functional Materials. 2020, 2006753.

Strong coupling in all-perovskite metasurface via bound state in the continuum

I. A. M. Al-Ani[1], K. As'Ham[1], L. Huang[1], A. Miroshnichenko[1], and H. T. Hattori[1]

[1] *School of Engineering and Information Technology, University of New South Wales at Canberra, Northcott Drive Canberra ACT 2610 Australia*
email: i.al-ani@student.unsw.edu.au

***Abstract**: We have demonstrated ultra-strong coupling with Rabi-splitting value of 375 meV in a high Q optical cavity based on all-perovskite nanostructure by exploring the physics of bound states in the continuum (BIC)*

Recently developed halide perovskite semiconductors have been viewed as an excellent platform to realize exciton-polariton at room temperature due to their large oscillation strength. Plasmonic resonators, such as metal nanoparticles and nanogap resonators, have been used to produce large Rabi-splitting values, mainly due to their ultrasmall mode volume[1]. However, metals have intrinsically high damping losses and heat up fast, degrading their performance over time. The conventional DBR-based cavities have also been proposed for strong coupling realization, however, such cavities have limited Q-factor, which induce the insufficient cavity polariton lifetime that prevents the realization of a polariton condensate. On the other hand, an all-dielectric optical cavity with a high Q-factor is a more attractive way to achieve strong coupling.

we use phenethylammonium lead iodide (PEPI) perovskite with the chemical formula $(C_6H_5C_2H_4NH_3)_2PbI_4$ as an example to illustrate the strong coupling between exciton and QBICs. The dielectric function of the PEPI perovskite material is given by the Lorentz oscillator model as follows:

$$\varepsilon(E) = n^2 + \frac{f}{E_{PEPI-exciton} - E^2 - i\Gamma E} \qquad (1)$$

where n= 2.4 is the background dielectric constant, $E_{PEPI\text{-}exciton}$ = 2.394 eV is the exciton energy, Γ = 0.03 eV is its homogeneous linewidth, and f = 0.85 eV^2 is the constant related to its oscillator strength[2]. The substrate is made of silica with the refractive index n_s=1.46 in the visible wavelength range. Initially, we have investigated the Q-factor as a function of the structure period at normal incidence while fixing other structure parameters at W=200nm, T=180nm, G=50nm, and C=10nm, respectively as shown in **Fig 1a**. Introducing the asymmetric slits within the NW induces the transition from BIC into QBIC, allowing it to be coupled to the plane wave excitation. **Fig 1b** shows the mapping data of absorption spectra as a function of the period of QBIC structure coupled to exciton in the PEPI perovskite material with a 180 nm thickness. A clear anti-crossing behavior is observed, indicating the strong light-matter coupling and formation of cavity polaritons half-light half-matter bosonic quasiparticles. To optimize the strong coupling between QBIC and PEPI exciton, we have studied the effect of the Q-factor and the thickness of the PEPI grating on the value of the Rabi-splitting. **Fig 1c** shows the Rabi splitting at different Q-factors, while **Fig 1d** shows Rabi-splitting as a function of the height of PEPI NW. It can be observed that the Rabi-splitting increases gradually with the increase of Q-factor and height of NW until it saturates at Q ~ 800 and T~180 nm.

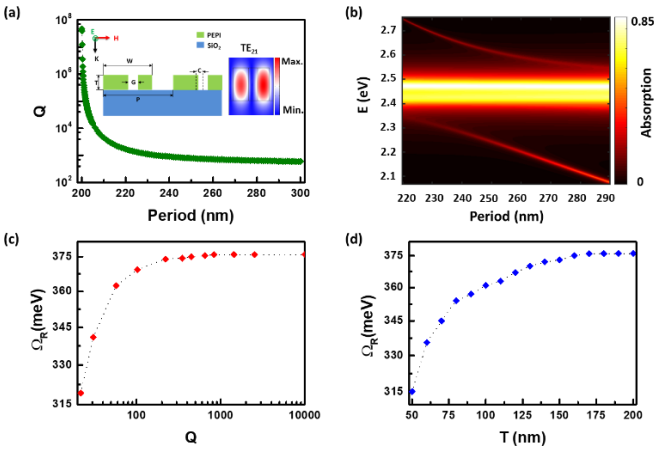

Figure 1: (a) Q-factor as a function of the period of the structure (b) absorption spectra as a function of the period of QBIC structure (c) and (d) Rabi-splitting as a function of Q-factor and height of the structure, respectively.

Therefore, in our report, we have proposed a high Q optical cavity by exploring the physics of bound states in the continuum (BIC) based on all-perovskite nanostructure to demonstrate ultra-strong coupling with a high Rabi-splitting value, which may help to significantly reduce the threshold of polariton lasing and enables the observation of polariton-condensation.

References:

1. Shang, Q.; Zhang, S.; Liu, Z.; Chen, J.; Yang, P.; Li, C.; Li, W.; Zhang, Y.; Xiong, Q.; Liu, X.; Zhang, Q. *Nano Letters* **2018,** 18, (6), 3335-3343.
2. Zhang, S.; Audebert, P.; Wei, Y.; Al Choueiry, A.; Lanty, G.; Bréhier, A.; Galmiche, L.; Clavier, G.; Boissière, C.; Lauret, J.-S.; Deleporte, E. **2010,** 3, (5), 3385-3406.

Selective Area Growth of InGaAs/InP Multiple Quantum Well Nanowire for Optoelectronic Device Applications

Fanlu Zhang[1,3], Xutao Zhang[2], Ziyuan Li[1], Ruixuan Yi[2], Zhe Li[4], Naiyin Wang[1], Xiaoxue Xu[7], Zahra Azimi[1], Li Li[5], Mykhaylo Lysevych[5], Xuetao Gan[2], Yuerui Lu[6], Hark Hoe Tan[1,3], Chennupati Jagadish[1,3], and Lan Fu[1,3]

[1] *Research School of Physics, The Australian National University, Canberra, ACT 2601, Australia*
[2] *School of Physical Science and Technology, Northwestern Polytechnical University, Xi'an, Shaanxi 710129, China*
[3] *Australian Research Council Centre of Excellence for Transformative Meta-Optical Systems, Research School of Physics, The Australian National University, Canberra, ACT 2601, Australia*
[4] *Advanced Research Computing, Virginia Tech, Blacksburg, VA 24061, USA*
[5] *Australian National Fabrication Facility ACT Node, Research School of Physics, The Australian National University, Canberra, ACT 2601, Australia*
[6] *Research School of Electrical, Energy, and Materials Engineering, College of Engineering and Computer Science,, The Australian National University, Canberra, ACT 2601, Australia*
[7] *Institute for Biomedical Materials and Devices (IBMD), Faculty of Science, University of Technology Sydney, NSW 2007, Australia*
email: lan.fu@anu.edu.au

***Abstract**: Miniaturized light sources and detectors are important component for the development of highly integrated optical systems. Here, we present a new strategy for growth of InGaAs/InP multiple quantum well (QW) nanowire array by selective area metalorganic vapor phase epitaxy. The nanowire exhibit excellent optical properties with room temperature optically pumped lasing at the wavelength of ~1 μm. Photoconductive detector based on n^+-i-n^+ InGaAs/InP 40-QW nanowire are demonstrated with broadband response (400 – 1600 nm) and high responsivities of 2175 A/W at 980 nm. High quality nanowire based on this growth strategy is promising for the development of future nanoscale optoelectronic devices.*

Owing to the small footprint and quasi-one-dimensional geometry, nanowire could be monolithically grown on various substrate with large lattice mismatch, which provide the promising compatibility with complementary metal oxide semiconductor (CMOS) technology for next generation on-chip optoelectronic devices [1].

III-V semiconductor nanowires integrated with quantum wells (QWs) are especially attractive for miniaturized photodetectors and light sources. However, most of the reported InGaAs/InP QW nanowires are based on wurtzite crystal structure and exhibit non–uniform morphology due to the complex heterostructure growth, making it challenging to incorporate multiple-quantum wells (MQW) for desired applications. [2]

In this work, we present selective area growth of InP nanowire with mixed zincblende and wurtizte crystal structure. The nanowire exhibit excellent optical quality with ~1 ns minority carrier lifetime, which could work as ideal platform for the subsequent InGaAs MQW growth. Based on the {110} faceted InP nanowire, InGaAs/InP nanowire with 5-, 10, 20 and 40 QWs are successfully demonstrated. Benefiting from the uniform morphology, the nanowire could form a Fabry–Pérot cavity and room temperature lasing was demonstrated under pulsed laser excitation, indicating the superior structural and optical properties.

Based on on n^+-i-n^+ InGaAs/InP 40-QW nanowire, broadband near-infrared photodetector was further demonstrated with high responsivities of 2175 A/W at 980 nm, outperforming those of conventional planar InGaAs photodetectors [2].

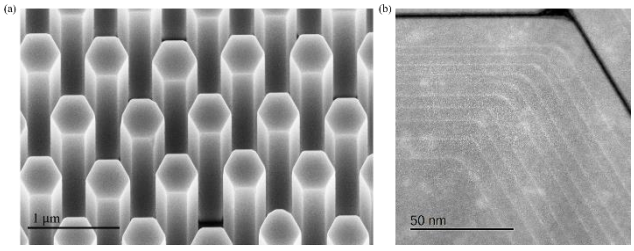

Figure 1: SEM (a) and TEM (b) image of representative InGaAs/InP MQW nanowire [2].

In summary, we present a new strategy for growth of InGaAs/InP MQW nanowire. The nanowire demonstrate excellent optical and electrical performance, which could pave way for future nanoscale optoelectronic applications.

References:

1. Chen, R., Ng, K., Ko, W. et al., *Nat Commun 5, 4325 (2014)*

2. Zhang, F., Fu L., et al., *Adv. Funct. Mater.* 2103057 (2021).

Aberration correction for printed microstructures

D. Armstrong[1], A. Stilgoe[1], and H. Rubinsztein-Dunlop[1]

[1]*School of mathematics and physics, The university of Queensland, QLD, 4067, Australia*
email: declan.armstrong@uq.edu.au

***Abstract**: Two-photon photopolymerised microstructures can be produced using structured light produced by a spatial light modulator (SLM) illuminated by a femtosecond laser. These structures are used in a broad variety of optical tweezers experiments. However, distortion throughout the optical train cause less than ideal focusing of the beam, reducing the achievable resolution. We quantify how these aberrations affect printing quality and how they can be corrected in-situ using an SLM.*

By exposing UV curing resin to a focused femtosecond laser, polymerized voxels can be stacked to form high resolution microscopic structures and used for optical tweezers experiments. These structures have far reaching applications in the study of molecular biology, fluid dynamics and colloidal sciences.

Common methods of printing include scanning a piezo-electric stage to trace out a predefined bitmap, or by deflecting the beam using a spatial light modulator (SLM). Ultimately, the resolution of these structures is limited by the size of the volume capable of exceeding the resins polymerization threshold [1]. Imperfections throughout the optical train lead to significant aberrations that increase this volume and negatively affect efficiency and printing quality.

Using an in-house inverted microscope with a femtosecond laser to illuminate an SLM, we quantify the effects of these aberrations and compare *in-situ* aberration correction techniques [2,3]. By analyzing interference patterns from partitioning regions of an SLM, we can reconstruct the beam amplitude and associated phase correction pattern irrespective of where in the optical train such distortions are introduced.

We analyze the limitations and computational trade-off of these techniques using an iterative algorithm and show that such corrections will be a necessary factor for holographic optical tweezers systems utilizing multiple focused spots. Such aberration correction techniques have applications in a range of optical experiments including microfabrication, microscopy and optical trapping through disordered media.

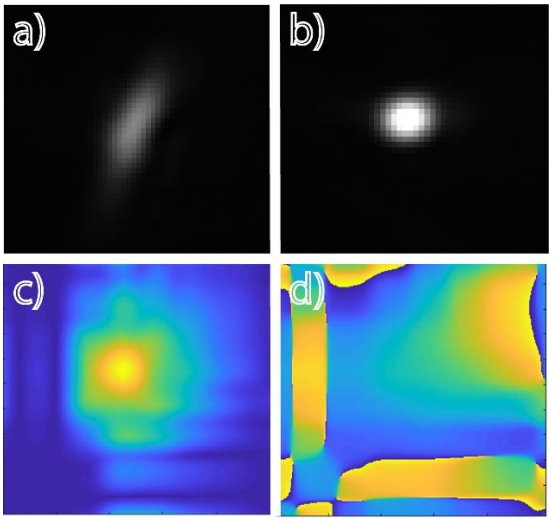

Figure 1: a) Uncorrected focused beam from a femtosecond laser. b) Aberration corrected focused beam. c) Beam amplitude on a spatial light modulator (SLM). d) Phase correction pattern displayed on SLM, used to construct a).

References:

1. A. Ostendorf and B. Chichkov, *Photonics Spectra*, 40.0 (2006).

2. T. Čižmár, M. Mazilu and K. Dholakia, *Nature Photonics* 4, 388-394 (2010).

3. A. Stilgoe and H. Runinsztein-Dunlop, *J. Opt.* 23, 085602 (2021).

An Integrated Platform for Superfluid Optomechanics

W. W Wasserman, R. A. Harrison, Y. L. Sfendla, C. G. Baker, G. I. Harris, A. Sawadsky and W. P. Bowen

ARC Centre of Excellence for Engineered Quantum Systems, School of Mathematics and Physics, The University of Queensland, St Lucia, Queensland 4072, Australia.
email: w.wasserman@uq.edu.au

***Abstract**: Superfluid is an extremely desirable medium for quantum optomechanics, however typically requires complex experimental apparatus. Here an integrated approach solves these complexities, requiring only a standard cryogenic system with optical fiber access.*

As a quantum fluid, superfluid ^{4}He has fascinating properties; it is highly deformable, demonstrates irrotational and nonviscous flow, has quantized vortices [1], has high thermal conductivity, and can self-assemble into thin films on all surfaces of a container [2]. These properties are of particular interest in quantum optomechanics but come with stringent experimental requirements—superfluids can leak through gaps which even gases find impermeable. This becomes complex with the need for custom cryogenic systems with connections for optical and electrical access to the experiment (see figure 1 for images). A simplified alignment-free approach to integrated superfluid optomechanics is presented, solving these requirements and requiring only optical fiber access within a standard cryogenic system. This is done by leveraging a standard silicon-on-insulator (SOI) platform, allowing novel superfluid optomechanical circuits to be designed. The result is a simple, robust, and flexible set-up. This approach is used to trap sound in superfluid using light, confine sound in superfluid phononic crystals [3], and achieve strong Brillouin (light-sound) coupling [4].

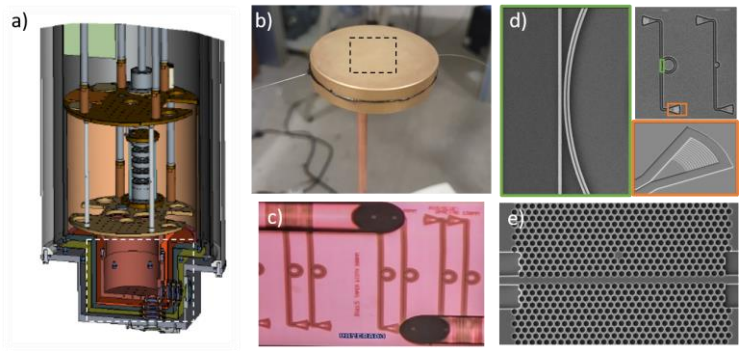

Figure 1: Superfluid experiment simplification. (a) The previous system - a modified dilution refrigerator with optical and electrical feedthroughs (5 IR windows, several electrical connections for motors). (b) The new fully sealed experiment, containing helium and a SOI photonic device. Simply securing the puck to the base of a cryogenic system with an optical fiber connection is sufficient. (c) Optical connection to the device can be via glued angle polished fibers. (d, e) SEM of photonic devices used in experiments.

References:

1. Y. Sachkou, et al., Science 366 6472 (2019).

2. G. Harris, et al., Nature Phys 12 788 (2016).

3. Y. Sfendla, et al. npj Quantum Inf 7 62 (2021).

4. G. Harris, et al., Opt. Express 28 22450 (2020).

Superfluid Brillouin Optomechanics

C. Baker, X. He, G. Harris, A. Sawadsky, W. Wasserman, R. Harrison, Y. Sfendla and W. Bowen

ARC Centre for Engineered Quantum Systems, School of Mathematics and Physics, The University of Queensland, Brisbane, Queensland 4072, Australia
email: c.baker3@uq.edu.au

***Abstract**: In this talk, I will present how the unique features of superfluid helium (absence of viscosity, high compliance, negligible optical absorption…) make it a compelling material for Brillouin scattering applications.*

Brillouin scattering has applications ranging from signal processing, sensing and microscopy to quantum information and fundamental science. Most of these applications rely on the electrostrictive interaction between light and phonons. In this talk, I will show how in liquids optically-induced surface deformations can provide an alternative and extremely efficient interaction. This is achieved here using a thin superfluid helium film covering the surface of an optical WGM resonator, as shown in Fig. 1, top. This system allows the demonstration of ultralow-threshold Brillouin lasing and strong phonon-mediated optical coupling [1], as well as the ability to tune between a standing wave `optomechanics-like' interaction and a travelling-wave Brillouin interaction. Configured as a Brillouin gyroscope this provides the prospect of measuring superfluid circulation with unprecedented precision, and exploring the rich physics of quantum fluid dynamics, from quantized vorticity to quantum turbulence [2].

I will also present experimental progress towards an on-chip liquid-based Brillouin system that is predicted to exhibit large phonon-photon coupling with exceptionally low acoustic dissipation. The system is comprised of a silicon-based slot waveguide filled with superfluid helium [3], (see Fig. 1, bottom). This type of waveguide supports optical and acoustical traveling waves, strongly confining both fields into a subwavelength-scale mode volume. It serves as the foundation of an on-chip traveling wave Brillouin resonator with a predicted electrostrictive single photon optomechanical coupling rate exceeding 240 kHz.

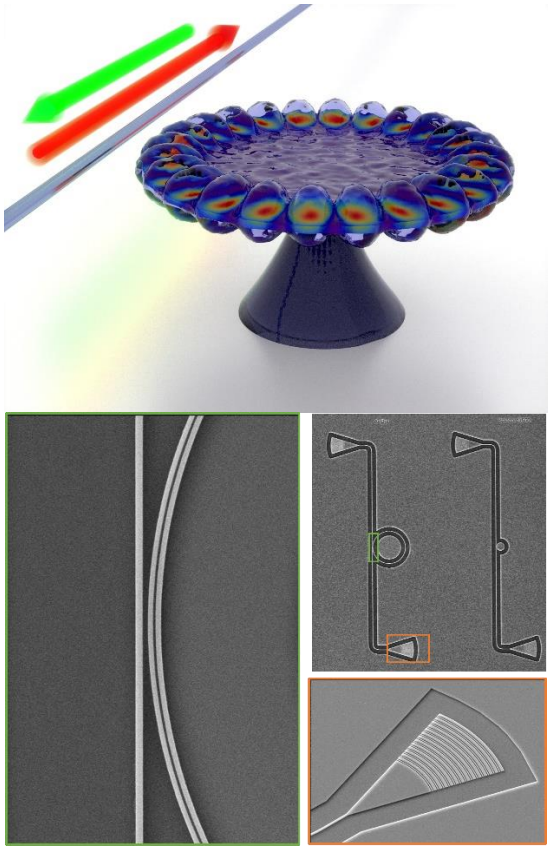

Figure 1: Top: Illustration of the backward Brillouin scattering process in a superfluid-covered optical resonator. Bottom: Silicon on insulator slot waveguide resonator.

References:

[1] X. He, G. I. Harris, C. G. Baker, A. Sawadsky, Y. L. Sfendla, Y. P. Sachkou, S. Forstner, and W. P. Bowen, *Strong Optical Coupling through Superfluid Brillouin Lasing*, Nature Physics **16**, 4 (2020).

[2] Y. P. Sachkou, C. G. Baker, G. I. Harris, O. R. Stockdale, S. Forstner, M. T. Reeves, X. He, D. L. McAuslan, A. S. Bradley, M. J. Davis, and W. P. Bowen, *Coherent Vortex Dynamics in a Strongly Interacting Superfluid on a Silicon Chip*, Science **366**, 1480 (2019).

[3] G. I. Harris, A. Sawadsky, Y. L. Sfendla, W. W. Wasserman, W. P. Bowen, and C. G. Baker, *Proposal for a Quantum Traveling Brillouin Resonator*, Opt. Express, **28**, 22450 (2020).

Optical-to-mechanical state transfer through feedback in optomechanics

Amy van der Hel[1,2], J.S. Bennett[1,2], and W.P. Bowen[1,2]

[1]School of maths and physics, the University of Queensland, St Lucia, QLD 4072, Australia
[2]ARC Centre of Excellence for Engineered Quantum Systems, St Lucia, QLD 4072, Australia
email: a.vanderhel@uq.edu.au

***Abstract**: This work revisits ground state cooling through feedback which is an established result in optomechanics. In particular we are optimising the feedback to achieve optical-to-mechanical state transfer.*

For optomechanical systems in the high quality (Q) factor limit a set of approximations reduces the interaction term to a beam splitter type interaction. These approximations can be made as a result of the small optical cavity linewidth and driving the optical cavity detuned from the resonance frequency by -Ω. The beam splitter interaction ultimately is a direct state-transfer and allows for cooling of the mechanical oscillator to the ground state.

It is difficult to fabricate high Q optical resonators and often optomechanical systems are in the low Q limit. In order to achieve ground state cooling of mechanical resonators with low Q optical cavities, feedback cooling was introduced [1]. The feedback scheme uses the information of the position of the mechanical oscillator that can be obtained from the optical signal, to reduce the momentum of the oscillator. The feedback scheme has been implemented successfully in experiments to cool mechanical oscillators with optical cavities in the low Q limit [2].

We revisit the feedback scheme, to investigate the fluctuations of the mechanical resonator after feedback has been applied. In particular we optimise the feedback force to transfer the optical fluctuations on to the mechanical oscillator. Using this optimisation optical-to-mechanical state transfer fidelities as high as 0.970 are found.

We also present the spatio-temporal mode that is transferred to the mechanical oscillator. Using the information of the spatio-temporal mode we are aiming to extend this work to include transfer of non-Gaussian optical states to the mechanical oscillator. That would add to the on-going research into macroscopic quantum states.

A separate extension of this work is to include an additional cavity at microwave frequencies. That microwave cavity would be in the high Q limit. The optimised feedback found through this work, can be applied to achieve optical-to-microwave state transfer with the mechanical oscillator mediating the state transfer.

References:

1. S. Mancini and D. Vitali and P. Tombesi, *Phys. Rev. Lett.* **80**, 688 (1998).
2. K.H. Lee and T.G. McRae and G.I. Harris and J. Knittel and W.P. Bowen, *Phys. Rev. Lett.* **104**, 123604 (2010).

Microwave Photonic Notch Filter for Suppression of Multi-Band Interferers

Matthew Garrett[1,2], Yang Liu[1,2], Moritz Merklein[1,2], Duk-Yong Choi[3], Kunlun Yan[3]
Stephen J. Madden[3] and Benjamin J. Eggleton[1,2]

[1]*The University of Sydne Nano Institute (Sydney Nano), The University of Sydney, NSW 2006, Australia*
[2]*Institute of Photonics and Optical Science (IPOS), School of Physics, The University of Sydney, NSW 2006, Australia*
[3]*Laser Physics Center, Australian National University, Canberra, ACT, 2601, Australia*
email: matt.garrett@sydney.edu.au

***Abstract**: We present a chip-based microwave photonic notch filter with three independently tunable notches up to 11 GHz with depth of 40 dB. We simultaneously filter multiple interfering signals to demonstrate the effectiveness of this filtering scheme in enhancing performance of wideband radio frequency receivers.*

Signals used in radio frequency (RF) communications and sensing systems are moving to higher frequencies. This drives the need for RF filters that operate over larger frequency ranges to suppress unwanted interfering signals. Microwave photonics (MWP) is a key enabling technology that delivers RF systems with frequency agility and tunability unmatched by traditional RF electronic systems [1,2]. Accordingly, MWP filters implemented on chip-scale platforms with multiple notches, tunable over wide frequency ranges are vital to enhance performance and reduce the size of wideband RF receivers [3,4].

A recent demonstration of an MWP filter [5] utilized an over-coupled micro ring resonator (MRR) and on-chip stimulated Brillouin scattering (SBS) [6] to form an RF notch with wideband tunability to 12 GHz and notch depths of 40 dB. While this approach is attractive in achieving high-performance RF filtering, the system was limited by the wide 3-dB bandwidth and limited tunability of the single MRR on the As_2S_3 chip. Therefore, a new hardware platform capable of delivering multiple, independently tunable RF notches over a wide frequency range must be implemented to meet the demands of the modern RF spectrum.

In this work, we utilise high performance Si_3N_4 MRRs and on-chip SBS in As_2S_3 waveguides as the key elements of an MWP filter with multiple notches. Optical processing by overlapping independently tunable MRR and Brillouin gain resonances form multiple RF notches over a wide frequency range (1-11 GHz) with large rejection up to 40 dB.

The key to achieving an RF notch in this architecture is through spectrally localised destructive interference of RF photocurrents and is outlined in Fig. 1 (a). An RF signal is modulated onto a continuous wave probe laser through intensity modulation (IM). A series of MRRs process the upper sideband of the optical signal, each imparts a π phase shift at its resonant frequency. The frequency of the Brillouin pump laser is tuned such that the SBS and MRR resonances overlap. The magnitude of the SBS gain overcomes losses from the MRR response. Optical processing from cascaded MRR and SBS resonances forms a deep RF notch upon photodetection, through destructively interfering RF photocurrents. Notches are added in Fig. 1 (b) by using additional MRR and SBS resonances. We demonstrate RF filtering from 3-10 GHz with notch depths of 40 dB. Fig. 1 (c) demonstrates the suitability of this scheme for wideband RF receivers where two notches attenuate strong interfering signals at 7.8 GHz and 11.3 GHz, whilst leaving a desired signal at 9.5 GHz unaffected.

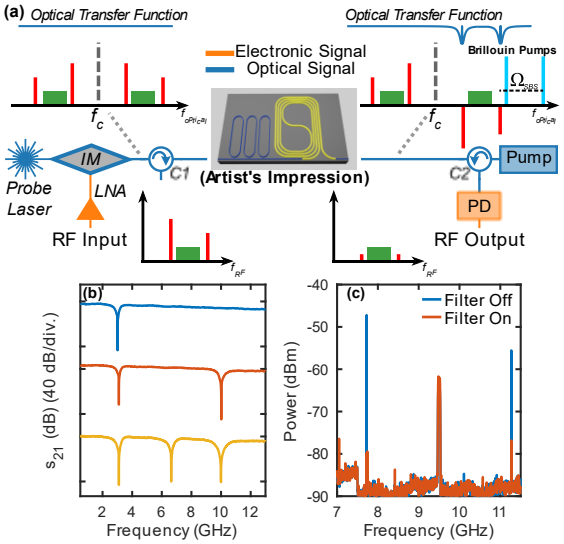

Figure 1: (a) Experimental setup and operating principle. LNA: Low-Noise Amplifier, IM: Intensity Modulator, C: Circulator, PD: Photodetector. (b) Wideband filter response tunability with multiple notches. (c) RF filtering over multiple frequency bands.

In conclusion, we demonstrated an MWP notch filter capable of removing multiple interfering signals over a wide RF frequency range, which plays a vital role in enabling next-generation wideband RF receivers.

References:

1. D. Marpaung, *Nat. Photonics* **13**, 80 (2019).
2. J. Yao, J. Light. Technol. **27**, 314 (2009)
3. Y. Liu *et al.*, *Adv. Opt. Photonics.* **12**, 485 (2020).
4. J. Capmany, J. Light. Technol. **24**, 201 (2006)
5. Y. Liu *et al.*, *APL Photonics* **4**, 106103 (2019).
6. B. Eggleton, *Nat Photonics* **13**, 664 (2019).

Ultra-deep image rejection mixer using stimulated Brillouin scattering in a chip-based platform

Luke McKay[1], Choon Kong Lai[1], Nicholas Athanasios[1], Duk-Yong Choi[2], Stephen J. Madden[2], Benjamin J. Eggleton[1], and Moritz Merklein[1]

[1]*Sydney Nano Institute (Sydney Nano), Institute of Photonics and Optical Science (IPOS), School of Physics, The University of Sydney,* Sydney, NSW 2006, Australia
[2]*Laser Physics Centre, The Australian National University,* Canberra, ACT, 2601, Australia

email: moritz.merklein@sydney.edu.au

***Abstract**: We demonstrate a microwave photonic chip-based mixer with ultra-deep image rejection using stimulated Brillouin scattering. We down-convert a signal from 11 GHz to 2GHz with -8dB conversion gain and 70 dB of image rejection.*

Frequency mixers are ubiquitous in modern radio frequency (RF) systems and are used to down-convert signals from the transmission frequency to an intermediate frequency (IF) where they can be detected by low frequency electronics [1]. However, signals with the same frequency separation between the local oscillator (LO) and the desired signal will down-convert to the same IF. This will induce distortion and cannot be removed with filtering after the down-conversion process [1]. This interfering component is referred to as the image.

Microwave photonics (MWP) can implement image rejection, and at the same time, enable very high carrier frequencies and broad bandwidths compared to electronic approaches. Image rejection has been shown in multiple ways [1], however, these demonstrations were implemented in optical fibre which are bulky and sensitive to environmental perturbations. Photonic integration significantly improves stability, while also reducing size, weight, and power (SWaP) characteristics.

Here, we build upon our previous SBS chip-based image rejection mixer [2] and significantly improve the image rejection while simultaneously reduce the required SBS gain. We demonstrate a chip-based ultra-deep image rejection mixer with 70 dB of image rejection. The image rejection was achieved with 5 dB of SBS gain generated by 20.1 dBm of optical pump power in a chalcogenide waveguide. The signal was down-converted from 11 GHz to 2 GHz, and we achieved a conversion gain of -8 dB and a spurious-free dynamic range (SFDR) of 87 $dB{\cdot}Hz^{2/3}$.

Initially, a laser is modulated by the LO at 9 GHz before continuing through to a second modulator driven by the RF signal (RF_{sig}) and image (RF_{img}) at 11 GHz and 7 GHz respectively (Fig. 1a). The modulated signal is coupled into a chalcogenide waveguide with a germanosilicate (Ge:SiO2) taper to reduce reflections from the chip-fiber interface [3]. On the chip the upper sideband component RF_{sig} is amplified by SBS gain (Fig. 1b).

After the chip, the optical signal is split into two paths, each path is filtered to retain the upper and lower sideband components of the carrier respectively (Fig. 1c) and each path is detected using a balanced photodetector (BPD) (Fig. 1d). The LO beats with the RF tones and produces the corresponding IF output signals. The components corresponding to RF_{img} are identical therefore destructively interfere, whereas the IF components corresponding to RF_{sig} are unbalanced due to the applied Brillouin gain and present at the output.

The down-converted component of RF_{sig} is measured on a spectrum analyzer and shown in Fig. 1e) in orange and RF_{img} in blue. There is 70 dB difference between the two down-converted components. The inset of Fig. 1e) shows RF_{sig} before down-conversion without SBS gain.

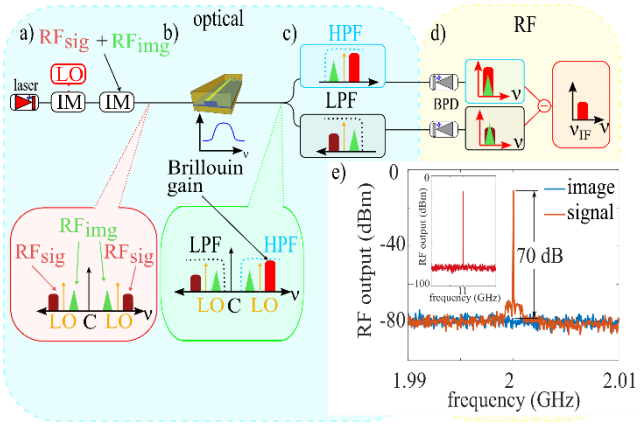

Figure 1: a-d) Image rejection mixer concept. e) Experimental result: An 11 GHz signal down-converted to 2 GHz (orange) and image (blue). C: carrier; HPF: high pass filter; LPF: low pass filter.

References:

1. Z. Tang, et al., Las. & Phot. Rev., vol. 14, no. 1, p. 1800350, 2020
2. Z. Zhu, Opt. Lett., vol. 45, pp. 5571–5574, Oct 2020.
3. Choon Kong Lai, et al. Adv. Funct. Mater. 2105230,2021,

Trapping Sound With Light

R.A Harrison, C.G Baker, W.W Wasserman, A. Sawadsky and W.P. Bowen

ARC Center of Excellence for Engineered Quantum Systems, School of Mathematics and Physics, The University of Queensland, Brisbane 4072, Australia
email: raymond.harrison@uq.edu.au

***Abstract**: In this talk I will show how strong optical forces with the extreme compliance of superfluid helium on photonic circuits allows the precise control of the local thickness of the film. This opens up a new regime for cavity optomechanics whereby the light no longer acts in a perturbative fashion on existing acoustic eigen modes, but allows the creating of optically defined acoustic eigen modes.*

The discovery of optical tweezers has enabled advances in many areas of science and the ability to finely control the motion of microscopic particles has helped advance our fundamental understanding of the internal physics of various microscopic systems [1]. Optical tweezers rely on radiation pressure to draw dielectric material into the focal point of a beam, this is often referred to as the gradient force.

In this talk I will present experimental results showing how this interaction can be leveraged in superfluid covered optical resonators [2] to create customized acoustic landscapes. The interaction of radiation pressure and photo thermal forces as shown in Fig. 1 (a) locally influence the superfluid film height, causing a localized change in the speed of sound. We have designed and build new devices shown in Fig. 1 (c) to isolate the effect of the radiation pressure to work as on chip optical tweezers that control the superfluid as shown in Fig. 1 (b) that will define new acoustic eigen modes.

Using this as a proof of concept a new regime will be possible for engineering systems for the precise control of superfluid mechanical modes and open fluid circuits that allow the controlled interaction of phonons in superfluids for sensing applications [3] and for fundamental investigations of the properties of superfluid [4,5].

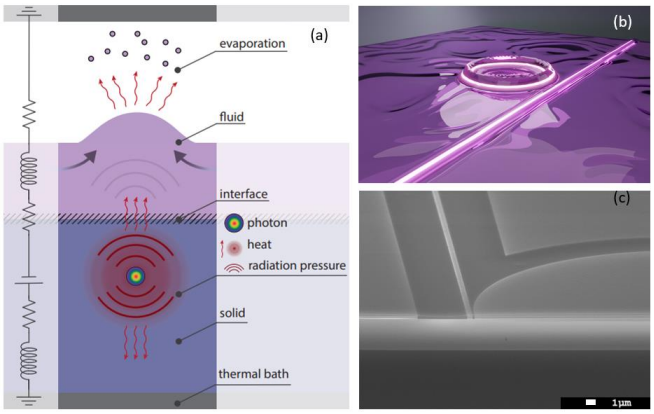

Figure 1: (a) Heat circuit alongside schematic of heat flow mechanisms for photon absorption in an optical resonator inside a dilution refrigerator with a thin film of superfluid He. (b) Illustration of an optical resonator device with localized bulging of the fluid from radiation pressure. (c) SEM of a fabricated optical resonator used in these experiments.

References:

[1] A. Ashkin,Phys. Rev. Lett. **24** 156 (1970).

[2] X. He, et al,Nat. Phys. **16** 4 (2020).

[3] Y. Sachkou, et al, Science **366** 6472 (2019).

[4] G. Harris, et al,Nat. Phys. **12** 8 (2016).

[5] Y. Sfendla, et al, npj Quantum Inf. **7** 62 (2021).

Progress toward the integration of high-speed photodetectors in lithium niobate on insulator photonic circuits

P. Kaur[1], A. Boes[1], G. Ren[1], T. Nguyen[1], and A. Mitchell[1]

[1]*Integrated Photonics and Application Centre, School of Engineering, RMIT University, 3000 VIC, Australia*

email: s3858721@student.rmit.edu.au

***Abstract**: We report the experimental demonstration of grating couplers in the of lithium niobate on insulator platform, which are suitable for the integration of high-speed photodetectors via transfer printing.*

The thin film lithium niobate on insulator (LNOI) platform has attracted a lot of attention recently and enabled for example high speed and low power electro optical modulator[1]. However, the optical detection of such high-speed signals is currently not feasible as high-speed detectors are still missing in LNOI.

In silicon photonics techniques have been developed to integrate no-native high-speed detectors, such as transfer printing of III-V photodetector[2] chiplets on grating couplers. A similar approach should also be suitable for the integration of high-speed detectors on LNOI. The coupling between the LNOI waveguide and the III-V detector can be achieved by using grating couplers, as it is illustrated in Fig. 1. The grating coupler directs the propagating light of the LNOI waveguide upward to the III-V photodetector, where it gets absorbed and generates an electrical signal.

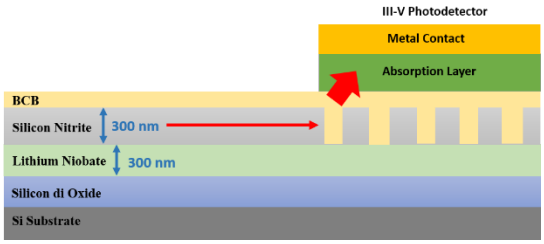

Figure 1: Cross-section of III-V photodetector integrated on LNOI grating coupler.

In this paper, we report on the first step that is required for the high-speed detector integration on LNOI, namely the fabrication of grating couplers.

For the fabrication of the waveguides and grating couplers we use silicon nitride (SiN) loaded lithium niobate thin films (see Fig. 1). For our application we are interested in the use of high-speed detectors for communications, hence we designed the grating couplers to operate at C-band wavelengths, which required a grating period of 940 nm, when using a fully etched SiN film with a thickness 300 nm and lithium niobate thin-film thickness of 300nm. Fig. 2(a) shows the SEM image of the fabricated grating coupler. The waveguide transmission of two grating couplers connected with a straight waveguide is shown in Fig. 2(b), when using a laser power of 0 dBm. One can see that the coupling efficiency per grating coupler is in the order of 10 dB, when assuming no waveguide losses.

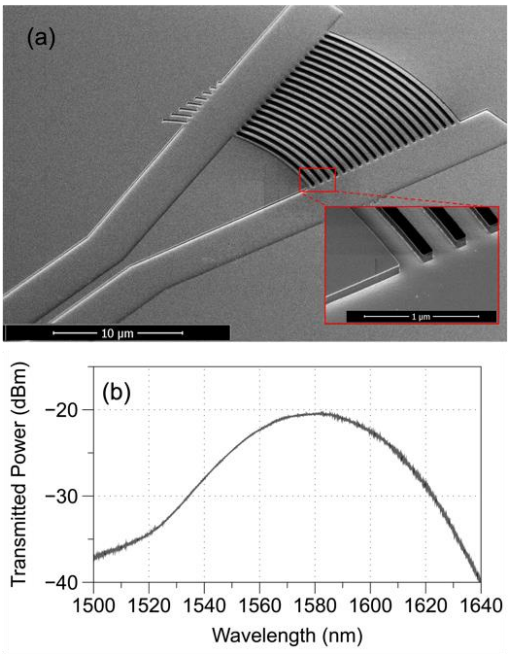

Figure 2: (a) SEM images of LNOI grating coupler, (b) transmission as the function of the wavelength for a straight waveguide in LNOI.

These results are promising for the next steps, which will include the integration of the III-V photodetector on the LNOI grating coupler using polymer bonding.

In this contribution, we presented the demonstration of LNOI grating couplers that are suitable for the integration of highspeed photodetectors via transfer printing. I will present the progress towards this aim by the time of the conference.

References:

[1] C. Wang, M. Zhang, X. Chen, M. Bertrand, A. Shams-ansari, S. Chandrasekhar, P. Winzer, and M. Lončar, Nature (2018).
[2] G. Chen, J. Goyvaerts, S. Kumari, J. Van Kerrebrouck, M. Muneeb, S. Uvin, Y. Yu, and G. Roelkens, Opt. Express **26**, 6351 (2018).

CMOS-compatible high-efficiency silicon photodetector with suspended nano-photonic structures

Oliver Bickerton[1,2], Shouyi Xie[1,2], Dennis Delic[3], and Benjamin J Eggleton[1,2]

[1]*School of Physics, The University of Sydney, NSW 2006, Australia*
[2]*University of Sydney Nano Institute (Sydney Nano)*
[3]*Defence Science and Technology Group, Edinburgh, SA 5111, Australia*
Email: shouyi.xie@sydney.edu.au

***Abstract**: Silicon photodetectors play an important role in imaging systems, LIDAR, and optical communication technologies. Improving the detection efficiency in the near infra-red (NIR) range has been challenging. In this work, we propose a CMOS-compatible silicon photodetector with enhanced external quantum efficiency in the wavelength range of 800-900 nm by integrating a suspended photonic crystal structure, showing an absorption efficiency as high as 85%.*

Photodetectors play an important role in a variety of applications such as imaging systems, LIDAR, and optical communication technologies. The development of high-performing Si photodetectors is vital for seamless integration with mature CMOS technologies to increase bandwidth, scalability and reduce both losses and costs. Modern communication technologies typically operate in the NIR range where the intrinsic absorption in Si is low. Improving the efficiency of Si photodetector in the NIR range has been challenging since there is always a trade-off between detection efficiency and response speed, both heavily dependent on the Si thickness.

Several photonic light-trapping structures have been proposed to enhance the detection efficiency of the Si photodetectors in the NIR range, including Bragg reflectors [1], diffraction gratings [1], waveguides [1], and nanostructured metasurfaces [2]. However, narrowband operation, low coupling efficiencies, and complex fabrication processes have limited their applications. Here we suggest a new design concept relying on a Si photonic crystal (PC) structure suspended in air with dimensions comparable to the wavelength of interest. Although similar structures have been previously implemented on silicon-on-insulator (SOI) devices, the enhancement of these earlier works was limited by the non-ideal vertical symmetry and index contrast [3]. Our proposed approach resolves this by implementing ideal vertical symmetry. Furthermore, it is fully CMOS-compatible and the added fabrication process has been widely implemented in other technologies like MEMS sensors [4].

The proposed structure can be seen in Fig 1a which in practice can be realised on SOI by adding a wet etch step to remove the SiO_2 underneath the cavities. We evaluate the optical performance of the structures via FDTD simulation as illustrated in Fig 1b. We compare the absorption in Si (normalised to the incident light) for planar SOI (i), PC on SiO_2 (ii), and suspended PC (iii) over the 800-900nm spectrum. The dimensions of the cavities for both structures have been optimised for a maximum peak absorption in the spectrum range.

Both the PC on SiO_2 and the suspended PC show significantly higher absorption than planar SOI. The suspended PC can achieve higher peak absorption (85%) than the PC on SiO_2 (65%), giving an enhancement of over 40 compared to the planar device. Moreover, the suspended PC design shows more peaks with higher absorption values at multiple wavelengths giving higher flexibility in wavelength of choice for practical applications.

In conclusion, we have proposed a design for a Si photodetector structure with broadband absorption enhancement in the 800-900 nm wavelength range by implementing a suspended PC structure on SOI. The peak absorption can be as high as 85%. This approach is fully CMOS-compatible and can be beneficial in a wide range of applications.

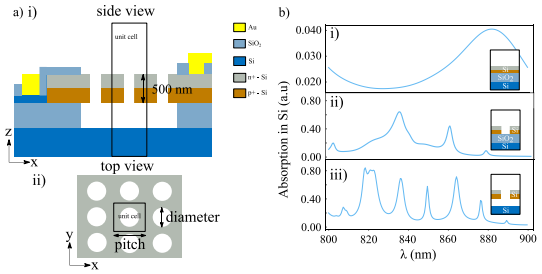

*Figure 1: **a)** Device structure **i)** side view and **ii)** top view. **b)** Normalised absorption for **i)** planar SOI. **ii)** PC on SOI with pitch: 800nm & diameter: 680 nm. **iii)** suspended PC structure with pitch: 750 nm & diameter: 450 nm.*

References:

1. S. Mokkapati and K. R. Catchpole, *J. Appl. Phys*, vol.112, no. 10, 2012
2. K. Zang *et al.*, *Nat. Commun.*, vol.8, no. 1, pp. 1–6, 2017
3. Y. Gao *et al.*, *Nat Photonics*, vol. 11, no. 5, pp. 301-308, 2017.
4. T. J. Peters and M. Tichem, *J. Micromechanics Microengineering*, vol. 25, no. 10, 2015

Generalised sixth order dispersion solitons

Y. Long Qiang[1], Tristram J. Alexander[1], C. Martijn de Sterke[1,2]

[1] *Institute of Photonics and Optical Science (IPOS), School of Physics, The University of Sydney, NSW 2006, Australia.*
[2] *The University of Sydney Nano Institute (Sydney Nano), The University of Sydney, NSW 2006, Australia.*
email: yqia7452@uni.sydney.edu.au

***Abstract**: We analytically and numerically evaluate and categorise soliton solutions comprised of even dispersion effects up to the 6th order, and identify an exact analytic solution within the solution space.*

Solitons are a physical phenomenon, that is characterised by the property of remaining unchanged as they propagate, traditionally a result of the nonlinear Kerr effect balancing with quadratic dispersion. The recent discovery of the pure quartic soliton has initiated research into the study of even higher order dispersion pure solitons, identifying that soliton formation can be achieved with anomalous dispersion at any even order, with experimental confirmation up to 10th order. [1] These studies also prompted the exploration of the 4th order phase plane, revealing a large family of soliton solutions formed by combined 2nd order and 4th order dispersion. [2] We outline an examination of the 6th order phase plane, of bright pulse-like soliton solutions, and provide a basis to predict the characteristics of soliton pulses for any combination of anomalous dispersion. We also identify an exact analytic solution, based upon the analytic solution observed by Karlsson and Höök in the 4th order case. [3]

The evolution of these solitons can be described by the modified nonlinear Schrodinger equation

$$\frac{i\,\partial\psi}{\partial z} - \frac{\beta_2}{2}\frac{\partial^2\psi}{\partial T^2} + \frac{\beta_4}{24}\frac{\partial^4\psi}{\partial T^4} - \frac{\beta_6}{720}\frac{\partial^6\psi}{\partial T^6} + \gamma|\psi|^2\psi = 0, \quad (1)$$

where ψ(z, T) is the pulse envelope, z the propagation coordinate, T the local time, γ the nonlinear parameter, which we take to be positive, and β_n is the nth order dispersion coefficient. Analysis of this equation leads to an analytic framework to identify distinct soliton pulse shapes, based on the nature of the tails of the pulses, where the nonlinear term can be neglected, and which we use to examine the order phase plane. We confirm these analytic results, with fully numerical solutions, and propagation simulations, confirming their pulse shape and stability. These analytic and numerical methods allow us to distinguish a 3-dimensional phase plane for the 6th order dispersion case, separated into 4 key distinct regions, as shown in Fig. 1. We first identify the black region, where no pulse-like solutions are expected to form. In the dark grey region Eq. (1) supports the formation of solutions with oscillations in the tails. In the light grey and white region, the solutions have purely exponential tails. We note that we locate an exact analytic solution within the white region of the phase plane, indicated by a purple cross. All these regions are distinguished by analytically defined boundaries.

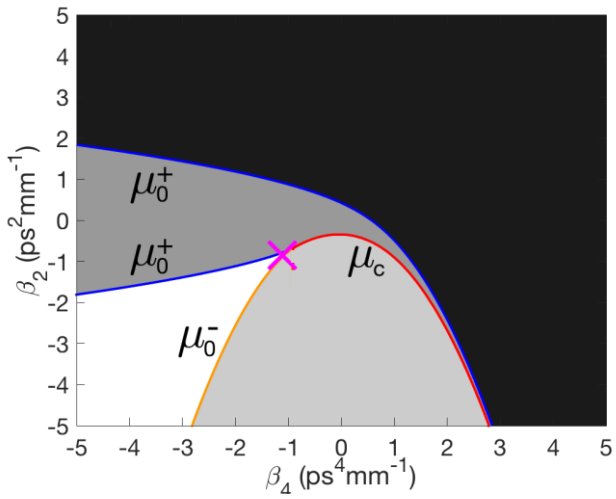

Figure 1: 2D cross section taken through 3D 6th order phase space with β_6 = -1 ps^6 mm^{-1} and μ = 1 mm^{-1} constant. The four key regions are separated by analytic boundaries $\mu_0^{\pm}$ and μ_c.

In summary, we have explored the 6th order dispersion phase plane, identifying novel regions of solutions. This includes a discovery of an exact analytic solution in the space, which we expect to utilise to find analytic solutions at higher dispersion orders. Our methods produce a framework to predict soliton solutions at any order, with experimental mechanisms already present to observe 6th order dispersion solitons. [1]

References:

1. A.F.J. Runge, Y. L. Qiang, T.J. Alexander, M. Z. Rafat, D.D. Hudson, A. Blanco-Redondo, and C. M. de Sterke, Physical Review Research **3**, 013166 (2021).
2. K.K.K. Tam, T.J. Alexander, A. Blanco-Redondo, and C.M. de Sterke, Phys. Rev. A **101**, 043822 (2020).
3. M. Karlsson and A. Höök, Opt. Commun. **104**, 303 (1994).

Simulation and design of circulators in lithium niobate on insulator

R. Russell[1], A. Boes[1], G. Ren[1], T. Nguyen[1], and A. Mitchell[1]

[1]*Integrated Photonics and Applications Centre, School of Engineering, RMIT University, Melbourne, VIC 3000, Australia*

email: s3412482@student.rmit.edu.au

***Abstract**: On-chip optical circulator are crucial for the vision of fully integrated optical circuits that include integrated light sources. In this contribution, we simulate and design integrated circulators that are based on spatiotemporal modulation in the low loss silicon nitride loaded lithium niobate on insulator platform.*

Optical circulators are non-reciprocal devices which direct light away from a source, blocking any reverse travelling light and redirecting it away to another port. Photonic integrated circuits (PICs) require such components for laser integration on chip for improved stability, in applications such as sensing and optical computing. Examples of integrated circulator demonstrations include the use of bonded magneto optical materials on optical waveguides[1, 2] and Nonlinear optical interaction such as stimulated Brillouin scattering[3]. Spatiotemporal non-reciprocity has been demonstrated on chip[4] in the form of an isolator.

However, no clear integration method has yet crystalised as the methods have downsides such as the relatively high optical losses of the magneto optical material [1] or the high pump powers for the nonlinear optical demonstrations[5]. Lithium Niobate on insulator (LNOI) offers new opportunities for integration on chip, recently the spatiotemporal circulator was demonstrated by a bulk component setup[5].

In this contribution, we theoretically investigate integrated circulators that are based on spatiotemporal modulation, using two electro optic Mach Zehnder modulators separated by delay lines, as shown in Figure 1.

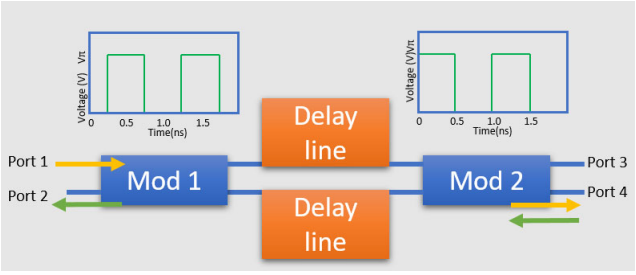

Figure 1: Illustration of the circulator configuration and working principle.

The working principle of the circulator is a follows, as the optical switches have square wave switching voltage with an amplitude of Vpi, a frequency of 1GHz and a time delay of 1/4T between M1 and M2 applied. The delay lines are used as a way to slow the light entering the next switch. For the forward direction this means that the modulation signal for both modulators stay in phase, resulting in the light exiting in port 4, whereas in the backward direction the modulation signal for from the second to the first modulator is out of phase, resulting in in the light exiting in port 2.

To simulate the Circulator performance IPKISS was used. For the simulations we assumed a modulation frequency of 1 GHz, which for a group index of LNOI waveguides of 2.21 means that the delay line length of the optical waveguides required is 33.91mm. For the modulators we assumed a modulator bandwidth of 5GHz and for the waveguides a realistic propagation loss of 0.5 dB/cm.

The results for forward operation are shown in figure 2(a) and the backwards operation is shown in Figure 2 (b). The results show that in forward direction the light is able to exit out port 4 and in backward direction the light exits out of port 2, demonstrating non-reciprocal function with 20dB isolation. One can also see that during the switching transitions the highest amount of light exits the undesired port, highlighting that high switching speeds are crucial for the good operation of the circulators.

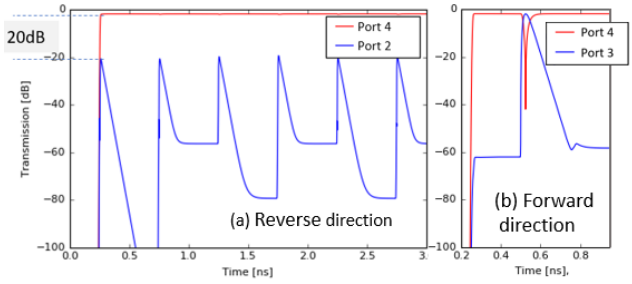

Figure 2: Circulator results.

In this contribution we showed that integrated circulators are feasible in the LNOI waveguide platform when using spatiotemporal modulation. Isolation values of 20dB appear to be feasible.

References

[1] D. Huang *et al.*, "Dynamically reconfigurable integrated optical circulators," *Optica,* vol. 4, no. 1, 2016, doi: 10.1364/optica.4.000023.

[2] P. Pintus, D. Huang, C. Zhang, Y. Shoji, T. Mizumoto, and J. E. Bowers, "Microring-Based Optical Isolator and Circulator with Integrated Electromagnet for Silicon Photonics," *Journal of Lightwave Technology,* vol. 35, no. 8, pp. 1429-1437, 2017, doi: 10.1109/jlt.2016.2644626.

[3] W. Fu, F. J. Shu, Y. L. Zhang, C. H. Dong, C. L. Zou, and G. C. Guo, "Integrated optical circulator by stimulated Brillouin scattering induced non-reciprocal phase shift," *Opt Express,* vol. 23, no. 19, pp. 25118-27, Sep 21 2015, doi: 10.1364/OE.23.025118.

[4] C. Galland, R. Ding, N. C. Harris, T. Baehr-Jones, and M. Hochberg, "Broadband on-chip optical non-reciprocity using phase modulators," *Opt Express,* vol. 21, no. 12, pp. 14500-11, Jun 17 2013, doi: 10.1364/OE.21.014500.

[5] L. Del Bino, J. M. Silver, M. T. M. Woodley, S. L. Stebbings, X. Zhao, and P. Del'Haye, "Microresonator isolators and circulators based on the intrinsic nonreciprocity of the Kerr effect," *Optica,* vol. 5, no. 3, 2018, doi: 10.1364/optica.5.000279.

Measuring the fundamental thermal phase fluctuations in a passive fibre resonator

J. P. Hedger[1], B. M. Sparkes[2], P. S. Light[1], S. Foster[2], and A. N. Luiten[1]

[1]*Institute for Photonics and Advanced Sensing (IPAS) and School of Physical Sciences, University of Adelaide, 5005 South Australia, Australia.*
[2]*Defence Science and Technology Group, Edinburgh SA 5111, Australia.*
email: jonathan.hedger@adelaide.edu.au

***Abstract**: We report on our work towards measuring fundamental phase fluctuations of passive optical fibre resonators.*

Optical fibre sensors provide a robust platform to perform strain measurements down to the sub-picostrain level [1]. This makes them ideal for sensing in harsh environments such as smelting furnaces or the seafloor. The sensitivity of all these devices is ultimately limited by unavoidable length fluctuations of the optical fibre, which are associated with fundamental thermal fluctuations. Until now, the leading edge for ultra-precise sensing has made use of sensors based on distributed-feedback fibre lasers, due to the benefits of having an autonomous sensor that produces its own output. However, theory suggests that this approach suffers from higher levels of thermal noise than could be achieved by using external optical interrogation of a "passive" fibre resonator [2].

This theoretical hypothesis has yet to be experimentally verified [3], but if the improvement in sensitivity can be realised, it might allow for the design of next-generation optical fibre sensors as well as providing experimental evidence for the correct theoretical form of this noise. Motivated by this, we have developed custom passive fibre resonators, optimized for measuring these fundamental thermal fluctuations (Fig. 1a). To minimise noise our experiments are conducted in a thermally- and acoustically-isolated environment (Fig. 1b) and in this presentation we will present our current results using this set-up.

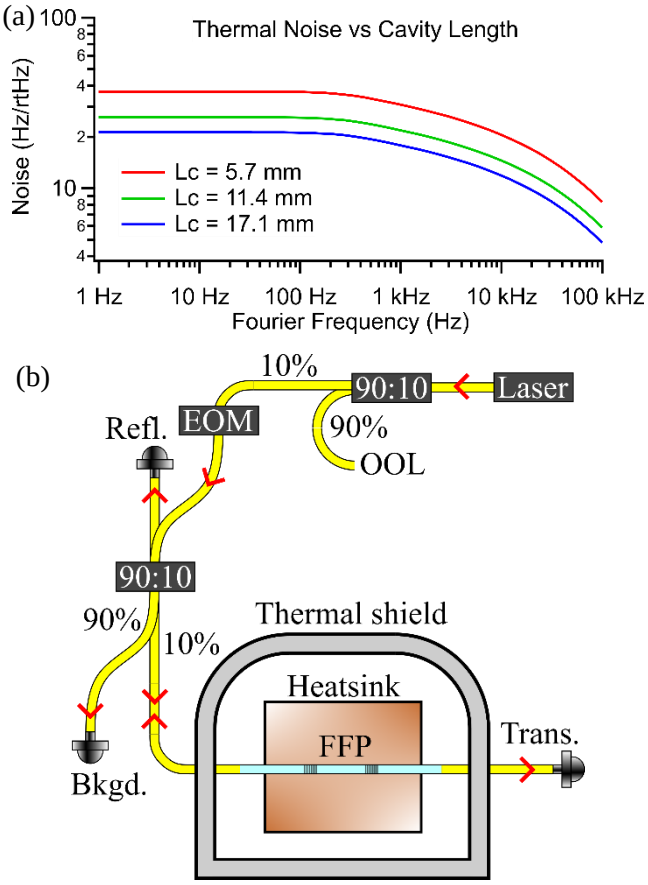

Figure 1: (a) Theoretical noise floors for the fundamental thermal phase fluctuations, for different cavity lengths. (b) Diagram of experimental set-up (OOL = out of loop measurement, EOM = electro-optic modulator, FFP = fibre Fabry-Perot, Refl. = reflected signal, Bkgd. = background signal, Trans. = transmitted signal).

References:

1. I. C. M. Litter et al., *Opt. Express*, **17** (13), 11077 (2009).
2. S. Foster, *Phys. Rev. A*, **86** (4), 043801 (2012).
3. G. A. Cranch and S. Foster, *Science*, **335** (6066), 286 (2012).

Soliton linear-wave scattering in a Kerr microresonator

Pierce C. Qureshi,[1,2] Vincent Ng,[1,2] Farhan Azeem,[1,3] Luke S. Trainor,[1,3] Harald G. L. Schwefel,[1,3] Stephane Coen[1,2], Miro Erkintalo[1,2] and Stuart G. Murdoch[1,2]

[1]*The Dodd-Walls Centre for Photonic and Quantum Technologies.*
[2]*Department of Physics, University of Auckland, Auckland, New Zealand.*
[3]*Department of Physics, University of Otago, Dunedin, New Zealand.*
email:pqur870@aucklanduni.ac.nz, s.murdoch@auckland.ac.nz

***Abstract**: Nonlinear scattering between a linear probe wave and a soliton in a Kerr microresonator is shown to generate an idler comb of identical FSR at a new frequency set by the probe detuning. This process enables the coherent spectral manipulation of the original soliton comb.*

Microresonator frequency combs (microcombs) are a highly attractive new technology with the potential to enable applications across fields ranging from precision measurement, to telecommunications and medical diagnostics [1]. In Kerr microresonators, coherent combs take the form of ultra-short pulses known as temporal cavity solitons (CS). In this abstract we experimentally demonstrate that a linear probe wave can nonlinearly scatter off a CS resulting in the generation of a new idler comb, fully coherent with the original CS comb, but offset in frequency [2–4]. In addition, we find that in the absence of higher order dispersion, the peak of the newly generated idler comb can be linearly tuned in frequency simply by changing the probe wave's detuning from its closest cavity resonance (Δ_2).

We experimentally investigate these effects in a MgF_2 microresonator with a free-spectral-range (FSR) of 56 GHz. In Fig. 1(a) we plot the output spectra with a CS excited at 1582 nm (P_S), and a linear probe signal injected simultaneously at 1550 nm (P_P). A third laser at 1534 nm (P_{AUX}) is also coupled into the resonator to enable thermal compensation. These spectra show the clear emergence of new idler comb components whose central frequency (indicated by the black dashed line) can be tuned simply by changing the probe detuning. Corresponding measurements of the comb's low-frequency RF power spectrum show a single narrowband beat note (*dv*). This confirms the presence of two separate coherent combs with identical FSRs, offset in optical frequency by this beat frequency. Measuring *dv* in each case allows us to infer the value of Δ_2, which we can then use to simulate the output comb spectrum via the Lugiato-Lefever equation. These simulations (red traces) are superimposed on top of the experimentally measured spectra, and show a good agreement. Finally, in Figs. 1(c,d), we plot experimentally measured spectra of single– and two–soliton combs with the probe detuning set to maximize the comb's spectral width. The superimposed red traces show the original spectral extent of the CS. We are able to demonstrate this effect both with the soliton at 1550 nm and probe at 1582 nm [Fig. 1(c)], and vice versa [Fig. 1(d)].

In conclusion, we have been able to demonstrate that the nonlinear interaction between a microresonator cavity soliton and a linear probe wave allows the generation of a frequency tunable idler comb, fully coherent with, but spectrally offset from, the original CS comb. This interaction offers a new mechanism for the flexible manipulation of microcomb spectra.

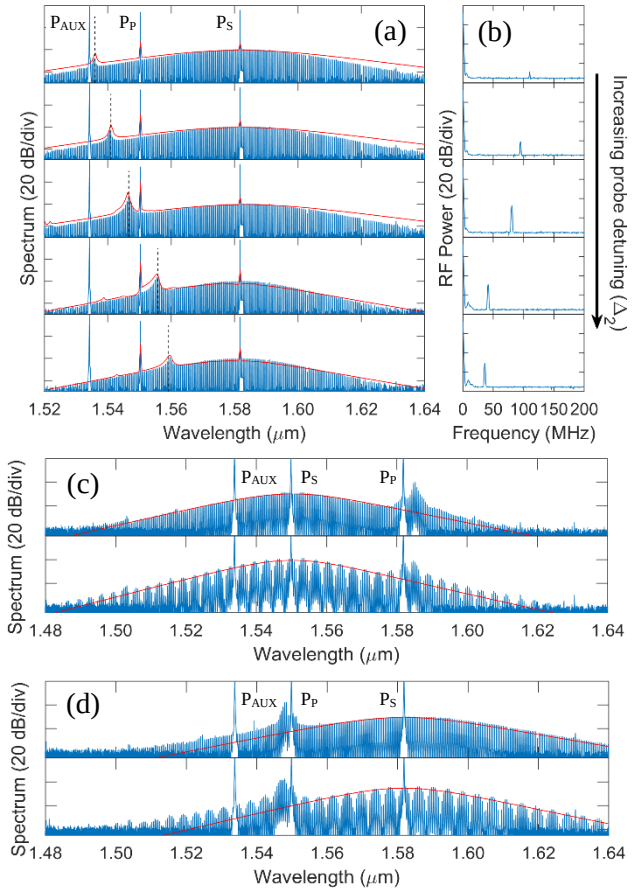

Figure 1: (a) Soliton and probe waves generate a tunable idler comb, (b) RF beat note between soliton and idler combs. (c,d) Spectral extension of single–soliton and two–soliton combs at 1550 and 1582 nm.

References:

1. T. Kippenberg et. al., Science **361**, eaan8083 (2018)
2. D. Skryabin and A. Yulin, Opt. Lett. **29**, 2411 (2004)
3. K. Webb et. al., Nat. Commun. **5**, 4969 (2014).
4. G. Moille et. al., arxiv.org/abs/2102.00301 (2021)

Ultra-fast vector imaging of surface plasmon polaritons

T. J. Davis [1,2,3], D. Janoschka [2], P. Dreher [2], B. Frank [3], H. Giessen [3], F.-J. Meyer zu Heringdorf [2]

[1]University of Melbourne, Parkville 3010, Australia
[2]University of Duisburg-Essen, Duisburg D-47057, Germany
[3]University of Stuttgart, Stuttgart D-70569, Germany
email: timd@unimelb.edu.au

***Abstract**: We describe our ground-breaking technique to image the electric field vectors of surface plasmon polaritons (SPPs) with sub-femtosecond temporal resolution and nanometre spatial resolution. We use the technique to directly study spin and topological properties of SPPs propagating and interfering on single crystal gold films.*

Surface plasmon polaritons (SPPs) are surface charge oscillations that propagate as waves over metal surfaces. The surface-charge electric fields rotate in time, creating a spin transverse to the direction of propagation that gives rise to novel spin properties [1]. Although many techniques exist to observe the wave properties of the SPP electric fields, very few enable the imaging of the three vector components. Recently we developed a technique using photo-emission electron microscopy (PEEM) that not only enables us to extract the field vectors but allows us to obtain these as a function of time with sub-femtosecond resolution at each location on the metal surface [2]. We describe this technique and present some recent results.

The imaging principle is based on a pump-probe laser technique performed in a photo-emission electron microscope. A single crystal gold film is chemically grown to create atomically smooth surfaces that improves imaging quality. A pump laser pulse with centre wavelength 800 nm is normally incident on the gold surface, launching SPPs from a series of grooves etched into the gold film. A probe pulse arriving some time $\Delta\tau$ later generates an interference pattern with the SPP that spatially modulates the rate of photo-electron emission as detected by the electron microscope. The result is an image of the SPP wave on the surface of the gold film at time $\Delta\tau$ (Fig. 1a).

A series of images as a function of time delay allows us to reconstruct the full spatio-temporal dynamics of the SPP. Sections from a time series (Fig. 1b). of the electric field vectors of the SPP shown in Fig. 1a highlight the transverse spin property. This profile is almost a textbook reproduction of the SPP field vectors, obtained from our pump-probe experiment exciting SPPs from a single groove etched in a gold film.

With growing interest in the topological properties of vector fields, there has been an increasing effort to create systems that generate vector fields amenable for study. An example topological field is the skyrmion that is equivalent to a uniform coverage of a sphere with vectors. We have studied the time dynamics of an SPP interference pattern that mimics a skyrmion field (Fig. 1c) and extracted the topological measures from the data, such as the Chern number [2].

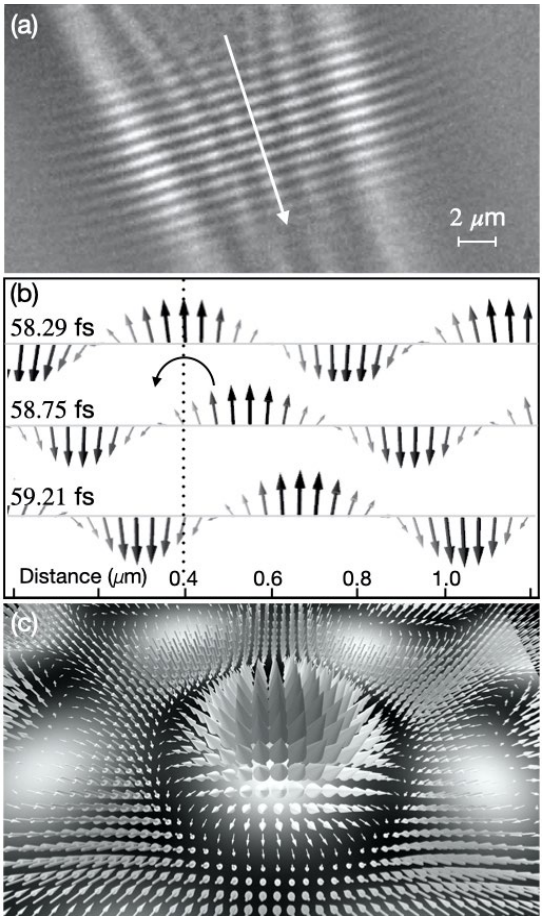

Figure 1: Examples of experimentally measured SPP fields: a) SPP plane wave; b) plane-wave SPP vectors at 3 time delays. The dashed line shows the rotation (spin) of a vector at a fixed location; c) SPP skyrmion at one moment in its oscillatory cycle.

For our current and future studies, we are measuring the topological properties of complex SPP spin textures, such as merons, which is only possible with our vector microscope technique.

References:

1. K.Y. Bliokh et al. Nat. Commun. 5, 3300 (2014)
2. T. J. Davis et al. Science 368, eaba6415 (2020)

Terahertz bend losses in cm-scale polyurethane flexible hollow-core fibers

A. Stefani[1], J.H. Skelton[1], and A. Tuniz[1,2]

[1]Institute of Photonics and Optical Science (IPOS), School of Physics, The University of Sydney, NSW 2006, Australia
[2]The University of Sydney Nano Institute (Sydney Nano), The University of Sydney, NSW 2006, Australia
email: alessandro.tuniz@sydney.edu.au

***Abstract**: We experimentally investigate bend losses in thermoplastic polyurethane (TPU) antiresonant waveguides, which are highly flexible despite their cm-scale thickness. Structured cladding waveguides outperform single tubes at small bend radii, but not at larger bend radii, due to coupling to cladding modes.*

Terahertz (THz) technology lacks convenient, flexible, and reconfigurable waveguides with low attenuation and small bend losses. Hollow-core THz waveguides offer some advantages [1], but often have centimeter-scale diameter and are therefore not flexible. Here we investigate two comparable hollow-core thermoplastic polyurethane (TPU) antiresonant waveguides (WGs) formed by one tube and six tubes which are extremely flexible [2]. We experimentally characterize transmission when strong bends occur (Fig. 1b, R_b: bend radius). Such WGs show overall comparable performances (transmission loss <1 dB/cm in their 0.1–1 THz transmission bands). Experiments are performed using a commercially available fiber-coupled THz Time Domain Spectroscopy system (Menlo TERA K15), maintaining alignment for all bend radii. Modal images are experimentally obtained by measuring the THz pulse while raster-scanning a 1 mm aperture at the WG output. These experiments showcase TPU as an extremely flexible THz fiber platform, allowing small bend radii (only ten times the WG diameter). Our experiments used WGs with ~1 cm cross-section, enabling guided-wave transmission below 10 cm bend radii for wavelengths up to 3 mm, analogous to a standard step-index fiber of 125 µm diameter guiding a 40 µm wavelength within a 1.2 mm bend radius. Such extreme WG bends introduced a maximum loss increase of 1dB/cm (Fig. 1c), with the transmitted field staying confined to the hollow core (Fig. 1d). Compared with a single tube, the six-tube waveguide shows resonant coupling to cladding tube modes for specific frequencies when the bend radii are greater than 10 cm, and outperforms the one-tube waveguide for smaller bend radii. Such WGs can be fabricated using standard fiber drawing techniques, which is critical for producing long waveguide lengths. Further harnessing the extensive amount of ongoing research on antiresonant fibers at higher frequencies is likely to improve their performance and extend their operating frequency, complementing ongoing efforts in fabricating extremely flexible fibers for a wide variety of optoelectronic applications [3]. This work demonstrates the potential of antiresonant TPU waveguides for making THz WGS in this frequency range more practical, flexible, and accessible.

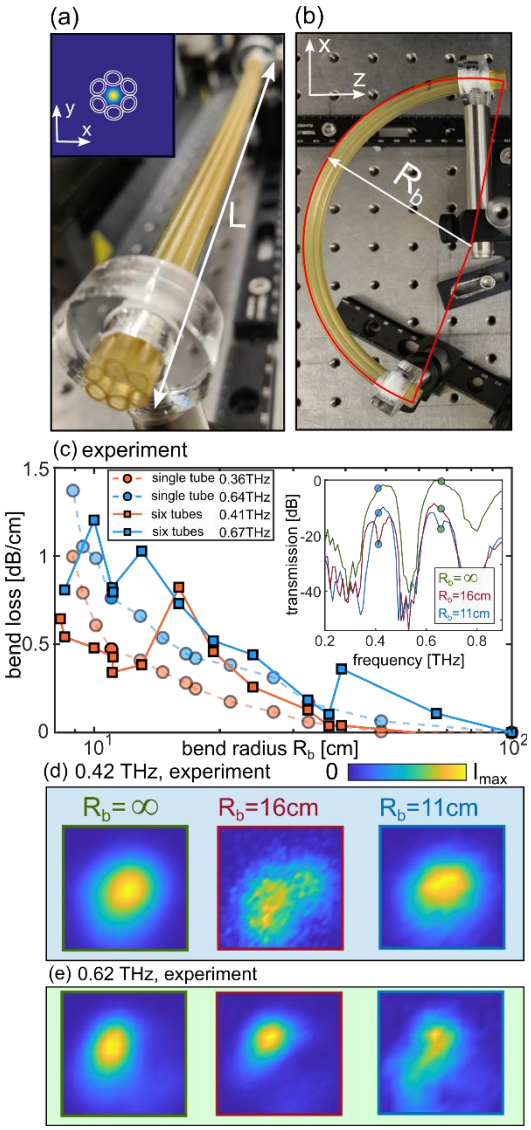

Figure 1: (a) Flexible TPU six-tube antiresonant THz waveguide and mode. (b) Example bent waveguide. (c) Representative bend loss in one- and six- tube waveguides. Inset: example transmittance measurements and cladding resonances. (d) Experimental images (0.42,0.62 THz) at different R_b.

References:

1. M. S. Islam et al., Opt. Express **28**, 16089–16117 (2020)
2. A. Stefani et al., APL Photonics **3**, 051708 (2018).
3. M. Chen et al., Adv. Fiber Mater. **3**, 1–13 (2021).

High-dimensional Stokes-space Spatial Beam Analyser

D. S. Dahl [1*], M. Plöschner [1], N.K. Fontaine[2], and J. Carpenter [1]

[1] *School of ITEE, The University of Queensland, Brisbane, QLD 4072, Australia*
[2] *Nokia Bell Labs, 600 Mountain Ave., New Providence, NJ, 07974, USA*
[*]*Email: daniel.king2@uq.net.au*

Abstract: We demonstrate a device for measuring the generalised Stokes parameters of a six spatial mode beam. The device is a single-shot wavefront sensor measuring spatial complex amplitude and coherence without an external phase reference. © 2021 The Author(s)

Measuring the spatial amplitude, phase, and coherence of a wavefront, without a well-defined external phase reference, is challenging. Current methods such as, homodyne/heterodyning techniques and self-reference techniques [1], both have their drawbacks. For homodyne and heterodyning techniques, a well-defined reference is needed, which is not always possible or desirable. Self-reference techniques incur loses for single-shot type methods and are relatively slow for sequential type methods. The device presented here removes these deficiencies and uses a theoretically lossless and static measurement configuration, performing single-shot spatial state tomography [2] on a beam (which is described through a higher-dimensional Stokes-space) with no need for an external reference beam.

The device works on the principle of multi-plane light conversion (MPLC) [3], which transforms a beam through a cascade of phase manipulations. The MPLC allows every spatial state in the higher-dimensional Stokes-space that describes the beam, to be interfered with every other spatial state in the space. The MPLC is made up of approximately order N phase planes, where N is the number of spatial states that the input beam is made up of. The device approximates a unitary transformation between an input beam composed of N=6 Laguerre-Gaussian (LG) spatial components, and an output array of $2N^2$-N=66 Gaussian spots. From the intensity of those spots the complete spatial state of the beam is acquired. This is similar to how the polarisation state of a beam (which is described by a 2-D Stokes-space) is measured from the intensity of a beam after passing through a combination of beam splitters and waveplates.

Fig. 1 illustrates preliminary experimental results from the device, where 6 pure state LG modes (Fig. 1 (a) Top row), that are measured by off-axis digital holography, have been passed through the device. The output from the device for each of the pure states is an array of spots (Fig. 1 (a) middle row), measured with a CCD camera. From the intensity of these spots the spatial state of the input beam was determined (Fig. 1 (a) bottom row), which shows good agreement with the measured input fields acquired through digital holography. Fig. 1 (b) illustrates the device's ability to measure a mixed spatial state that contains equal parts of all the pure states. The top and middle images show the sum of their respective rows from Fig. 1 (a). For this type of state, it is expected that all 66 spots should have equal intensity and the squared density matrix (ρ^2) should be diagonal with trace equal to 1/N=0.167 (0.199 in Fig.1 (b)), which is in good agreement.

1. H.Ji, *et al*, *Opt.Lett.*, 44, 2065–2068 (2019)
2. M.Agnew, *et al*, *Phys. Rev. A*, 84 (2011)
3. N.K.Fontaine, *et al*, *Nat.Commun.*, 10, 1865 (2019)

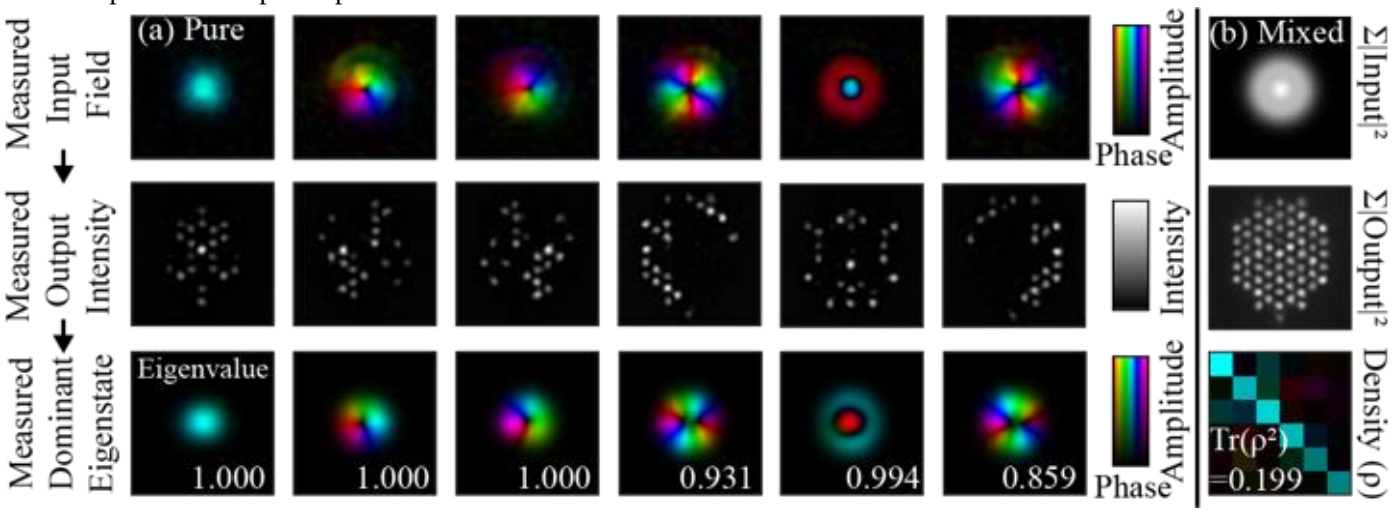

Fig 1: (a) (Top row) Comparison of input field as measured by off-axis digital holography for the first 6 LG modes. (Middle row) intensity of output spot array on CCD camera. (Bottom row) Measured dominant eigenstate, with corresponding eigenvalues, of the Stokes-space representation constructed for the intensities measured in the spot array. (b) Example of tomography on a completely mixed state.

Personal Thermal Management with Large Scale Kevlar Textile

Nusrat Alim[1], Ahasanul Haque[1], Lujun Huang[1], Evgeny Morozov[1], Haroldo T. Hattori[1], Svetlana Boriskina[2], and Andrey Miroshnichenko[1]

[1] *School of Engineering and Information Technology,University of New South Wales, Canberra, Australia*
[2]*Department of Mechanical Engineering, Massachusetts Institute of Technology, Cambridge, MA, USA*
email: n.alim@student.adfa.edu.au

***Abstract**: Kevlar, a large-scale producible aramid textile, is proposed to achieve passive radiative cooling to ensure thermal comfort. The performance of the Kevlar textile is evaluated based on both experimental and numerical analysis. We found that, it can exhibit around 2.5K temperature reduction in the indoor environment.*

Over the years, personal thermal management technology based on thermal textiles has become important. It provides a cost-effective and energy-efficient solution to control human body temperature and its surrounding by reducing reliance on air-conditioners and thermal heaters. Typically, in the indoor environment, almost over half of the total body heat loss occurs due to heat dissipation (emissivity 98%) from human skin through thermal radiation [1]. Based upon these facts, thermal radiative textiles have emerged, providing an easy way to dissipate thermal radiation from the human body.

In this work, we consider Kevlar fabric to effectively transmit heat to outer space to achieve localized cooling. This fabric can offer around 90% emissivity in the mid-infrared spectrum, almost 40% solar reflection, and a low thermal conductivity of 0.012 W/m, being qualified as a suitable choice for achieving passive radiative cooling that utilizes an atmospheric channel to radiate heat to the outer space (3K temperature) [2]. On the contrary to the conventional cotton fabric, it can produce almost 1.5K temperature reduction, making it a promising candidate for cooling purposes. At indoor environment, the fabric can exhibit around 2.5K temperature gradient, which is desirable for better cooling performance in hot weather conditions.

The net cooling power of the Kevlar fabric when it is subjected to heater power can be expressed by the following power balance equation [3]:

$$P_{net\_cool}(T) = P_{rad}(T) - P_{atm}(T_{atm}) - P_{heater}(T) - P_{con+conv}(T, T_{atm}), \quad (1)$$

where P_{net_cool} is the net power outflow at Kevlar surface temperature T, P_{rad} is the hemispheric radiation power from the fabric's surface, P_{atm} is the absorbed power density due to thermal radiation of air particles at ambient temperature T_{atm}, P_{heater} is the heater power absorbed by the fabric, $P_{con+conv}$ is the power loss due to conduction and convection process. When the net power outflow is zero, the fabric top surface temperature reaches a steady-state temperature. A couple of thermocouples are used to measure top and bottom surface temperature of Kevlar fabric and the heater in indoor environment.

Figure 1 shows a good agreement between calculated and measured temperatures of Kevlar fabrics at different values of heating power. The highest 1.97 K temperature difference can be found between the measured and calculated temperatures of Kevlar fabric at the heater power ranging between 0.04 and 2.5 W.

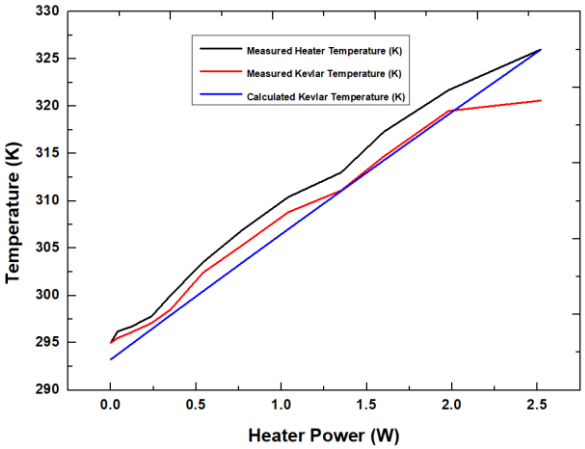

Figure 1: Experimentally measured heater, Kevlar fabric, and calculated fabric temperature as a function of heater power.

Finally, a 5K temperature difference can be achieved for the heater power of 2.52 W due to nonlinear effects. Even more significant temperature reduction can be achieved in outdoor use, when the outer space can be used as the heat sink.

References:

1. W. Li, and S. Fan, *Opt. Express* **26**,1601-16017 (2018).
2. M. Alberghini, S. Hong, L. Lozano, V. Korolovych, Y. Huang, F. Signorato, S. Zandavi, C. Fucetola, I. Uluturk, M. Tolstorukov, G. Chen, P. Asinari, R. Osgood, M. Fasano and S. Boriskina, *Nat. Sustain.* **4**, 715 (2021).
3. H. Luo, Y. Zhu, Z. Xu, Y. Hong, P. Ghosh, S. Kaur, M. Wu, C. Yang, M. Qui and Q. Li, *Nano Lett.* **21**, 3879 (2021).

Optical Fibre Photodetector for COMET Phase-I

S.Dekkers[1], Y.Fujii[1], and J.Nash[1]

[1]*Monash University, VIC 3800, Australia*
email:sam.dekkers1@monash.edu

***Abstract**: The COMET experiment aims to search for neutrinoless muon to electron conversion at new sensitivity levels. In Phase-I, a trigger hodoscope detector will be used for increased timing resolution in high momentum electron hits. This detector consists of scintillator counters with silicon photomultiplier detectors to read photon signals, coupled by optical fibres. We present initial tests on photon efficiency and time resolution in this system.*

The COMET experiment (COherent Muon to Electron Transition) is an experiment aiming to measure the charged lepton flavour violating process $\mu+N \rightarrow e+N$, a process forbidden in the Standard Model of particle physics, at new sensitivity levels [1]. To measure this process, the world's highest intensity muon beam will be directed at aluminium stopping targets. The CyDet (Cylindrical Detector) used in Phase-I will be centred around these stopping targets in order to observe the decay of the muons within the presence of the aluminium nuclei. Surrounding the stopping targets are a 1 T detector solenoid and CDC (Cylindrical Drift Chamber) detector with the CTH (Cylindrical Trigger Hodoscope) detector occupying each end of the detector region. The CDC detector will provide momentum measurements for signal electrons while the CTH detector will provide important timing information.

The CTH detectors consist of concentric rings of scintillator counters, with the main trigger condition on high momentum signal electrons being 4-fold coincident hits while suppressing as many backgrounds as possible. These counters will be coupled to multi-pixel photon counters (MPPC) for light signal readout via optical fibres. The fibres are necessary due to the high radiation environment present [2] - no sensitive photodetectors can be located near the counters, meaning a small number of near-UV photons must be transported efficiently via fibres. This means photon fibre transmission (at least 5 m), detecting small numbers of photons at the MPPC side and having fast pulse reading for good timing resolution (1 ns) due to the high hit rate environment are key design issues. Preliminary tests on fibre transmission and timing resolution in fibre versus direct coupling to scintillator have been made. In each case the MPPC used was the S14160-3015PS model from Hamamatsu, and the scintillator was the BC-408 from Saint-Gobain Crystals.

The first test performed was an analysis on the fibre attenuation utilizing a variety of different wavelength LED test pulses impinged on the MPPC surface through different length and material fibres. The main conclusion was that although glass fibres have a longer attenuation length, plastic PMMA optical fibres are suitable for the CTH design goals in their attenuation around the BC-408 peak emission wavelength.

The second test was a preliminary time resolution measurement. A small scintillator counter was used, one end coupled directly to an MPPC and the other end coupled to an MPPC via plastic PMMA fibres, both with transparent grease.

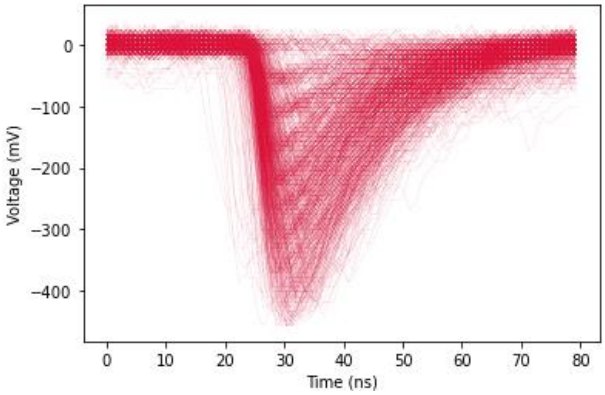

Figure 1: Signals from scintillator fibre-connected MPPC, showing distinct differences between different number of photoelectron peaks.

Using two other trigger counters above and below the centre of the main counter, MPPC waveforms were recorded using cosmic rays. Figure 1 shows a sample of waveform data taken from the fibre connected MPPC, showing distinction between number of photoelectron peaks. By accounting for time-walk correction, the time resolution of the fibre connected channel was found to be almost 1 ns.

Following these tests, measurements are starting with an improved system with better couplings, so that a better measure of system photon efficiency and time resolution can be made.

References:

1. The COMET Collaboration,et al., "COMET Phase-I technical design report,"Progress of Theoretical and Experimental Physics, vol. 2020, no.3, pp.2050-3911, Mar. 2020, doi: 10.1093/ptep/ptz125.

2. Y.Nakazawa, et. al., "Radiation hardness study for the COMET Phase-I electronics," Nucl. Instrum. Method A, vol. 955, 163247, 2020, doi: 10.1016/j.nima.2019.163247

Fabrication of thermally stable fiber Bragg gratings with high reflectivity for the mid-infrared

Luyi Xu, Toney T Fernandez, Benjamin Johnston, Simon Gross, Michael Withford, Alex Fuerbach

[1]*MQ Photonics Research Centre, Department of Physics & Astronomy, Macquarie University*
email: alex.fuerbach@mq.edu.au

Abstract: Thermally stable fiber Bragg gratings at mid-IR wavelengths are demonstrated. Unlike previous reports where grating strength and design wavelength vary with annealing, current report demonstrates grating structures which are resilient to temperatures up to 200°C.

The demonstration of femtosecond laser inscribed fiber Bragg gratings (FBGs) into fluoride fibers has enabled the development of alignment free, Watt-level all-fiber mid-infrared laser systems [1]. Poor thermal stability of FBGs is particularly concerning for high power lasers that unavoidably operate at elevated temperatures. From previous reports, Goya et al. used fs laser direct inscription technique with a target wavelength of 2800 nm ending up having a blue shift of 2.067 nm after annealing at 150°C [2]. Bharathan et al. used the same technique and also had a blue shift of 2 nm with an increase in κ of 39% at 150°C [3]. Heck et al. inscribed a long period fiber grating ending up having a strong blue shift of 11 nm along with 18% increase in κ value after 30 minutes of annealing at 75°C [4]. In this paper we propose an entirely new fabrication window to produce highly stable grating structures both at the designed reflectivity and peak wavelength for temperatures in excess of 200°C and 48 hours of annealing time.

Using 190 fs laser pulses at 1030 nm (Light Conversion, Pharos), we explored pulse repetition regimes of 1 - 150 kHz, inscribing line-by-line, type-I gratings. Inscription was performed directly through the jacket in a passive ZBLAN fiber (LeVerre Fluore) with a core of 6.5 μm, cladding of 125 μm and polymer coating of 190 μm in diameter. Focusing was done with a 0.6 NA lens and pulse energies between 100-350 nJ (between modification threshold up to visual damage in the fibre) were considered. A 20 μm/s feed rate of the laser spot was found to provide the strongest (saturated) index contrast upon inspection with phase contrast microscopy. A pulse energy of 300 nJ was found to be optimal independent of repetition rate, resulting in smooth grating structures with strongest transmission dips. Figure 1(a) shows a bright-field microscope image of the line-by-line structures inscribed with 50kHz, 300 nJ and 20 μm/s. Figure 1(b) shows the grating strength obtained at various repetition rates from 1 kHz to 150 kHz, written with 300 nJ and 20 μm/s. The spectral transmission profiles of 5 mm and 10 mm long, 1 kHz and 50 kHz written gratings are shown in Figure 1(c). The highest grating strength of κ = 448 m^{-1} was obtained at 1 kHz repetition rate followed by κ = 365 m^{-1} for 50 kHz. Both these gratings were annealed at 150°C and it was found that that the 50 kHz grating showing less than 5% reduction in its κ value whereas the strength of the 1 kHz grating was reduced by more than 20% (Fig. 1(d)). The Bragg wavelength of the 50 kHz grating shifted from 2146.6 nm to 2146.0 nm after 8 hours of annealing at 150°C, compared to a 2.067 nm shift for the 1 kHz grating [2]. Raising the temperature of the 50 kHz grating to 200°C for an additional 26 hours reduced the κ value by less than 5%.

In this work, we have systematically canvased a larger range of repetition rates for line-by-line inscription in fluoride fibres than is currently considered in the literature. We have clearly identified two modification regimes in the fluoride glass, typified by the annealing characteristics of the gratings inscribed at 1kHz and 50 kHz (Fig. 1d). We believe that this is an important step towards higher power scaling and long term stability for all-fiber mid infrared lasers.

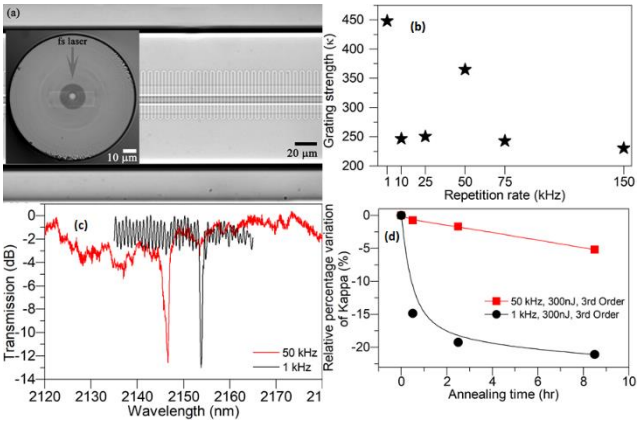

Figure 1: (a) Bright field image of the grating structures written at 50kHz, 300 nJ & 20 μm/s (b) Transmission dips for 50 & 1 kHz repetition rate written gratings (c) Relative percentage change of the κ values when annealed at 150°C (d) annealing characteristics for 1 kHz and 50kHz

References:

1. V.Fortin et al. Opt. Lett. **44**, 491 (2019)
2. K. Goya et al. Optics Express **25**, 33305 (2018)
3. G. Bharathan et al. Opt. Lett. **44**, 423 (2019)
4. M. Heck et al. Opt. Lett **43**, 1994 (2019)

Laboratory Scintillation Emulator for the Optical Low Earth Orbit Satellite Downlink Channel

K. Mudge[1], E. Jager[1], J. Kodithuwakkuge[1], B. Clare[1], V. Devrelis[2], G. Bolding[1] and K. Grant[1]

[1]DST Group, Edinburgh SA 5111, Australia
[2]*Gadzooks Pty Ltd, SA 5096, Australia*
E-mail: kerry.mudge@dst.defence.gov.au

***Abstract**: The implementation of a laboratory based optical channel emulator for the synthesis of the optical downlink channel from a low Earth orbit satellite to an optical ground station is described and the performance characterised. The optical channel emulator can be used for hardware-in-the-loop evaluation of optical modems and optical receivers for laser satellite communications applications.*

Optical data downlinks from low Earth orbit (LEO) satellites have the potential to significantly increase the downlink data capacity compared to RF technology. This is advantageous, for example, in reducing bottlenecks in transmitting the large amounts of sensor data generated for Earth-observation missions to ground stations. In addition to the potential for very data high rates, optical links have other desirable attributes including enhanced security, smaller payloads, immunity to interference and jamming and no RF spectrum licensing requirements.

Direct-to-Earth (DTE) links to an optical ground station (OGS) involve transmission through the Earth's turbulent atmosphere, which manifests as small temperature inhomogeneities resulting in fluctuations in the refractive index of the air over different length and time scales. The cumulative effect of these turbulence cells over the propagation path leads to intensity/irradiance fluctuations (scintillation), which can result in frequent and deep signal dropouts on millisecond timescales, known as optical fading [1]. Additionally, fluctuations in received signal can result from pointing jitter of the narrow laser beam widths transmitted from the satellite.

To combat the optical fading, various channel-coding schemes such as forward error correction (FEC) or data interleaving are proposed and implemented. Currently work is being undertaken by the Consultative Committee for Space Data Systems (CCSDS) [2] to standardise optical communication data formats to facilitate the global implementation and utilisation of OGSs for DTE links.

To aid in the development of channel coding schemes, and enable comparable performance investigations by different developers, a set of eight numerically generated, representative received power vectors (time-series) for optical downlinks has been defined [3]. These power vectors are based on models and measurements of laser transmission from satellites and include effects of both pointing jitter and optical turbulence. We extend these results by implementing an optical channel emulator test-bed to output the power vectors as an optical signal to enable a hardware-in-the loop testing of optical receivers, transmitters and modems. This allows testing to include the effects of the various technical noise sources and non-idealities present in the system such as detector noise or signal distortion. In the test-bed, shown in Figure 1, power vectors are imposed onto a laser source via an acousto-optic modulator (AOM) controlled by National Instruments data acquisition card and a custom LabVIEW program.

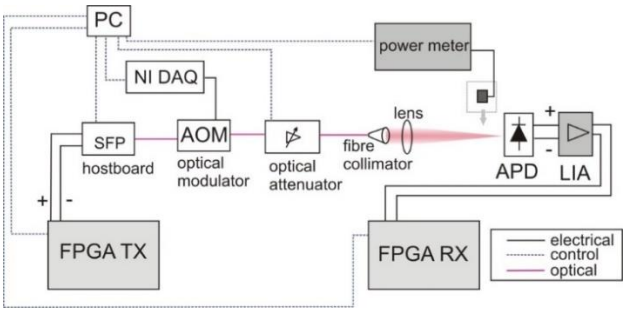

Figure 1 Optical channel emulator schematic.

Communication bit-error-ratio (BER) characterisation is highly dependent on the statistics of the fading, particularly in the tails of the distribution. We will present our experimental results on BER measurements to characterise the range of validity of our optical channel emulator. We will also present results demonstrating the utility of the hardware-in-the-loop optical channel emulator by using it to characterise optical receivers for communications and downlink channel measurements.

References:

1. L. C. Andrews and R. L. Philips, *Laser Beam Propagation through Random Media*, 2nd Ed. (2005)
2. CCSDS-website https://public.ccsds.org/Publications/default.aspx
3. D. Giggenbach, A. Shrestha, F. Moll, C. Fuchs and K. Saucke, IEEE International Conference on Space Optical Systems and Applications (ICSOS) (2019)

Cloud free sky comparison for optical ground station sites in Australia

V. Devrelis[1], H. C. Chedzey[2], M. J. Lynch[2], B. D. Nener[3], K. A. Mudge[4], B. Clare[4], and K. J. Grant[4]

[1]*Gadzooks Pty Ltd, SA 5096, Australia*
[2]*Curtin University, Perth WA, Australia,*
[3]*University of Western Australia, Perth WA, Australia*
[4]*DST Group, Edinburgh SA 5111, Australia*
email: vladimir.devrelis@dst.defence.gov.au

***Abstract**: Cloud free skies are important in the effectiveness of ground to space optical communication systems. To assess this, satellite data covering a decade have been analysed for locations of convenience in Australia. A comparison of the probability of cloud free line of sight for assessing sites is used in planning for the development of an optical ground station for infrared laser communications.*

The effectiveness of ground to space optical communication systems relies on cloud free skies since the presence of clouds cover either interferes or inhibits laser communication between an optical ground station (OGS) and a satellite. A four decade cloud climatological study for Australia was undertaken by Chedzey *et al* [1], and it is on this data that this analysis is based. By knowing the amount of cloud cover over specific geographic location it is possible to determine the amount of clear sky over a period of time. Clear skies infer the presence of a clear line of sight between the ground and space and thus availability for an optical communication channel.

The Earth's climate is a complex system [2] composed of multiple processes operating across all spatio-temporal scales, with non-linear behaviours [3] between its variables. Recent studies have shown that that cloud amount has changed in recent decades [4] and as such the focus is limited between 2009-2018, as older timelines may not reflect today's conditions.

The OGS uses a 0.5 m diameter aperture telescope for detecting and tracking a satellite and a laser at 1550nm and 1064nm wavelengths. To assess and compare OGS locations in terms of link availability, good knowledge of the atmosphere and its climate is needed Additional factors like proximity to services and infrastructure are also important for OGS locations.

The chosen data set from PATMOS-x AVHRR provide cloud information, with a 0.1° spatial resolution grid, from which monthly averages and standard deviations are extracted. These numbers are then used to derive a probability value for the cloud free line of sight (CFLOS) for a specified confidence interval. The effect of zenith angle on CFLOS and laser transmission is also examined. Different sites across Australia are examined to compare their CFLOS amount scaled from 0.0 to 1.0. Two contrasting locations have been chosen, one at the Northern (near Darwin) and another in the Southern (near Adelaide) regions of Australia.

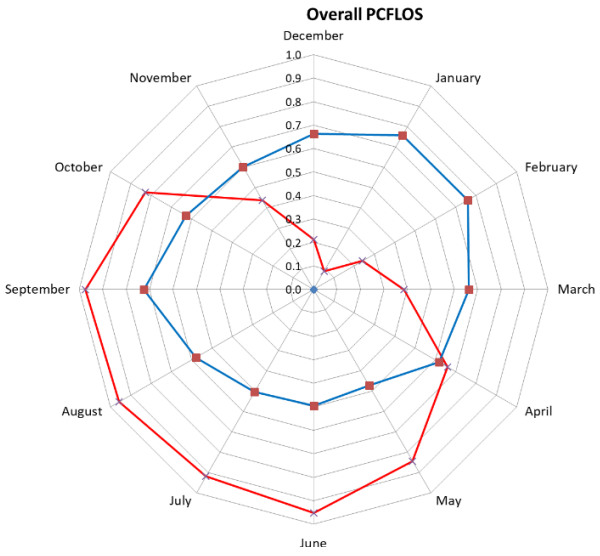

The plot in Figure 1 gives the probability of CFLOS for a site in the vicinity of Adelaide (blue) and Darwin (red). It indicates that the probability for laser communication is higher in summer than in autumn or winter, where sites at the North, near Darwin, have the reverse conditions.

As link availability is a key factor in determining the effectiveness of direct-to-Earth laser satellite communications, CFLOS analysis comparing various sites across Australia provides key information to guide practitioners on best placement of future OGS.

References:

1. H. C. Chedzey et al., *Proceedings of the 37th International Communications Satellite Systems Conference (ICSSC)*, 1, (2019).
2. Rind, D. Complexity and climate. *Science* **284**, 105–107 (1999).
3. Franzke, C. L. E. Nonlinear climate change. *Nature Climate Change* **4**, 423 (2014).
4. A. Delgado-Bonal et al., *Nature Sci Rep* **10,** 922 (2020).

The Mount Stromlo Optical Communication Ground Station

M. Birch[1], F. Bennet[1], D. Chandler[1], M. Copeland[1], D. Grosse[1], N. Herrald[1], and T. Travouillon[1]

[1]*Research School of Astronomy & Astrophysics, Australian National University, Canberra*

***Abstract**: The Australian National University is building a 0.7m telescope facility at Mount Stromlo for free space optical communication with satellites.*

The Research School of Astronomy and Astrophysics at the Australian National University (ANU) is building an optical communication ground station (OCGS) on Mount Stromlo in Canberra to be commissioned in 2022. The OCGS will be capable of transmitting and receiving communication laser signals from low Earth orbit to deep space. Free space optical communication (FSO) is a critical emerging technology as it allows space links with bitrates that are hundreds to thousands of times faster than radio, and supports ultra-secure quantum communication. This facility will therefore provide an important testbed for domestic FSO research, and tie Australia to the global network of ground stations already established.

The OCGS will take part in numerous FSO experiments, leveraging existing space missions and a swathe of upcoming missions. Low earth orbit relay demonstrations, deep space communication to the Moon, and quantum communication with satellites are primary goals of the OCGS.

Adaptive optics, the method of deforming a mirror in real-time to correct for wavefront distortions, will be used to reduce turbulence-induced errors that otherwise impact the bitrate. Adaptive optics for quantum communication is also currently being investigated over a horizontal channel to highlight the importance of this technology for quantum communication with satellites. The application of adaptive optics for FSO will leverage the existing expertise at the ANU, where numerous instruments have already been built to improve the wavefront for astronomy and satellite imagery.

The OCGS facility is a two-storey building, with a 0.7m aperture telescope in the upper dome and a lower-level laboratory. Received light will be transmitted through a Coudé path down the hollow pier supporting the telescope, where it can be directed onto one of four optical benches in the laboratory. The facility will support up to four major experiments on these benches, which may extend beyond FSO to the space situational awareness and astronomical research that is ongoing at Mount Stromlo Observatory. An auxiliary telescope may also be mounted on the primary telescope for transmitting lasers such that we can investigate bi-directional communication with satellites or laser guide stars for improved adaptive optics.

We report on the status of this project, provide an overview of proposed experiments, and expected outcomes from the OCGS.

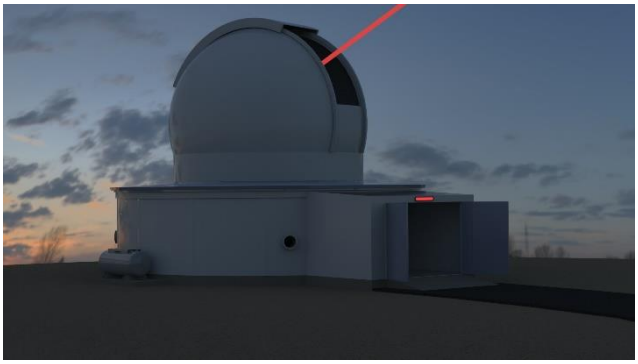

Figure 1: Render of the Mount Stromlo Optical Communication Ground Station with artistic render of laser downlink

Ultrastable dual frequency combs generation using whispering gallery resonators

N. J. Lambert[1, 2], L. S. Trainor[1, 2], H. G. L. Schwefel[1, 2]

1. Department of Physics, University of Otago, Dunedin, New Zealand
2. The Dodd-Walls Centre for Photonic and Quantum Technologies, New Zealand
email: nicholas.lambert@otago.ac.nz

***Abstract**: Frequency combs can be generated using second order effects in lithium niobate. We demonstrate the generation of dual combs with orthogonal polarisations; because both combs are generated in the same resonator, they have a mutual repetition rate stability better than 1 mHz.*

A frequency comb is a spectrum consisting of equally spaced lines. They are generated by optical sources which emit intensity pulses with a highly stable repetition rate, and are therefore a link between time and frequency measurements. They are now ubiquitous in applications of photonic technologies, having a wide range of uses [1] including frequency multiplexing of telecoms signals, optical frequency atomic clocks, calibration of astronomical instrumentation and low noise generation of microwave frequencies, as well as enabling studies of basic physical phenomena such as soliton dynamics and atomic coherence.

By combining two sources with slightly different repetition rates, a dual frequency comb can be generated. These offer an integrated photonic solution to a wide range of technological challenges, including spectroscopy, range finding, material characterisation and hyperspectral imaging. Such applications require a high level of mutual coherence between combs [2], but achieving such stability can be demanding.

In this work, we demonstrate an electro-optic frequency comb [3], in which microwave frequency modulation of the refractive index of an electro-optic nonlinear material creates new frequencies of light as sidebands around an optical pump. Here we simultaneously generate two combs centred around ~ 192 THz, using microwave tones of 7.814 GHz and 7.934 GHz. Furthermore, we show that by exploiting the rich structure of the electro-optic tensor in lithium niobate, we can create dual combs for which the two individual combs naturally have orthogonal polarisations.

To enhance the non-linear effects in lithium niobate, we fabricate whispering gallery mode (WGM) resonators with Q-factors of ~ 10^8. This leads to resonant enhancement of the optical fields supported by the modes, and an effective increase in the electro-optic coefficient. We also embed the resonator in a metallic microwave cavity to enhance the GHz frequency field; our scheme is therefore fully resonant.

The resulting combs are efficiently generated and ultrastable. Our combs have a relative linewidth of ~ 500 μHz, and require no stabilisation or post-processing methods. Neither do they require any careful navigation of the thermal landscape for initiation of the comb generation, as can be the case for Kerr combs. They therefore represent a turn-key dual comb solution, suitable for the most demanding of applications.

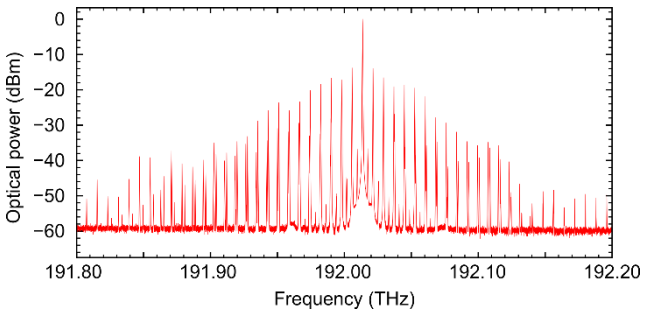

Figure 1: The dual frequency comb resulting from driving our fully resonant electro-optic system with two microwave tones.

References:

[1] T. J. Kippenberg, A. L. Gaeta, M. Lipson, and M. L. Gorodetsky, Science **361**, eaan8083 (2018).

[2] P. Trochaz, et al, Science **359**, 887 (2018).

[3] A. Rueda, F. Sedlmeir, M. Kumari, G. Leuchs, and H. G. L. Schwefel, Nature **568**, 378 (2019)

Parametric study of waveguide inscription into mid-infrared compatible glasses

S. Rehman*, T.T. Fernandez, S. Gross and A. Fuerbach

MQ Photonics Research Centre, Faculty of Science and Engineering, Macquarie University, New South Wales 2109, Sydney, Australia
*sobia.rehman@students.mq.edu.au

***Abstract**: We report the results of a systematic study into the femtosecond laser inscription of optical waveguides into two different mid-infrared transparent glasses, the fluorophosphate glass Schott N-FK58 and the fused silica glass Heraeus Suprasil 3001. Refractive index change profiles induced by femtosecond laser irradiation are presented.*

The goal of our work is to fabricate fibre-coupled glass chips that would enable the development of fully integrated and thus field deployable mid infrared laser sources. N-FK58 and Suprasil both feature good transmission up to 4 µm, yet compared to fluoride, tellurite, or chalcogenide glasses, both materials exhibit high thermal and mechanical stability.

Results and Discussions

Utilizing the femtosecond laser direct-write technique (FLDW), a systematic parameter study is conducted using different writing methodologies to explore the optimum waveguide inscription window for the fabrication of low loss waveguides in N-FK58 and Suprasil for operation in the 3 – 4 µm wavelength range.

A 5.1 MHz repetition rate femtosecond laser emitting pulses with a duration of 50 fs at a centre wavelength of 800 nm [1] is used to initially inscribe structures with a 1.4 NA oil immersion objective for a wide range of pulse energy (50 nJ - 120 nJ) and feed-rates (9 mm/min - 15 mm/min) values at a depth of 170 µm below the surface. The onset of cumulative heating was observed for energies beyond 70 nJ. A maximum refractive index contrast of 2×10^{-2} was observed for structures fabricated with 110 nJ and 9 mm/min, yet the size of the positive index-change region was limited to 2 - 2.5 µm. Thus, structures were also fabricated using lower NA objectives (1.25 NA and 0.45 NA), resulting in a maximum refractive index contrast of 1×10^{-3} for structures fabricated with 140 nJ pulse energy, 12 mm/min feed rate and 1.25 NA objective.

Next, using multi-scan waveguide writing with a 1.25 NA oil immersion objective, rectangular waveguides were written that exhibit a strong positive refractive index change with a band of strong negative refractive index change underneath as shown in figure 1. The maximum value of the induced positive refractive index change was as high as 8×10^{-2} with an overall height of the waveguide structure of about 3 - 4 µm.

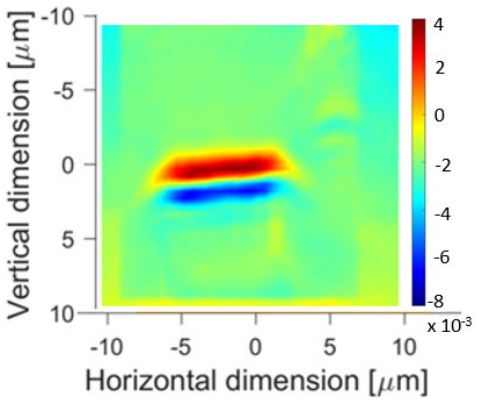

It is believed that only certain elements in this glass are responsible for the observed strong increase in the refractive index upon femtosecond laser irradiation and spatially resolved elemental analysis and micro-Raman measurements will be utilized to further study the material response.

Similar work was also carried out on Suprasil 3001 glass. Initial experiments using a high repetition rate (5.1 MHz) inscription laser are promising and point towards improved performance compared to previous attempts in the same glass using a low repetition rate (500 kHz) inscription laser [2].

References:

[1] A. Fuerbach *et al.*, "Chirped-pulse oscillators for the generation of high-energy femtosecond laser pulses," Laser and Particle Beams 23, 113 (2005).

[2] J. Martinez *et al.*, "3D laser-written silica glass step-index high-contrast waveguides for the 3.5 µm mid-infrared range," Optics Letters 40, 5818 (2015).

High-Q yttrium lithium fluoride whispering-gallery mode resonator

J. Christensen[1,2], F. Azeem[1,2], L. S Trainor[1,2], N. J. Lambert [1,2], and H. G. L. Schwefel[1,2]

[1]*The Dodd-Walls Centre for Photonic and Quantum Technologies, New Zealand*
[2]*Department of Physics, University of Otago, 730 Cumberland Street, Dunedin 9016, New Zealand*
email: harald.schwefel@otago.ac.nz

***Abstract**: The first yttrium lithium fluoride (YLF) whispering-gallery mode (WGM) resonator was successfully fabricated and explored. The YLF WGM resonator demonstrated an ultra-high quality factor (Q-factor) and was utilised in a set of experiments including a novel method of beam alignment. This YLF WGM resonator has the potential to generate frequency combs and further suggests rare-earth doped YLF WGM resonators may be suitable candidates to observe third harmonic generation (THG).*

YLF is a transparent, anisotropic, centrosymmetric crystal of which by symmetry disallows second harmonic generation processes but in which third harmonic generation THG and other third order processes, such as Kerr-frequency combs are allowed. Furthermore, YLF is an excellent host of rare earth ions, as the yttrium ion is of similar size and can be exchanged without changing the crystal dimensions.

In order to investigate nonlinear phenomena in YLF we fabricate a YLF WGM resonator. WGM resonators are known to have large cavity confinement times, or Q-factors [1] that, combined with their small footprint, allow them to generate the high field intensities required to observe non-linear optical phenomena [2]. The fabrication by a single point turning machine using diamond tools produced a 2.94 mm YLF WGM resonator that resulted in an ultra-high Q-factor resonator ($Q \approx 5\times10^8$) in the near-infrared telecommunication spectrum. To the best of our knowledge this is the first and the highest recorded Q-factor for YLF.

We also report a novel method of resonator alignment for evanescent coupling. The resonator was imaged through the back side of a trapezoidal coupling prism where Newton rings around the contact point were observed (see Figure 1). These Newton rings provide a direct measure of the resonator to prism separation as well as direct feedback on the position of an incident coupling beam. By overlapping the beam profile with the Newton rings, coupling was achieved. This process is shown in Figure 1.

Furthermore, a series of experiments was performed with the resonator showing that good temperature control is possible in the configuration, and we observed that differently polarized modes obeyed different sensitivities to temperature changes, as expected.

We expect these studies to lay the groundwork for a new material to be explored for both third harmonic generation, as well as its reverse, and in Kerr soliton formation.

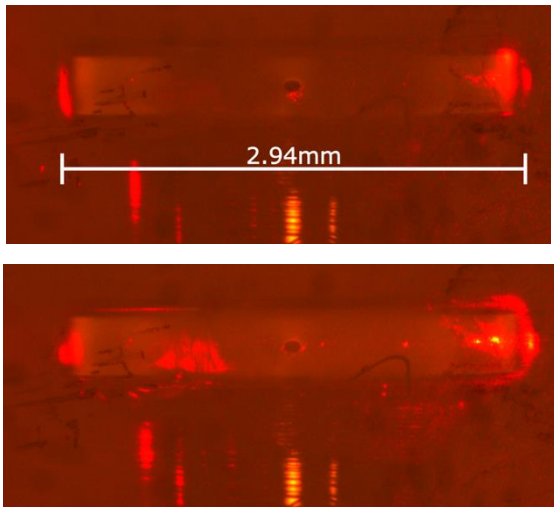

Figure 1: Observation of Newton rings at the contact point between prism and resonator, seen in the center of each image. Top figure shows an incident red laser beam misaligned just below the Newton ring. Bottom figure shows alignment of beam and Newton ring resulting in coupling seen through the resonator as a red glow.

In conclusion, this study has shown YLF to be an excellent high-Q optical material and a promising candidate for THG and Kerr-comb generation. This study also found a novel technique in the imaging of Newton rings for use in beam alignment into the resonator through a trapezoidal prism. A technique which may provide alternatives in beam alignment of experimental arrangements which could have restricted geometry or require finer tuning.

References:

1. D. V. Strekalov, et al., *J. Opt.* **18**, 123002 (2016).
2. L. S. Trainor, et al., *Phys. Rev. Appl.* **9**, 024007 (2018).

Using convolutional neural networks for nonlinear frequency division multiplexing

W. Q. Zhang[1], Terence H. Chan[2], and S. Afshar V.[1]

[1]*Laser Physics and Photonic Devices Laboratories, STEM, University of South Australia, SA 5095, Australia*
[2]*Institude for Telecommunications Research, University of South Australia, SA 5095, Australia*
email: wenqi.zhang@unisa.edu.au

***Abstract**: A 0.5 MB serial and a 128 MB parallel CNN designs are proposed for receiving 128-subcarrier 16-QAM NFDM signals. Both networks were successfully trained to 99.9% accuracy.*

Nonlinear Fourier Transform (NFT) is a novel technique that has the potential to break through the Shannon linear capacity limit in optical fibres [1]. It has been experimentally demonstrated that NFT can outperform conventional optical communication methods under the same conditions [2,3]. Previously, a convolutional neural network (CNN) is shown to be useful to decode nonlinear frequency division multiplexing (NFDM) signals [4]. In this work, we propose two network designs based on the previous work to detect NFDM signals using CNNs that aimed at small network size and high performance separately. The proposed work will allow us to take the advantage of the fast-developing deep learning hardware industry to boost the efficiency of developing NFT-ready devices.

NFDM, as shown in Eq. (1), is similar to its linear counterpart, except the nonlinear spectrum of the signal $Q(\lambda)$ is used instead of the linear spectrum $q(\omega)$, $\lambda = 2\omega$ is the nonlinear frequency and ω is the linear angular frequency.

$$Q(\lambda) = \sum_n c_n w_n(\lambda)\,, \qquad (1)$$

where n is the number of subcarriers, c_n is the complex data symbols, $w_n(\lambda)$ is the carrier wave.

The neural network designs in this work take the linear spectrum of the signal $q(\omega)$, whose nonlinear spectrum is $Q(\lambda)$, as the inputs and outputs the complex data symbols c_n. In the serial design, a gate function is applied to the pulse spectrum to pick out a subcarrier with its most influential neighbouring subcarriers to significantly reduce the input size to the network. A CNN, as shown in Fig. 1 (top), is trained for only 1 subcarrier (subcarrier n). To decode any other subcarriers using this network, a segment of the pulse spectrum $q(\omega)$ around a subcarrier is taken out and shifted in the linear frequency domain using

$$\tilde{q}_n(\omega, z) = \tilde{q}(\omega - 2\lambda_n, z)e^{jt_n(\omega-\lambda_n)}, \qquad (2)$$

where λ_n is the central nonlinear frequency of subcarrier n, $t_n = 4\lambda_n z$. Equation (2) is built into the network as a translation layer.

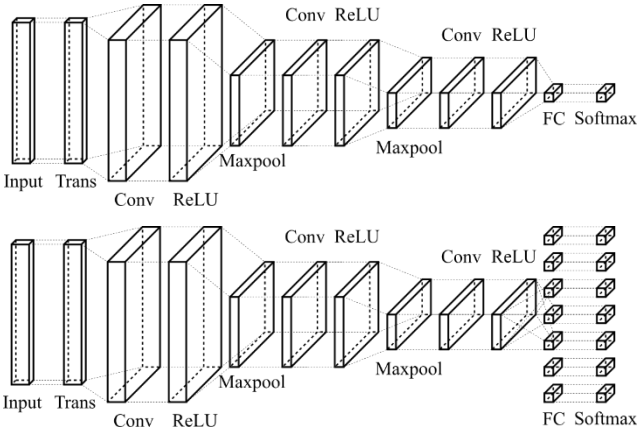

Figure 1: The conceptual designs of the serial (top) and parallel (bottom) network.

In contrast to the serial design, a parallel network, shown in Fig. 1 (bottom), can be designed to process all the subcarriers at once to boost the processing speed. The parallel design takes the whole spectrum $q(\omega)$ as the input and outputs c_n of all subcarriers simultaneously. For this network, the following equation is needed as the translation layer:

$$\tilde{q}^c(\omega, z) = \tilde{q}(\omega, z)e^{-j\omega^2 z}\,. \qquad (3)$$

Both networks are trained with simulated 128-subcarrier 16-QAM optical bursts and reach 99.9% accuracy at the end of their training cycles. The trained parallel network occupies 128 MB of memory for an input size of 4096 elements while the trained serial network occupies merely 0.5 MB for an input size of only 64 elements. The parallel network requires about 2.8 times more operations than the serial network, but the parallel network can be computed in parallel.

1. M. I. Yousefi and F. R. Kschischang, *IEEE Transactions on Information Theory*, 60, 4312 (2014),
2. S. T. Le and H. Buelow, in *Photonic Networks; 19th ITG-Symposium*, 1 (2018).
3. S. T. Le, K. Schuh, F. Buchali, and H. Buelow, in *2018 Optical Fiber Communications Conference and Exposition (OFC)*, 1 (2018)
4. W. Q. Zhang, T. H. Chan, and S. Afshar V., *Opt. Express*, 29, 11591 (2021).

Successful Intracellular Microrheology of Living Macrophages

M. L. Watson[1], A. B. Stilgoe[1], I. A. Favre-Bulle[1,2], J. Stow[3], and H. Rubinsztein-Dunlop[1]

[1]*University of Queensland, QLD 4072, Australia*
[2] *Queensland Brain Institute, QLD 4072, Australia*
[3]*Institute for Biomedical Sciences, QLD 4072, Australia*
email: m.l.watson@uq.net.au

***Abstract**: We present the successful use of rotational optical tweezers to determine the microrheology within a macropinosome of a living macrophage cell. This work provides the foundation for wideband microrheological studies of intracellular compartments and opens a new research direction to study macropinocytosis and other biological processes.*

Studies of mechanical properties of living cells can unravel the physical phenomena that govern well defined biological functions. Macropinocytosis [1], a cellular mechanism involving the uptake of extracellular fluid and formation of macropinosomes, has a variety of crucial cell-specific roles most notably in immune cells [2] and cancer cells [3].

The microrheology of macropinosomes, large cytoplasmic vesicles resulting from macropinocytosis [4], provides an intriguing source of information that has previously been concealed by the accessibility of the vesicle, its micro-litre volume, and the highly dynamic nature of the mechanism. Here we show that during macropinocytosis, a probe microsphere can be successfully internalised and used for intracellular microrheology of living macrophage cells. This is achieved using rotational optical tweezers [5] via the transfer of optical angular momentum from the trapping beam to an internalised birefringent probe particle. Vaterite microspheres were used as the photonic probes because they are strongly birefringent, can be synthesised in batch, and are not toxic to the cell.

Microrheometry performed in the rotational regime has a crucial advantage over linear techniques as wall effects reduce with distance cubed rather than distance squared [6]. Hence, the rotational regime provides the best opportunity to study the rheometry of enclosed microenvironments. This is especially important studying macropinosomes because they undergo shrinkage during an early maturation phase.

For this proof-of-concept work, macrophage cells were treated with the protein inhibitor YM201636 which prevented macropinosomal shrinking. This facilitated observation of internalised probe particles within the macropinosome.

After this treatment, vaterite microspheres were added to the cells and naturally internalised via macropinocytosis. A single internalized microsphere was trapped and rotated using rotational optical tweezers with varying trapping power. By measuring the torque on the microsphere and the corresponding rotation rate [5], we determined viscosity within the macropinosome. Additionally, the cells remained alive and active despite measurements being performed at room temperature.

The results confirm the usefulness of the presented method for quantitative and dynamic measurements of viscosity within extremely small volumes during biologically relevant processes.

Since many biologically important fluids consists of polymers, their viscoelastic response over a wide frequency should be studied. These results indicate wideband microrheometry is feasible and can be achieved by monitoring the angular position of the birefringent probe as it experiences an alignment torque via active and passive methods [7].

To summarise, this work confirms that microrheometry within living cells is achievable with rotational optical tweezers and provides the foundation for future wideband microrheological investigations. It reveals a novel research avenue to address processes involving macropinocytosis including macropinosomal shrinking, variations between cell types, pathogen entry, cellular feeding, and antigen presentation.

References:

1. Lewis, W. H. *Bulletin of the Johns Hopkins Hospital* **49**: 17-27. (1931).
2. Sallusto, F., et al. *The Journal of experimental medicine*, **182**(2), 389-400. (1995).
3. Commisso, C., et al. *Nature*, **497**(7451): 633-637. (2013).
4. Kerr, M. C., et al. *Traffic*, **10**(4): 464-371. (2009).
5. Bishop, A. I., et al. *Physical Review Letters*, **92**(19):198104. (2004).
6. Leach, J., et al. *Physical Review E*, **79**(2), 026301. (2009).
7. Zhang, S., et al. *Optica*, **4**(9), 1103-1108. (2017).

Biosensing with high Q-factor dielectric metasurfaces

S. Manjunath[1], B. Karawdeniya[1], A. Damry[2], C. Jackson[2], and D. Neshev[1]

[1]ARC Centre of Excellence TMOS, Research School of Physics, Australian National University, Acton, 2601, Australia
[2] Research School of Chemistry, Australian National University, Acton, 2601, Australia

email: shridhar.manjunath@anu.edu.au

***Abstract**: We employ dielectric high quality-factor nano resonators to sense very low concentrations of Bovine Serum Albumin. Also, we demonstrate high sensitivity, selectivity, non-invasive, label-free biosensor which can be easily integrated into point-of-care devices.*

Metasurfaces are arrays of subwavelength particles which strongly interact with the electromagnetic radiation. Metasurfaces provide a great platform for point-of-care devices as they are non-invasive, label-free, rapid, and robust [1-2]. A typical plasmonic metasurface confines the light partially, hence exhibits low quality-factor (Q-factor) and high dissipative losses. For effective sensing applications, the Q-factor should be increased several times over the plasmonic resonators. Recent work shows that high Q-factors can be achieved by employing high-index dielectric metasurfaces based on the concept of Bound States in Continuum (BIC) [3]. BIC modes have infinite Q-factor but do not couple with continuum electromagnetic spectrum. Hence, we introduce a small degree of structural asymmetry to overlap resonance mode with the BIC mode, thereby forming a quasi-BIC. As shown in the figure 1a, one of the ovals is squeezed along the y-axis to introduce asymmetry. By controlling the dimensions of these ovals, we were able to obtain a very high Q-factor (~180) and high sensitivity (~210 nm/RIU).

Metasurfaces sensing works based on refractometry yet lacks the capability to selectively sense the target analyte. This challenge can be addressed by immobilizing bio-receptors on top of metasurfaces that provide very high selectivity to target biomarkers.[4] Here, we immobilize anti-BSA (Bovine Serum Albumin) through protein G, to obtain very high selectivity to BSA. As shown in figure 1b, we attach protein G-antibody complex by using a silane linker. As demonstrated in figure 1b, we observed a 4 nm shift in resonance frequency after binding 10 µM BSA. The combination of high selectivity and highly sensitive metasurface provide an excellent platform for bio-sensing applications. This process can be replicated for other antibody-antigen combinations, including for testing of type-I diabetes and other diseases.

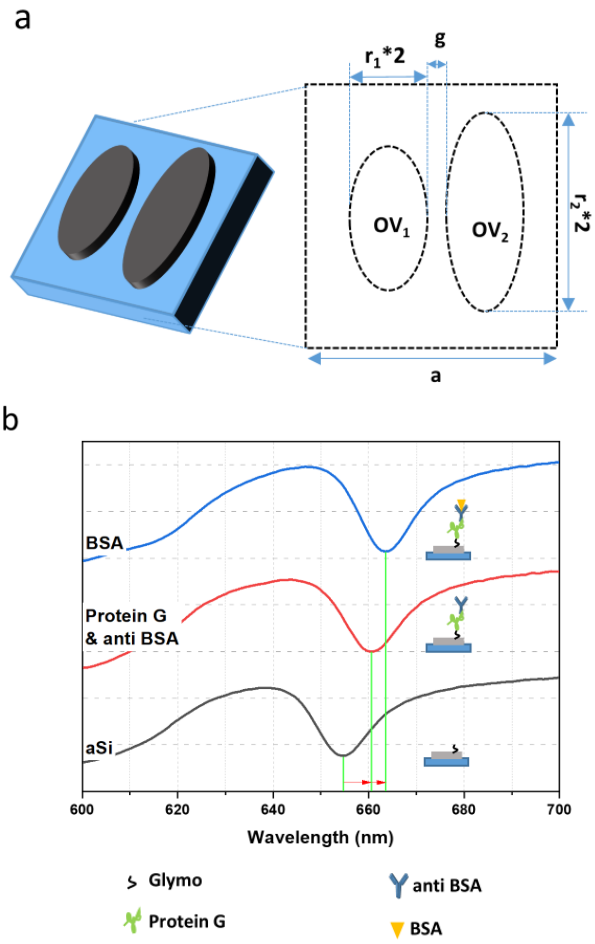

Figure 1: a) Schematics of a single unit-cell of the metasurfaces, where a = 420 nm, r_1 = 60 nm, g = 60 nm, r_2 (OV_1) = 130 nm, r_2 (OV_2) = 160 nm, and height of the disks is 70 nm. b) Transmission spectra measured after attaching each biomolecule.

References:

1. O. Yavas, et al, *Nano Lett.* **17**, 4421-4426 (2017).
2. N. Bontempi, et al, *Nanoscale.* **9**, 4972 (2017).
3. Yesilkoy, et al, *Nat. Photonics.* **13**, 390 (2019).
4. R. Aoni, et al, *Adv. Funct. Mater.* 2103143 (2021).

Centimetre-Spatial-Resolution Photonic Radar Using Low-Speed Electronics

Ziqian Zhang[1,2], Yang Liu[1,2], and Benjamin J. Eggleton[1,2]

[1]*Institute of Photonics and Optical Science (IPOS), School of Physics, The University of Sydney, NSW 2006, Australia*
[2]*The University of Sydney Nano Institute (Sydney Nano), The University of Sydney, NSW 2006, Australia*
email: ziqian.zhang@sydney.edu.au

***Abstract**: A novel photonic radar system with over 10 GHz bandwidth scalability and 1.2-centimetre resolution based on an MHz-RF-driven optical frequency-shifting modulation is demonstrated to detect and recognise unmanned aerial vehicles (UAVs) as a proxy for real-world resolution-demanding applications.*

High-resolution radars are employed in ubiquitous scenarios such as environment sensing, penetrating security inspection, and self-driving vehicles [1]. However, conventional radar systems that use electronics purely suffer from inherited bandwidth and flexibility bottlenecks, limiting the performance and potential applicability [2]. Photonic radars can overcome these weaknesses, enabling broadband, high-resolution detection, and adaptable operating frequency to cope with requirements for broader applications [3]. Although photonics-assisted radars are reported with centimetre resolution, the use of high-speed, high-priced, and bulky RF electronics made them unrealistic when developing such systems for mobile and handheld sensing purposes [4-6]. Therefore, a photonics-based radar system that uses low-speed electronics and has the potential for photonic integration is highly desirable for real-world performance-demanding applications.

In this work, we demonstrate a novel photonic radar system with a range resolution of 1.2 centimetres enabled by a broadband stepped-frequency (SF) radar signal over 10 GHz. The broadband SF waveform is built on steady frequency-increased pulses synthesised using a frequency-shifted optical modulation driven by an electronic signal oscillating at 80 MHz. The system can resolve the distance and velocity information of targets that are translated to electric signals at the MHz level using photonics-based coherent demodulation. In this radar scheme, the use of low-speed electronics releases the signal processing burdens by generating much less data, which low-cost, off-the-shelf devices can easily handle, making the detection in real-time, which eliminates the need for bulky, high-performance, and expensive apparatus required by conventional electronic radars and photonic radars.

Fig. 1a shows the schematic of the proposed photonic SF radar system. A continuous-wave light is split into two paths. One is chopped into a pulse train by an optical switch (OS), seeding the optical frequency-shifting loop and frequency-shifted by 80 MHz every round-trip time using an acousto-optic modulator (AOM) to generate the SF waveform optically. The other is frequency downshifted by 28 GHz and recombined with the optical SF signal, generating an RF carrier through the heterodyning in the photodiode (PD). Fig. 1b is the time-frequency plot of the SF signal in the baseband, demonstrating the bandwidth scalability above 10 GHz to enable the ultra-fine resolution of the system, which remains challenging using conventional electronics with narrow bandwidths. A clear range-Doppler image of the drone's propellers is reconstructed in Fig. 1c, proving the performance of the proposed system with centimetre resolution.

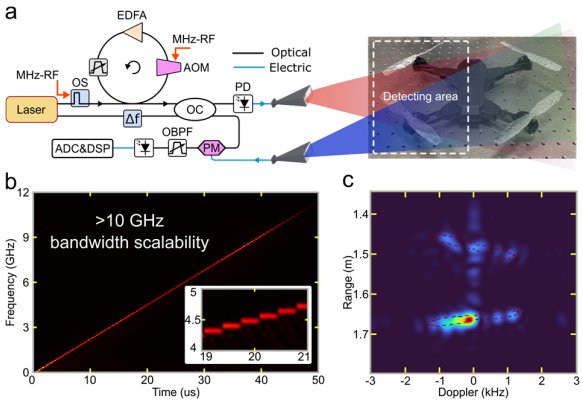

Figure 1: (a) Experimental setup for drone imaging, (b) time-frequency plot of the generated SF signal, (c) reconstructed radar image of a drone's propellers.

In conclusion, we demonstrated a novel photonic radar that offers a new path towards high-resolution, low-speed electronics controlled, and light data load radar sensing module. Drone detections serving as a proxy of practical and resolution-demanding applications showed a promising future of the proposed system.

References:

1. Scheer, Jim, et al., Principles of modern radar *(2010).*
2. Ghelfi, Paolo, et al., *Nature. 507.7492.* (2014).
3. Pan, Shilong, et al., Journal of Lightwave Technology (2020).
4. Li, Simin, et al., *Laser & Photonics Reviews* (2020).
5. Zhang, Ziqian, et al., *2020 Conference on Lasers and Electro-Optics (2020).*
6. Peng, Shaowen, et al., *Optics Express 26.2* (2018).

Distributed temperature and strain measurements at an active plate-bounding fault using fiber optic sensors

Shahna M Haneef[1], James Loveday[1], John Townend[2] , Rupert Sutherland[2] Kasper Van Wijk[1] and Neil Broderick[1]
[1]Department of Physics, University of Auckland, New Zealand, 2
[2] Victoria University of Wellington, New Zealand
email: Shahna.haneef@auckland.ac.nz

***Abstract**: New Zealand attracts people for its liveliness, but its geology calls for more seismic event. Alpine faults is one of the largest source of such activities. Deep fault drilling project 2B is commissioned to explore and understand the geophysical properties of the fault at depth, which involves the distributed temperature and strain monitoring of boreholes in the Whataroa valley. Here, we report the development and field deployment of the distributed fiber optic sensors based on Raman and Brillouin scattering.*

The Alpine Fault, located at the boundary between the Pacific and Australian tectonic plates, is a unique-natural laboratory for researchers across multiple countries. At 850 km long, this transform fault spans the entire length of South Island and poses one of the greatest sources of seismic risk to NZ. Paleo-seismic records at the central section of fault reveal that a great earthquake of Mw > 8 occurs on interval of 330 ± 60 years, and that an event is due. An event of this magnitude would propagate hundreds of kilometers uninhibited, causing significant impact to both land and community [1].

Aiming at investigating the ambient and geophysical conditions before large earthquakes, the Deep Fault Drilling Project scientific borehole (DFDP-2B) was drilled in the Whataroa valley to a depth of 893 m. As part of this campaign, a fibre-optic cable was installed in the borehole for, distributed temperature profiling and to better understand the fault at depth [2]. We developed a hybrid distributed strain sensor (DSS) and distributed temperature sensors (DTS) based on Brillouin and Raman scattering in optical fiber, operating at 1550nm for continuous monitoring of the temperature and strain using the single-mode (SM) and multi-mode (MM) fibres in the installed cable. Unlike the conventional method, distributed fiber optic sensors offer a high spatio-temporal resolution and can be used at extreme geophysical conditions [3-4].

Fiber optic DSS relies on Brillouin scattering in optical fiber, where the frequency shift (BFS) back scattered Brillouin Stokes signal is sensitive both temperature and strain changes in the medium. In order to differentiate the effects of temperature and strain perturbation, an independent temperature measurement is carried out using the Raman DTS. The ratio of Raman anti-Stokes to Stokes back-scattered intensity is the parameter used to accurately measure the temperature at any point along the fiber length. Since only one of the installed cable is accessible to the interrogator, the above two measurements are carried out in the optical time domain reflectometry configuration. In this paper, we report the temperature and strain measurements carried out using the developed sensor along the 893m deep borehole in the Alpine fault. A permanent continuous monitoring of the temporal variation of temperature and strain will lead to a better understanding of the processes in the damage zone of the Alpine fault

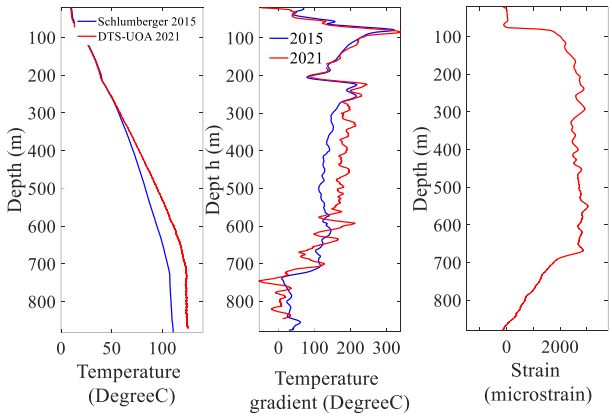

Figure 1: Estimated (a) temperature, (b) gradient of temperature and (c) strain along the length of the borehole measured using Raman and Brillouin OTDRs.

References:

1. R. Sutherland, *Earth and Planetary Science Letters* 177, no. 3-4 (2000): 141-151.
2. R. Sutherland, *Scientific drilling* 8 (2009): 75-82.
3. M.A. Soto, Electronic Letters 43, 862-84 (2007)
4. M. Nikles, *Journal of Lightwave Technology*, vol. 15, pp. 1842-1851 (1997)

Machine learning for sensing with a multimode exposed core fiber specklegram sensor

D. Smith[1], L.V. Nguyen[1], D.J. Ottaway[1], T.D. Cabral[2,3], E. Fujiwara[3], C.M.B. Cordeiro[1,2], and S.C. Warren-Smith[1,4,5]

[1]*Institute for Photonics and Advanced Sensing and School of Physical Sciences, The University of Adelaide, Adelaide, SA 5005, Australia*
[2]*"GlebWataghin" Institute of Physics, University of Campinas, Campinas 13083-859, Brazil*
[3]*School of Mechanical Engineering, University of Campinas, Campinas 13083-860, Brazil*
[4]*Australian Research Council Centre of Excellence for Nanoscale BioPhotonics, The University of Adelaide, SA 5005, Australia*
[5]*Future Industries Institute, University of South Australia, Mawson Lakes, SA 5095, Australia.*
email: darcy.smith@adelaide.edu.au

***Abstract**: Deep neural networks are applied to the problem of fibre specklegram sensing and correlating changes in a specklegram with changes in an environmental parameter to be sensed. They are shown to solve issues present with a traditional correlation method.*

Fibre specklegram sensors (FSSs) are optical fibre sensors which correlate changes in the specklegram output of a multimode fibre (MMF) with changes in an environmental measurand of choice [1]. This change in a specklegram is traditionally quantified through two statistical methods: correlation and subtraction, which use pixel-wise multiplication and subtraction respectively between specklegrams.

We have previously demonstrated the use of the zero-normalised cross correlation (ZNCC) function to make an FSS out of an exposed core fibre for temperature and water depth sensing [2], by mapping a specklegram's correlation score against a reference specklegram to a measurand value.

Despite this method functioning as a sensor within certain temperature/depth from the reference, the correlation method suffers from a range issue in that once the specklegrams are sufficiently different from the reference specklegram, changes in the measurand and specklegram no longer produce meaningful changes in the ZNCC score, i.e. the correlation saturates.

In this work we show that deep neural networks (DNNs) are a more sophisticated way of mapping changes in an MMF's specklegram to changes in a measurand and overcome this range issue.

We employ a convolutional neural network (CNN) based on the VGG-16 architecture [3], trained to predict air temperature/water depth labels when given specklegrams. We use the same specklegram data as in [2], and compare our results from the CNN to the ZNCC method presented therein.

We show that within the ZNCC method's dynamic range, both methods function well for sensing with comparable accuracy, but that the CNN does not suffer from the dynamic range issue that the ZNCC method does, and instead shows the potential for a much larger range of sensing.

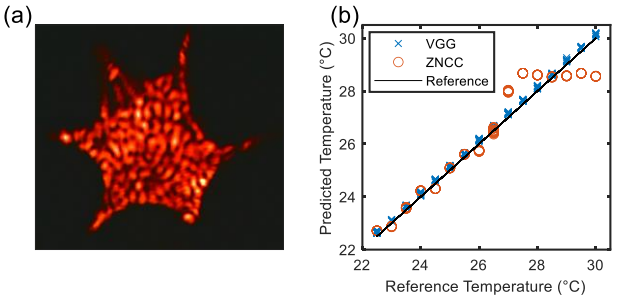

Figure 1: (a) example specklegram, (b) air temperature predictions from the two methods

We demonstrate the robustness of the CNN method as it continues to accurately map a specklegram to its temperature label despite being given artificially translated specklegram images, something the ZNCC method fails at. This highlights the power of utilising the entire specklegram along with the CNN's feature recognition capabilities as opposed to reducing the specklegram to a single correlation value for sensing.

Funding: ARC Future Fellowship (FT200100154). Optofab node of the Australian National Fabrication Facility utilizing Commonwealth and South Australian State Government funding. ARC Centre for Nanoscale BioPhotonics (CE14010003). The São Paulo Research Foundation (FAPESP) under grant 2018/10409-7

References:

1. S. Wu, S. Yin, and F. T. S. Yu, Appl. Opt. **30**, 4468-4470 (1990).
2. T. D. Cabral, E. Fujiwara, S. C. Warren-Smith, H. Ebendorff-Heidepriem, and C. M. B. Cordeiro, Opt. Lett. **45**, 3212-3215 (2020).
3. K. Simonyan and A. Zisserman, in *ICLR*, (2015).

Simultaneous measurement of high temperature and pressure using pure silica microstructured optical fiber

Mohammad Istiaque Reja[1,2,3*], Linh V. Nguyen[1], Heike Ebendorff-Heidepriem[1,2], and Stephen C. Warren-Smith[1,2,4]

[1]*Institute for Photonics and Advanced Sensing, School of Physical Sciences, The University of Adelaide, Adelaide, SA 5005, Australia*
[2]*ARC Centre of Excellence for Nanoscale BioPhotonics, The University of Adelaide, Adelaide, SA 5005, Australia*
[3]*Department of Electrical and Electronic Engineering, Chittagong University of Engineering and Technology, Chattogram 4349, Bangladesh*
[4]*Future Industries Institute, University of South Australia, Mawson Lakes, SA 5095, Australia*
**email: mohammadistiaque.reja@adelaide.edu.au*

***Abstract**: We report a pure silica microstructured optical fiber based interferometric sensor for pressure measurement at high temperature up to 800°C. Using a Fourier technique and sensitivity matrix approach the sensor can compensate the cross-sensitivity of temperature on the pressure measurement. The sensor is demonstrated to exhibit excellent stability with a detection limit of 8.86 kPa at 800°C temperature. This compact and potentially low-cost sensor is promising for extreme environment applications.*

Fiber optic sensors have been demonstrated for high temperature sensing and pressure measurement at high temperature using different approaches like fiber Bragg grating (FBG), Fabry-Perot interferometer (FPI), and multimode interferometer [1, 2]. However, a big challenge for pressure measurement at high temperature is the temperature compensation. In our work [3] we have used a multimode interferometer created by splicing a polarization-maintaining single-mode fiber to a four-hole asymmetric multimode microstructured optical fiber (Fig. 1 inset). The multimode interference spectrum has many fast Fourier transform (FFT) peaks corresponding to interference between pairs of modes.

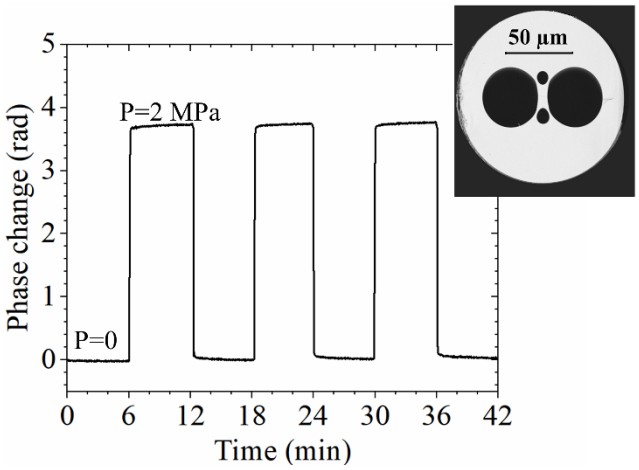

Figure 1: Demonstration of pressure measurement with the pressure sensing fiber (inset) at 800°C. Within 42 minutes time duration, nitrogen gas pressure of 2MPa was turned on and off alternately, for a period of 6 minutes in each step [3].

We tracked two different interference peaks having different temperature and pressure sensitivities and used a sensitivity matrix approach to measure both parameters simultaneously. We measured a pressure sensitivity of 2.29 rad/MPa, which matched closely with numerical simulations. Fig. 1 shows the pressure measurement at 800°C for 42 min where nitrogen gas pressure was alternately turned on and off. The pressure measurement was stable up to 700°C and showed slight drift at 800°C (less than 0.012 rad/min). We measured the minimum detectable pressure by considering the standard deviation of the phase fluctuation at 800°C and 2 MPa pressure. The detection limit was found to be 8.86 kPa, which compares favourably to other reported sensors [4].

Acknowledgements

Australian Government Research Training Program Scholarship, Australian Research Council (ARC) Future Fellowship (FT200100154), Ramsay Fellowship from the University of Adelaide. Optofab node of the Australian National Fabrication Facility utilizing Commonwealth and South Australian State Government funding. ARC Centre for Nanoscale BioPhotonics (CE14010003).

References:

1. Warren-Smith, Stephen C. et al., *Optics express* 24.4, p.3714-3719 (2016).
2. Zhang, Z., et al., *Optics letters*, 43.24, p. 6009-6012 (2018).
3. Reja MI et al., Journal of Lightwave Technology, submitted (2021)
4. Ma, W., Y. Jiang, and H. Gao, Measurement Science and Technology, 30.2, p. 025104. (2019)

Probing the electromagnetic response of dielectric antennas by vortex electron beams

A. Konečná[1,2], M.K. Schmidt[1,3], R. Hillenbrand[4], and J. Aizpurua[1,5]

[1]*Materials Physics Center, CSIC-UPV/EHU, 20018 Donostia-San Sebastian, Spain*
[2]*Central European Institute of Technology, Brno University of Technology, 612 00 Brno, Czech Republic*
[3]*Macquarie University Research Centre in Quantum Engineering (MQCQE), MQ Photonics Research Centre, Department of Physics and Astronomy, Macquarie University, NSW 2109, Australia*
[4]*IKERBASQUE, Basque Foundation for Science, CIC NanoGUNE and UPV/EHU, 20018 Donostia-San Sebastian, Spain*
[5]*Donostia International Physics Center DIPC, 20018 Donostia-San Sebastian, Spain*
email: mikolaj.schmidt@mq.edu.au

***Abstract**: We theoretically explore the possibility of near-field probing of electric and magnetic resonant modes in high-refractive-index nanoantennas with focused electron beams. We present a theoretical framework to calculate electron energy loss spectra corresponding to electron beams with both zero and non-zero orbital angular momentum interacting with arbitrarily shaped nanostructures. We demonstrate that a focused electron beam represents a versatile probe to characterize complex spectral response of the dielectric nanoantennas and that electron energy loss spectroscopy might be used to distinguish modes of electric and magnetic nature. We also analyze dichroism in spatially-resolved electron energy loss spectra when chirally-arranged nanostructures are probed by vortex electrons.*

Electron microscopy forms a versatile set of tools for interrogating the physical, and chemical properties of nanosystems. In particular, in Electron Energy Loss Spectroscopy (EELS), electron beams are used as broadband sources of electromagnetic waves to map out the optical response of the surroundings (see Fig. 1(a)) – specifically, the electric component of the Local Density of States (e-LDOS).

Over the last decade, the ultra-high spatial resolution offered by EELS was complemented by increasing its spectral resolution, and efficient coupling to electron-beam-forming optics [1]. Another recent innovation in electron microscopy was the introduction of Vortex Electron Beams (VEBs) made up of electrons with large Orbital Angular Momentum [2]. In VEBs, the circulating electrons create an effective magnetic current $\mathbf{J}_m$, which can probe the magnetic LDOS, complementing the capabilities of the standard EELS (see Fig. 1(b)).

In this work we introduce a full quantum-mechanical description of the *magnetic EELS*. This treatment allows us to account for the considerable spatial extension of the electrons, or the interference between the electric and magnetic currents [3-5]. We then identify the semi-classical limit of this problem to build a complete analogy with the EELS technique.

Finally, we show how the magnetic EELS can interrogate the magnetic response of several 2D and 3D systems of interest in nanophotonics: dielectric nanoantennas, waveguides, and simple chiral structures.

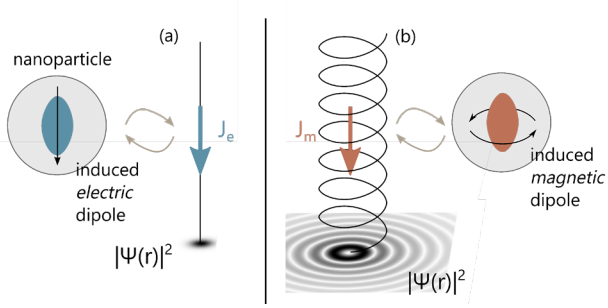

Figure 1: Schematic representation of the Electron Energy Loss Spectroscopy using (a) electrons without, and (b) with OAM, interacting with a nearby dielectric nanoparticle and probing its electric and magnetic response. Bottom plots represent the approximate density of the electron function.

References:

1. F.J. García de Abajo, and A. Konecna, Phys. Rev. Lett. 126, 123901 (2021).
2. J. Verbeeck, H. Tian, and P. Schattschneider, Nature 467, 301 (2010); S. M. Lloyd, M. Babiker, G. Thirunavukkarasu, and J. Yuan, Rev. Mod. Phys. 89, 035004 (2017).
3. A. Konečná, M.K. Schmidt, R. Hillenbrand, and J. Aizpurua, in preparation.
4. A. Asenjo-Garcia and F. J. García de Abajo, Phys. Rev. Lett. 113, 066102 (2014).
5. Z. Mohammadi, C. P. Cole P. Van Vlack, S. Hughes, J. Bornemann, and R. Gordon, Opt. Express 20, 15024 (2012).

Trapped aerosol sizes in dual beam optical fiber-based traps

L. Zhang[1,*], K. Cook[1], B. Liu[1], A. Szmalenberg[1], L. Ding[2], F. Wang[1,2], D. McGloin[1,2]

[1]School of Electrical and Data Engineering, University of Technology Sydney, NSW 2007, Australia
[2]School of Mathematical and Physical Sciences, University of Technology Sydney, Sydney, NSW 2007, Australia
Email: Ling.Zhang-9@student.uts.edu.au

***Abstract**: Quantifying the size range of aerosols that can be trapped in a counter-propagating (CP) dual fibre tapping configuration is important in determining trapping parameters and particle dynamics within the trapping volume. Here, we present simulations and experiments that describe the trapped aerosol size range variations under different fibre separations, fibre powers, radial and angular offsets. By doing so, we can determine the size area plot for stable aerosol trapping and predict regimes where multiple stable trapping points exist.*

Since Ashkin first used lasers to demonstrate the optical trapping and manipulation of microscopic particles [1], this technique has been extending into various disciplines of biology, physics, materials, and chemistry. In the past 15 years, an emerging field has been the optical trapping, manipulation, and characterization of a single aerosol particle [2-6]. To stably trap these airborne particles and probe their physical and chemical properties has great significance for studies of atmospheric chemistry and human health, as many processes at the single aerosol level are still not yet fully understood. They are obviously crucial for comprehending the global atmospheric processes developing more accurate climate models.

Unlike liquid environments, optical trapping and manipulation in air offers different challenges. One reason is the very low viscosity of the suspending medium, making the suspended aerosol more sensitive to the surrounding fluctuations. The other reason is the higher relative refractive index of the aerosols in air, which makes it more likely to push the aerosol away from the trapping field due to the greater scattering force [7]. Therefore, to accomplish stable three-dimensional (3D) aerosol trapping in air, it is of necessity to balance the scattering and gradient components generated by the light-matter interaction. When using optical fiber traps to manipulate aerosol particles, there are clear advantages in terms of system integration. However, most recent works in this area focus on either optical tweezers of free-space multibeam traps. Accurate quantification of particle properties within such a trap are useful in developing future trapping systems and in assessing the limits of such systems to misalignment.

In this paper, a CP dual fiber trap configuration is used to trap and manipulate aerosol particles. We develop a model that enables trapped sized particles to be predicted for a set of trap parameters. In Fig.1, we show the trapped aerosol sizes under different fiber separations, and fiber power with good alignment. Then we demonstrate the variations of the trapped aerosol sizes under different fiber separations, particle sizes and fiber power with the fibers experiencing different levels of misalignment, based on radial and angular offsets. We find situations where stable trapping positons shift from the center of the fibers to positons close to the fiber ends, and instances where the dynamics of the particles alter due to the modified trapping potentials presented. We observe that misalignment may, in some cases offer richer trapping possibilities, while also not being a major concern if using fiber trapping integrated devices.

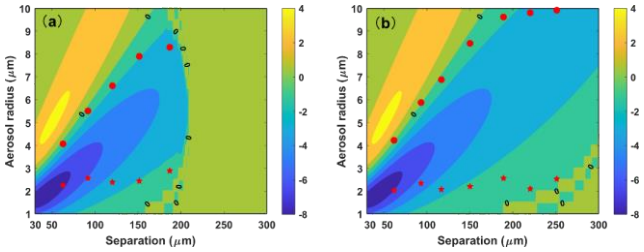

Figure 1: Area plots describing the expected 3D trapped aerosol size range at the midpoint under different fiber powers with (a) 20mW and (b) 100mW. The red dot and pentagrams represent the maximum and minimum aerosol sizes that can be trapped in the experiment, respectively. For legend bar, the negative value means the stable 3D trap can be achieved. Regarding the value of 0, it indicates the position where the midpoint is neither stable nor unstable for 3D trapping.

References:

1. Ashkin, A., Physical review letters, 1970. 24(4): p. 156.
2. Reich, O., et al., Communications Physics, 2020. 3(1).
3. Gong, Z., et al., Applied Spectroscopy, 2019: p. 000370281982880.
4. Gong, Z., et al., Journal of Quantitative Spectroscopy and Radiative Transfer, 2018. 214: p. 94-119.
5. Parmentier, E.A., et al., Journal of Aerosol Science, 2021. 151: p. 105660.
6. Purohit, P., et al., Analytical Chemistry, 2021.
7. van der Horst, A., et al., Applied optics, 2008. 47(17): p. 3196-3202.

Quantitative photoacoustic velocimetry technique using multi-angle observations

Caitlin Smith[1], Jami Shepherd[1], Guillaume Renaud[2] and Kasper van Wijk[1]

[1]*Dodd-Walls Centre for Photonic and Quantum Technologies, Department of Physics, University of Auckland, New Zealand*

[2]*Department of Imaging Physics, Delft University of Technology, The Netherlands*
email: csmi310@aucklanduni.ac.nz

***Abstract**: Photoacoustic velocimetry is a technique that automatically quantifies the direction and speed of moving absorbers such as blood. By synthetically changing the receiving angle of each pixel in post-processing, the photoacoustic Doppler equation can be solved using a least-squares approach to reveal the axial and lateral flow components of each pixel.*

Photoacoustic imaging (PAI) is a rising medical diagnostic modality in which the absorption of laser light generates high frequency pressure waves, which can be detected using clinical ultrasonic transducers and reconstructed to locate the position of optical absorbers [1, 2]. By recording a sequence of images, the phase shift of each pixel can be used to determine the movements of these absorbers.

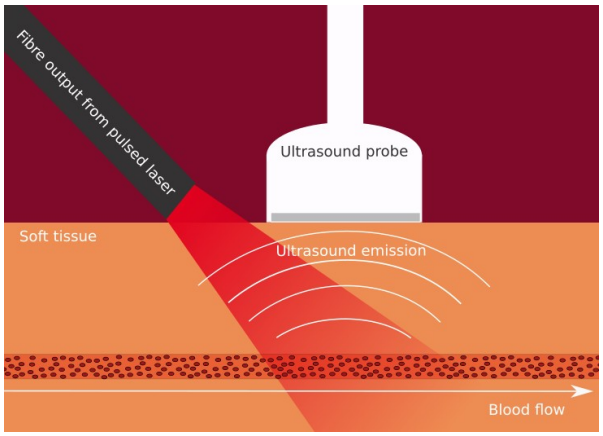

Figure 1: Photoacoustic velocimetry diagram. Moving blood cells absorb pulsed laser light which causes them to emit ultrasonic waves. These ultrasonic waves are detected by an ultrasound probe on the tissue surface.

Even though ultrasound methods are already used clinically to measure and map blood flow, the nature of measuring flow with PAI has the potential to be more powerful in many scenarios. PAI inherently offers a better SNR than ultrasound for determining blood flow as there is a high optical contrast between chromophore-rich red blood cells and the surrounding tissue while in ultrasound, acoustic waves are only weakly reflected by these cells. In low flow-rate scenarios, the signal reflected by blood flow can be overpowered by slow-moving respiratory or cardiac motion in ultrasound. However, in PAI this problem is less prominent as the photoacoustic waves are emitted primarily from blood flow and not tissue walls, resulting in less signal clutter. As a result, PAI is a promising technique to map the flow speeds in micro-vasculature, which has eluded ultrasound to-date.

Existing photoacoustic flow methods require the angle of flow to be known a priori, which is rarely the case, particularly in small, complex vasculature. In this presentation, I will discuss the development of a new technique, termed photoacoustic velocimetry (PAV), which computes both the magnitude and direction of flow automatically. By harnessing advancements from ultrasonic vector flow imaging, our PAV technique solves the Doppler equation using a least-squares approach [3]. We will demonstrate the validation of this novel technique through simulations and bench-top experiments.

References:

1. Beard, Paul. "Biomedical photoacoustic imaging." Interface focus 1.4 (2011): 602-631.
2. Bücking, T. M., Van Den Berg, P. J., Balabani, S., Steenbergen, W., Beard, P. C., & Brunker, J. (2018). Processing methods for photoacoustic Doppler flowmetry with a clinical ultrasound scanner. Journal of biomedical optics, 23(2), 026009.
3. Yiu, B. Y., & Alfred, C. H. (2016). Least-squares multi-angle Doppler estimators for plane-wave vector flow imaging. IEEE transactions on ultrasonics, ferroelectrics, and frequency control, 63(11), 1733-1744.